

**SUSTAINING HYDRAULIC CONDUCTIVITY IN SOFT/ACID
DAMAGED CARBONATE FRACTURES: CHEMICAL
TREATMENT FOR ENHANCED PERFORMANCE**

BY

MAHMOUD HASSAN MOHAMED DESOUKY

A Dissertation Presented to the
COLLEGE OF GRADUATE AND INTERDISCIPLINARY STUDIES

KING FAHD UNIVERSITY OF PETROLEUM & MINERALS

DHAHRAN, SAUDI ARABIA

In Partial Fulfillment of the
Requirements for the Degree of

DOCTOR OF PHILOSOPHY

In

PETROLEUM ENGINEERING

December 2023

KING FAHD UNIVERSITY OF PETROLEUM & MINERALS

DHAHRAN- 31261, SAUDI ARABIA

DEANSHIP OF GRADUATE STUDIES

This thesis, written by **MAHMOUD DESOUKY** under the direction of his thesis advisor and approved by his thesis committee, has been presented and accepted by the Dean of Graduate Studies in partial fulfillment of the requirements for the degree of **DOCTOR OF PHILOSOPHY IN PETROLEUM ENGINEERING.**



Dr. Dhafer Abdullah Al Shehri
Department Chairman



Dr. Suliman Saleh Al-Homidan
Dean of Graduate Studies

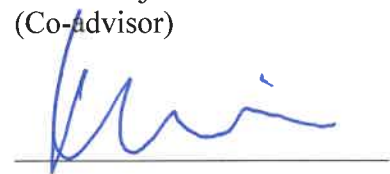
Date




Dr. Murtada Al-Jawad
(Advisor)



Dr. Abduljamiu Olalekan Amao
(Co-advisor)



Dr. Theis Ivan Solling
(Member)



Dr. Abdulazeez Abdulraheem
(Member)



Dr. Dhafer Abdullah Al Shehri
(Member)

© Mahmoud Desouky

2023

To my dearest father and mother, whose boundless love and unwavering support have shaped the person I am today. No words can express the depth of gratitude I feel for your endless sacrifices, tireless guidance, and unconditional belief in my dreams. I am forever indebted to you both.

ACKNOWLEDGMENTS

I am profoundly grateful to my esteemed advisor, **Dr. Murtada Al-Jawad**, whose dedicated support, invaluable guidance, and unwavering belief in my abilities have been the cornerstone of this dissertation. **Dr. Al-Jawad's** mentorship and tireless efforts have paved the way for the completion of this research, overcoming numerous challenges along the way.

I want to express my deepest gratitude to **Dr. Abduljamiu Amao** for his profound insights into the theoretical concepts explored in this research. His expertise and valuable contributions have significantly enriched the quality of this work.

I would also like to extend my heartfelt appreciation to **Dr. Theis Solling**, whose exceptional commitment, innovative thinking, and remarkable problem-solving skills have played a pivotal role in shaping the outcome of this work. His insightful contributions and dedication have been truly invaluable.

I am sincerely thankful to **Dr. Dhafer Al-Shehri** for his continuous encouragement and support throughout my academic journey. His guidance and genuine interest in my success have been a source of inspiration.

Lastly, I am immensely grateful to **King Fahd University of Petroleum & Minerals (KFUPM)** and the **College of Petroleum and Geosciences (CPG)** for their generous scholarship that has made this research possible. Their support and resources have been instrumental in shaping my academic path.

TABLE OF CONTENTS

ACKNOWLEDGMENTS	V
TABLE OF CONTENTS	VI
LIST OF TABLES	IX
LIST OF FIGURES	X
LIST OF ABBREVIATIONS	XII
ABSTRACT.....	XV
ملخص الرسالة.....	XVII
CHAPTER 1 INTRODUCTION.....	1
1.1 Problem Description	2
1.2 Research Objectives.....	3
CHAPTER 2 TEMPERATURE, PRESSURE, AND DURATION IMPACTS ON THE OPTIMAL STIFFENING OF CARBONATES AGED IN DIAMMONIUM PHOSPHATE SOLUTION.....	4
Abstract	4
2.1 Introduction.....	5
2.2 Materials and Methods.....	9
2.2.1 Rock Samples and Chemicals.....	9
2.2.2 Instrumental setups.....	10
2.2.3 Statistical Significance	14
2.3 Results	15
2.3.1 Temperature-Pressure Interaction Effect on Stiffness.....	15
2.3.2 Treatment Duration Effect on Stiffness.....	18

2.3.3	Catalysis Effect on Stiffness	19
2.3.4	Determination of Reaction Depth Using XRF	21
2.3.5	Characterization of Mineral Composition Using XRD and EDS.....	22
2.3.6	Morphological Changes Observed with SEM.....	23
2.4	Discussion	27
2.5	Conclusion	33

CHAPTER 3 ENHANCING FRACTURE CONDUCTIVITY IN SOFT CHALK FORMATIONS WITH DIAMMONIUM PHOSPHATE TREATMENT: A POTENTIAL SOLUTION FOR LONG-TERM PERFORMANCE..... 35

Abstract	35
3.1 Introduction.....	36
3.2 Experimental Design.....	39
3.2.1 Materials	40
3.2.2 Instruments and Procedure.....	40
3.2.3 Statistical Analysis	45
3.3 Results and Discussion.....	46
3.3.1 Samples Characterization	46
3.3.2 Chemical Treatment and E * Improvement.....	50
3.3.3 Statistical Analysis	53
3.3.4 Hydraulic Conductivity and Deformation	55
3.3.5 SEM and EDS.....	59
3.4 Conclusion	62

CHAPTER 4 DIAMMONIUM PHOSPHATE TREATMENT FOR SUSTAINED HYDRAULIC/ACID FRACTURE CONDUCTIVITY IN CHALK AND LIMESTONE FORMATIONS..... 64

Abstract	64
4.1 Introduction.....	65

4.2	Methodology	69
4.2.1	Rock Samples.....	69
4.2.2	Roughness Measurements	69
4.2.3	Elastic Stiffness Measurements	70
4.2.4	Acid Etching.....	71
4.2.5	Specimen's Chemical Treatment.....	72
4.2.6	Hydraulic Conductivity Measurements and Deformation.....	73
4.3	Results	77
4.3.1	Changes in Elastic Stiffness Following Acid Etching	77
4.3.2	Changes in Roughness Following Acid Etching.....	80
4.3.3	Hydraulic/Acid Conductivity	85
4.3.4	Deformation	89
4.4	Discussion.....	91
4.5	Conclusion	95
CHAPTER 5 CONCLUSION, FUTURE WORK, AND RECOMMENDATION... 96		
5.1	Conclusion	96
5.2	Future Work.....	97
5.3	Recommendation.....	98
REFERENCES.....		99
VITAE.....		114

LIST OF TABLES

Table 2-1:	Different Treatments Design	12
Table 2-2:	Two-way ANOVA Analysis of Temperature and Pressure as Factors.	17
Table 2-3:	Two-way ANOVA Analysis of Temperature and Pressure as Factors.	20
Table 3-1:	Summary of the roughness measurements in mm for the samples used in Experiment #2.	47
Table 3-2:	Statistical Summary of E*.	53
Table 3-3:	Summary of Two-way ANOVA Analysis.....	54
Table 3-4:	Failure Stress (psi) as Deduced from LVDT and Conductivity Trendlines.	58
Table 3-5:	Elements Composition by Weight (Wt.) Percent as measured by EDS at locations Specified in Figure 12B.	60
Table 4-1:	Summary of samples' data and corresponding experimental conditions....	76
Table 4-2:	Summary of the roughness measurements.	84

LIST OF FIGURES

Figure 1-1:	The proposed hardening stage after the acid fracture job.	2
Figure 2-1:	Austin Chalk Sample.....	9
Figure 2-2:	Workflow of the Experimental Analyses.....	14
Figure 2-3:	Pre- and Post-Elastic Stiffness Distribution Under Varying Pressure and Temperature Treatments.	16
Figure 2-4:	Tukey's HSD for Comparison Among Different Pressure Groups.	18
Figure 2-5:	Pre- and Post-Elastic Stiffness Distribution Under Increasing Time Treatments.....	19
Figure 2-6:	Pre- and Post-Elastic Stiffness Distribution for Catalyzed and Uncatalyzed Treatments.....	20
Figure 2-7:	Pseudo-colored Images Showing Phosphorous Concentration in a. Untreated, b. Treated Chalk Samples.	21
Figure 2-8:	Intensity of Phosphorous with Location Across the Untreated and Treated Samples.	21
Figure 2-9:	XRD Spectra of Powder from Treated and Untreated Chalk Samples.	23
Figure 2-10:	Colorized SEM Images of a. Intact Separate Calcite Grains, b. Niddle- shape HAP Crystals, c. Rose-shape HAP Crystals, d. Rod-shape HAP Crystals, e. Spikey -shape HAP Crystals.	24
Figure 2-11:	SEM Images of a. Treated Chalk Samples at 2,000 psi and 25 °C Showing Calcite and Needle-like HAP, b. Colorized and Closer View of Image 11a, c. Treated Chalk Samples at 2,000 psi and 75 oC, d. Colorized and Closer View of Image 11c, e. Treated Chalk Samples at 2,000 psi and 120 °C, and f. Colorized and Closer View of Image 11e	26
Figure 3-1:	Flow chart of the experimental work.	40
Figure 3-2:	A schematic for the fracture conductivity apparatus.....	43
Figure 3-3:	Sample preparation for the conductivity experiment.	45
Figure 3-4:	Example of surface roughness measurement and profiles along the long and short sides of 3C.....	48
Figure 3-5:	The chalk sample surface shows E* measurement grid.....	48
Figure 3-6:	Clustering of heterogenous chalk samples by measuring E*	50
Figure 3-7:	Distribution of E* measurements.....	52
Figure 3-8:	Treated and Untreated Hydraulic Conductivity Comparison of Experiment 1.....	55
Figure 3-9:	Comparison of Hydraulic Conductivity Between Treated and Untreated Samples in Experiments 2 and 3.....	57
Figure 3-10:	Comparison of Compaction Between Treated and Untreated Samples.	58
Figure 3-11:	The Long-term Conductivity Comparison.	59
Figure 3-12:	SEM image of A) intact chalk sample shows the calcite grains, B) treated chalk with minerals identified with EDS, C) treated chalk sample shows	

	the host calcite grains and the newly formed HAP, and D) closer view of treated chalk sample showing dendrite shape of HAP.....	62
Figure 4-1:	Illustration depicting the process of acid etching and subsequent brine flushing.	72
Figure 4-2:	A) Samples subjected to acidization B) Attachment of two sister samples to synthesize the fracture C) Molded samples utilized in hydraulic conductivity experiments.....	73
Figure 4-3:	Measurement of gas conductivity of the acid fracture and samples' deformations (Desouky et al., 2023a).....	74
Figure 4-4:	Mean stiffness 95% confidence interval of the limestone samples.....	78
Figure 4-5:	Comparison of initial Indiana limestone elastic stiffness and the impact of acid and DAP treatment.....	79
Figure 4-6:	Comparison of initial Austin chalk elastic stiffness and the impact of acid and DAP treatment.....	80
Figure 4-7:	Areal mean roughness profile and histogram for A) Sample LS1 without acidization, B) Sample LS5 after acidization, and C) Sample LS6 after acidization.....	82
Figure 4-8:	Areal mean roughness profile and histogram for A) Sample Ac5 after acidization and B) Sample Ac6 after acidization.....	83
Figure 4-9:	Short-term fracture conductivity of Indiana limestone A) Experiments 1 and 2, and B) Experiments 3 and 4.....	85
Figure 4-10:	Long-term fracture conductivity of Indiana limestone Experiments 1 and 2.....	86
Figure 4-11:	Short-term acid fracture conductivity of Austin chalk A) Experiments 1 and 2, and B) Experiments 3 and 4.....	88
Figure 4-12:	Long-term acid fracture conductivity of Austin chalk Experiments 3 and 4.....	89
Figure 4-13:	Deformation of the samples under stresses for Indiana limestone A) Experiments 1 and 2, and B) Experiments 3 and 4.....	90
Figure 4-14:	Deformation of the samples under stresses for Austin chalk Experiments 1 and 2.....	91

LIST OF ABBREVIATIONS

2D	:	Two Dimension
ANOVA	:	Analysis of Variance
API	:	American Petroleum Institute
C	:	Control
C₁	:	Conductivity When Stress Is Zero
C₂	:	Conductivity Decline Rate With Closure Stress
DAP	:	Diammonium Phosphate
E	:	Elastic Modulus/Young's Modulus
e	:	Euler's Number
E*	:	Reduced Modulus
EDS	:	Energy Dispersive X-Ray Spectroscopy
F value	:	Value Obtained From An F-Test
HAP	:	Hydroxyapatite
Hrs.	:	Hours
hf	:	Width Of Samples Comprising The Fracture
Tukey HSD	:	Tukey's Honestly Significant Difference
ID	:	Identification
k_f	:	Fracture Permeability
k_{rw}_i	:	Fracture Hydraulic Conductivity
L	:	Length Between First And Third Ports In The Api Conductivity Cell
L/S ratio	:	Liquid/Solid Ratio

LNH	:	Lithium Nitrate Hydrate
LVDT	:	Linear Variable Differential Transformer
M	:	Molecular Gas Mass
p	:	Probability
p₁	:	Pressure Measured At The First Port In The Api Conductivity Cell
p₂	:	Pressure Measured At The Third Port In The Api Conductivity Cell
p_{cell}	:	Arithmetic Average Of p ₁ And p ₂
Pr (>F)	:	P-Value Associated With The F-Statistic In An Anova
q	:	Nitrogen Flow Rate
R	:	Universal Gas Constant
S_a	:	Areal Arithmetic Mean Roughness
SEM	:	Scanning Electron Microscopy
sq.	:	Square Root
SRA	:	Surface Roughness Analyzer
S_{RE}	:	Rock Embedment Strength
T	:	Treatment Or Temperature
UCS	:	In The Context Of Materials, Ucs Stands For The Unconfined Compressive Strength
w_i	:	Fracture Aperture Width
XRD	:	X-ray Diffraction
XRF	:	X-ray Fluorescence

Z	:	Compressibility Factor
Δp	:	Difference Between p_1 And p_2
μ	:	Gas Viscosity
ν	:	Poisson's Ratio
ρ	:	Gas Density
σ_c	:	Closure Stress

ABSTRACT

Full Name : Mahmoud Hassan Mohamed Desouky

Thesis Title : Sustaining Hydraulic Conductivity in Soft/Acid Damaged Carbonate Fractures: Chemical Treatment for Enhanced Performance

Major Field : Petroleum Engineering

Date of Degree : December 2023

The successful implementation of hydraulic/acid fracture operations in carbonate formations heavily relies on the mechanical properties of the rock post-treatment. Preserving the integrity of the rock is crucial for maintaining conductivity in the created fractures under stress. However, weak formations or excessive acid etching can lead to significant declines in productivity due to rock failure and creep. To address this issue, strengthening chemicals are being explored to enhance rock strength and sustain high stresses, thereby preserving fracture conductivity. Previous studies have demonstrated the ability to alter the mechanical properties of carbonate rocks using strengthening chemicals such as diammonium phosphate (DAP). In the context of acid fracturing, adopting the concept of rock strengthening is vital for sustaining fracture conductivity, which is directly influenced by the stiffness of the rock.

Therefore, a systematic experimental methodology was developed to investigate the efficacy of the DAP-strengthening chemical in altering the mechanical properties of carbonate rocks for acid fracturing applications. The stiffness of the rock samples was

measured using the non-destructive impulse hammering technique, while acid etching and hydraulic/acid fracture conductivity were evaluated using the API conductivity cell. Various analytical techniques, including Scanning electron microscopy (SEM), X-ray diffraction (XRD), X-ray fluorescence (XRF), and energy dispersive microscopy (EDS), were employed to analyze the treated samples and gain insights into the accompanying changes. Statistical analyses were performed to assess the significance of the strengthening effect, and the parameters of pressure, temperature, and time were systematically varied to understand their influence on the overall outcomes.

The results revealed that 1M DAP solution has the potential to enhance the stiffness of the soft and acid-damaged samples significantly by the formation of hydroxyapatite (HAP). As a result, the hydraulic conductivity in both DAP-stiffened intact and DAP-stiffened acidized fractures showed significant improvement, with at least a twofold increase in the short-term and long-term performance in Indiana limestone and even up to eightfold enhancement in Austin Chalk. Furthermore, temperature was identified as the most critical parameter influencing the DAP reaction with calcite in the tested carbonate samples, making it a practical solution for reservoir conditions. These findings promise to address a common challenge in the petroleum industry and mitigate its impact.

ملخص الرسالة

الاسم الكامل: محمود حسن محمد دسوقي

عنوان الرسالة: الحفاظ على قابلية التوصيل الهيدروليكي في الكسور الكربوناتيّة اللينة/المتلفة بالحمض: معالجة كيميائية لتحسين الأداء

التخصص: هندسة البترول

تاريخ الدرجة العلمية: ديسمبر ٢٠٢٣

تعتمد نجاح عمليات كسر صخور الكربونات بالماء المضغوط والأحماض بشكل كبير على الخواص الميكانيكية للصخور بعد المعالجة. ولهذا ، الحفاظ على سلامة الصخور أمر حاسم للحفاظ على قدرة التوصيل في الشقوق التي تكونت تحت الإجهاد. ومع ذلك ، يمكن أن تؤدي التكوينات الضعيفة أو التآكل الحمضي الزائد إلى انخفاض كبير في الإنتاجية بسبب فشل وانزلاق الصخور. لمعالجة هذه المشكلة ، يتم استكشاف المواد المقوية لتعزيز قوة الصخور والحفاظ على الضغوط العالية ، وبالتالي الحفاظ على قدرة التوصيل في الشقوق. أظهرت الدراسات السابقة قدرة تغيير الخواص الميكانيكية للصخور الكربونات باستخدام المواد المقوية مثل فوسفات ثنائي الأمونيوم. في سياق كسر الصخور بالأحماض ، فإن اعتماد مفهوم تقوية الصخور ضروري للحفاظ على قدرة التوصيل في الشقوق ، والتي تتأثر مباشرة بصلابة الصخور.

لذلك ، تم تطوير تجارب منهجية للتحقيق من فعالية المواد المقوية في تغيير الخواص الميكانيكية لصخور الكربونات لتطبيقات كسر الصخور بالأحماض. تم قياس صلابة عينات الصخور باستخدام تقنية الصدمة غير المدمرة بواسطة المطرقة النبضية ، في حين تم حقن الحمض وقياس قدرة التوصيل الهيدروليكي / الحمضي باستخدام خلية التوصيل المعتمدة من معهد البترول الأمريكي. وعلاوة على ذلك تم استخدام تقنيات تحليلية مختلفة ، بما في ذلك المجهر الإلكتروني الماسح وتفاوت الأشعة السينية وتفاوت الأشعة السينية التفاعلية والمجهر الإلكتروني ذو الانتشار الطاقوي ، لتحليل العينات المعالجة واكتساب رؤى حول التغيرات المصاحبة. تم إجراء تحليلات إحصائية لتقييم أهمية تأثير التقوية ، وتم تغيير معاملات الضغط ودرجة الحرارة والوقت بشكل نظامي لفهم تأثيرها على النتائج العامة.

أظهرت النتائج أن محلول الفوسفات ثنائي الأمونيوم بتركيز ١ مولار له القدرة على تعزيز صلابة العينات اللينة والتالفة من الحمض بفعالية كبيرة من خلال تشكل هيدروكسيباتيت. نتيجة لذلك ، أظهرت قدرة التوصيل الهيدروليكي المقواة في الحالة السليمة والمعالجة بالأحماض تحسناً كبيراً ، مع زيادة بنسبة مضاعفة على الأقل في الأداء القصير الأجل والطويل الأجل في الحجر الجيري إنديانا ، وحتى زيادة تصل إلى ثمانية أضعاف في الحجر طباشيري أوستن. علاوة على ذلك ، تم تحديد درجة الحرارة بأنها العامل الأكثر أهمية يؤثر على تفاعل محلول الفوسفات ثنائي الأمونيوم مع الكالسيوم في العينات الكربونات المختبرية المختبرة ، مما يجعلها حلاً عملياً لظروف الخزان. تعد هذه النتائج واعدة في مواجهة تحدي شائع في صناعة البترول والحد من تأثيره.

CHAPTER 1

INTRODUCTION

Acid fracture has been widely used in carbonate formations to boost productivity since the 1960s. The job involves the injection of an acid with pressure exceeding the fracture pressure to initiate new fractures or revive existing natural ones. The ideal role that acid is supposed to play is etching the fracture surfaces differentially to create uneven surfaces. The least principal stress closes the fracture after stopping the acid injection. However, the uneven surface does not fully close, leaving a path for the formation fluid to flow into the wellbore.

The flow capacity of the created fracture is known as acid fracture conductivity. Different acid systems control the fracture extent and etching pattern for optimized acid fracture conductivity. The etching pattern, the effective stress, and the strength of the fracture-supporting pillars greatly impact the acid fracture conductivity. Acid fracturing is successful when the developed conductivity is preserved for a long time.

In case of weak formation or over-etching, the pillars that keep the fracture open lack the strength to hold the fracture open under stress for a long time. Consequently, productivity decay is observed shortly after the fracture job.

The main objective of this study is to harden the soft fracture surface to be more deformation-resistant. The deformation resistance will extend the life of the fracture by

reducing the fracture conductivity decline and increasing the stress that the fracture can support. As a result, the well productivity will be enhanced, and the need for refracting can be greatly reduced.

The hardening of the fracture surface will be approached by treating soft carbonate rock surfaces, i.e., chalk with diammonium phosphate. Although there are some studies to harden carbonate rocks, none of these studies investigated the effect of hardening on fracture conductivity. Proving the practical significance of hardening the fracture surface on the fracture conductivity proposes adding a hardening stage to the acid fracturing process (see **Figure 1-1**).

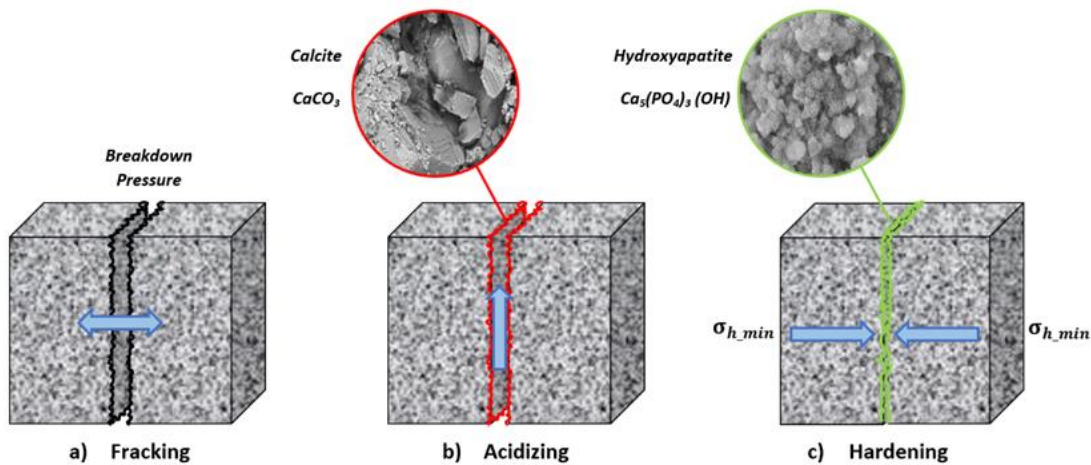


Figure 1-1: The proposed hardening stage after the acid fracture job.

1.1 Problem Description

Reduction in the fracture conductivity that occurs after acid fracturing is attributed to the combined effect of the elastic, plastic, and creeping deformations in response to the in-situ stress. Early-stage creeping is responsible for roughly one-third of the production rate

decline due to the acid-softening effect on the rock. Furthermore, production increases the effective least principle stress, making the asperities more prone to compressive failure.

The problem is more pronounced in limestone and chalk rather than dolomite due to the hard nature of the latter. Hence, if the rock surface hardness of chalk and limestone is enhanced, the expected deformation will be less, and a more sustainable acid fracture productivity can be attained.

1.2 Research Objectives

This research aims to test the effect of the hardening chemicals to enhance the acid fracture conductivity by mimicking the reservoir conditions of stress, temperature, pressure, etc. Toward this end, the following tasks should be conducted:

- 1) Understand the hardening effect by measuring the hardness at different conditions.
- 2) Design an appropriate experimental procedure to quantify the hardening treatment effect.
- 3) Study if the rock surface hardening can withstand high stresses after using hardening chemicals to sustain long-term fracture conductivity.

Examine the impact of chemical treatment on the ability of the formation to deliver fluid to the fracture and determine whether this effect is statistically significant and practically significant.

CHAPTER 2

TEMPERATURE, PRESSURE, AND DURATION

IMPACTS ON THE OPTIMAL STIFFENING OF

CARBONATES AGED IN DIAMMONIUM PHOSPHATE

SOLUTION

Abstract

DAP has been proven effective in improving the stiffness of weak or acid-damaged carbonates, thereby preserving hydraulic fracture conductivity. The reaction between DAP and calcite in chalk formations primarily produces hydroxyapatite (HAP), which is stiffer than calcite. However, the optimal reaction outcomes vary greatly with factors such as DAP concentration and reaction conditions. This study investigated the DAP-calcite reaction duration, pressure, and temperature effects on the stiffness magnitude of soft Austin chalk. Also, the catalyst effect and depth of HAP formation were examined. The study involved the assessment of stiffness, non-destructively (impulse hammering), mineralogy (XRD, SEM), and elemental composition (XRF). The study tested 15 different DAP-chalk reaction variations, where the pressure, temperature, time, and catalyst addition were modified in each case. The samples' elastic stiffness distributions were then collected and compared to the pre-reaction ones. The results showed that the elastic

stiffness increased in all treated samples, with an 181% maximum increase achieved after 72 hrs at 1,000 psi and 75°C. However, the pressure effect was minor compared to the temperature. The SEM images revealed different HAP morphology corresponding to different treatment conditions. Although the treated samples showed an increased intensity of phosphorus throughout the entire sample, the near-surface zone (4-6 mm) was the most affected, as inferred from the XRF elemental analysis. The study's findings can help optimize hydraulic fracturing operations in weak carbonate reservoirs, improving production rates and overall well performance.

Keywords: Soft Carbonates, Hydroxyapatite, Chalk, DAP Treatment, Stiffening

2.1 Introduction

Maintaining fracture conductivity is crucial to hydraulic fracturing operations, where rock stiffness greatly impacts (Jansen, 2014). Minerals are the rocks' building blocks; their composition and crystal structure uniquely define them (Smyth & Bish, 1988). At the mineral level, hardness is determined by the strength of the chemical bonding and is related to a mineral's resistance to scratching (Broz et al., 2006). For example, calcite and apatite have 3 and 5 on Moh's scale, respectively (Nesse, 2012). In comparison, macro hardness is the ability to resist deformation, such as indentation, which may be related to how the grains are cemented (Broitman, 2017). Constituent minerals contribute to the overall hardness of the rock they form (Ayatollahi et al., 2020; Li et al., 2021). Therefore, the minerals forming the rock and how the grains are cemented reflect the final rock's elastic stiffness (Viktorov et al., 2014). As long as calcium (Ca) and phosphate (PO₄) ions exist, apatite can exist in various forms. Thus, replacing a relatively soft mineral, i.e., calcite, with a harder one, i.e., apatite, can result in stronger structures than the original (Desouky

et al., 2021). Yaşar & Erdoğan (2004) investigated the relationship between hardness value and physicochemical properties of constructional and cover rocks and concluded that physicochemical properties can be estimated using hardness methods. In the context of hydraulic fracture conductivity, stiffness is a superior and more precise indicator of a rock's mechanical properties compared to macro hardness. While there may be some correlation between the two in certain types of rocks, stiffness measurements provide a more comprehensive understanding of the rock's mechanical behavior. Stiffness directly correlates with the rock's ability to withstand deformation, making it a more reliable indicator of its capacity to endure applied pressure and retain its shape during hydraulic fracturing.

Several methods are commonly used to prepare HAP (a specific type of apatite mineral that contains hydroxide ions OH^-), including hydrothermal, precipitation, solvothermal, spontaneous combustion, micro-emulsion, ultrasonic synthesis, bionic and solid-state reaction, or wet and dry methods (Ma, 2019). On the one hand, the precipitation process used in the formation of HAP from calcite typically involves the reaction of calcium carbonate with a phosphate source, such as diammonium phosphate ($\text{NH}_4\text{H}_2\text{PO}_4$), known as DAP, in the presence of water (Liu et al., 2001). On the other hand, hydrothermal is similar to precipitation but at high temperature and pressure (Roy & Linnehan, 1974). Also, researchers suggested that the HAP crystals can be synthesized from calcite crystals through hydrothermal treatment. Specifically, studies conducted by Yoshimura et al. (2004), (Neira et al. (2009), and Zhang & Vecchio (2007) have all reported successful production of HAP crystals using this method.

Different synthesis approaches results in different HAP crystal structure. The shape variations of HAP are attributed to the distinct reactivity level of each exposed calcite crystal plane towards the surrounding solution (Kim et al., 2012). For instance, the (100) plane of calcite is more reactive than the (111) plane, which has a thicker coverage of newly formed HAP. The shape of HAP crystals produced under hydrothermal conditions is affected by several factors, including the solubility of the starting material, processing temperature, pH of the solvent additives, residence period, and others (Ashokan et al., 2022). Also, the concentration of the reactants plays a crucial role in determining the morphology of HAP crystals. Higher concentrations of DAP and CaCO_3 can promote faster nucleation and growth of HAP crystals, forming smaller crystal sizes and different morphologies (Liu et al., 2001).

The hydrothermal process is a commonly used method for the synthesis of HAP from calcite, as it allows for the control of the particle size, morphology, and crystallinity of the HAP product. As a result, the HAP produced by this method is widely used in various applications. For example, hydrothermally-formed HAP has prosthetic and other biomedical applications (Mucalo, 2015; DileepKumar et al., 2022). Also, Pai et al. (2020) reviewed the use of HAP and its composites as adsorbents for removing pollutants from wastewater, including heavy metals, organic compounds, and dyes. They described the mechanisms of adsorption and the factors that affect the adsorption performance, such as pH, temperature, and initial pollutant concentration. In addition, Ashokan et al. (2022) described a dissolution precipitation method to produce HAP microspheres for Chromatographic uses. In art preservation, using the DAP has proved to be a promising technique in restoring damaged carbonate rock's aesthetic and mechanical integrity

(Barriuso et al., 2017). According to recent findings by Murru & Fort (2020), the immersion of limestone in DAP has resulted in a significant enhancement of mechanical performance, which was assessed through variations in ultrasonic measurements.

In recent experiments conducted by Samarkin et al. (2023), hydrothermal treatment was utilized to form HAP in weak chalk samples for use in petroleum applications. The purpose of this technique was to enhance fracture surface elastic stiffness and sustain hydraulic fracture conductivity. The results of the experiment revealed that the surface elastic stiffness of the weak chalk samples was significantly improved, ultimately leading to a higher hydraulic conductivity of the fractures (Desouky et al., 2023a; Desouky et al., 2023b). These findings offer valuable insight into the potential for HAP to improve the effectiveness of hydraulic fracturing techniques in the petroleum industry. Such developments hold the promise of enhancing the industry's efficiency and reducing costs.

Thermodynamics favors the mineralogical exchange to convert calcium carbonate into HAP by DAP treatment (Ashokan et al., 2022). However, little is known about the time scale for the exchange at reservoir conditions (i.e., high pressure and high temperature). A fast reaction is favored for the process to be applicable in petroleum-related operations. Therefore, the DAP-calcite reaction and HAP generation speed must be addressed and fully understood. This study aimed to determine the effectiveness of strengthening chalk specimens by adjusting key factors such as pressure, temperature, and time in the formation of HAP. Additionally, the study conducted a detailed analysis of the distribution of HAP in the treated chalk samples. Finally, the research investigated the catalytic effect of Li ions on the DAP reaction with calcite.

2.2 Materials and Methods

2.2.1 Rock Samples and Chemicals

The experimental work in this study was conducted using 15 slabs of Austin chalk, which was chosen as reference material due to its low stiffness. The Austin chalk slabs have dimensions of 177.8 mm in length, 38.1 in width, and 12.7 mm in thickness, as shown in **Figure 2-1**. Two chemicals were used in the current study. The first is a high-purity DAP ($(\text{NH}_4)_2\text{HPO}_4$) from Sigma Aldrich, with a purity exceeding 99%. This water-soluble salt serves as a chalk consolidation agent in the present study. The other one is lithium nitrate hydrate (LNH), a chemical compound with the formula $\text{LiNO}_3 \cdot 3\text{H}_2\text{O}$. It is an odorless, colorless, and water-soluble salt primarily used as a precursor to produce other lithium compounds, including lithium carbonate. Thus, LNH was tested for its potential to catalyze the DAP-chalk reaction.

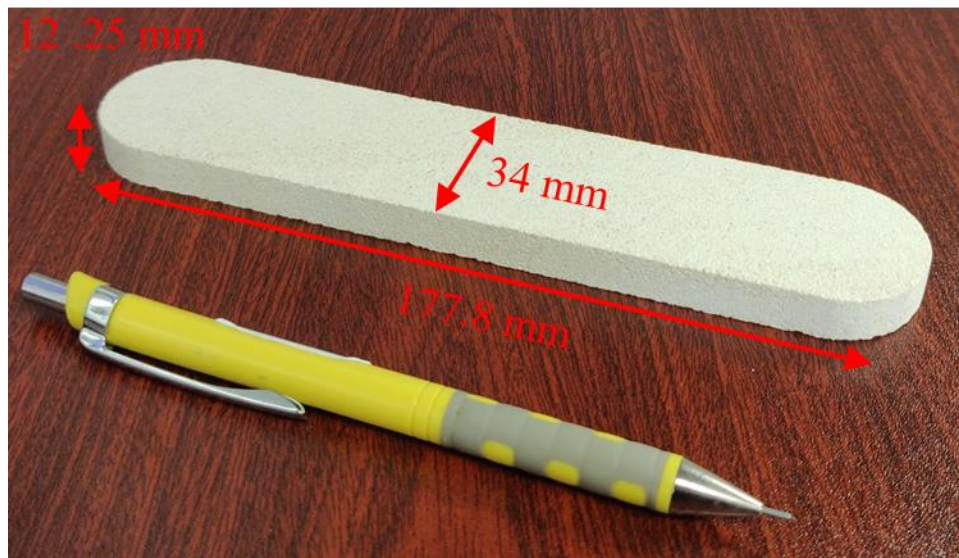


Figure 2-1: Austin Chalk Sample

2.2.2 Instrumental setups

In order to capture the variation in elastic stiffness of the chalk samples, multiple measurements were taken across the entire surface of each sample (30 points), covering different locations uniformly. First, elastic stiffness was assessed by the New England Research AutoScan by impulse hammering. The mechanical elastic stiffness probe is used to assess the elastic stiffness of a material, while the sensitive point measurements can detect fluctuations in inelastic stiffness and strength (i.e., heterogeneity). Once the elastic stiffness of the samples had been evaluated, they were subjected to one of the aging conditions specified in Table 2-1 by being placed in a Hastelloy steel cell for 24 hrs. following the vacuuming of the cell. In the first set of experiments (see **Table 2-1**), 9 samples with similar initial elastic stiffness distribution, 3.7 GPa on average, were aged at different pressure and temperature combinations. Every sample was treated at ambient, 1,000, or 2,000 psi pressure at each temperature inside a 3L-aging cell filled with 1M DAP. Following the treatment, the samples were extracted and rinsed with deionized water to eliminate any residual treatment solution. The samples were then dried for 24 hrs. in an oven at a temperature of 75°C. The aging process is highly similar to the hydrothermal synthesis used to synthesize various materials by subjecting reactants to high-pressure and high-temperature conditions in an autoclave closed vessel. The method is widely used in materials science and engineering, particularly for synthesizing inorganic materials such as HAP from DAP-calcite reactions. After the aging process, the surface elastic stiffness of the samples was assessed again to understand the effect of aging on them.

In the subsequent experiments, three samples underwent DAP treatments at an increment in treatment time (6, 18, 36, and 72 hrs) at 1000 psi and 75 °C. After each treatment interval,

the samples were taken out of the aging cell, washed thoroughly with DI water, and dried in the oven before their elastic stiffness was assessed using the Autoscanner. The same procedure was repeated for all the planned intervals, where the residual effluents from each previous interval were used in the subsequent one. For the final set of experiments, three samples with comparable elastic stiffness were subjected to an identical treatment using 1M DAP for six hrs. at 1,000 psi and 75°C, but with the addition of 5 grams of LNH per liter of DAP. The remaining procedures were carried out in the same manner as the previous experiments. The aim was to accelerate the creation of HAP by catalyzing the exchange process using direct methods and identifying the conditions that promote bonding between DAP and carbonate. The method focused on enhancing the interaction between an electron donor and an acceptor. Therefore, Li^+ was introduced to improve the electron acceptor (carbonate) by adhering to the O of the C=O group and drawing electrons from the carbon. This change might facilitate the attachment of DAP to the carbonate and thus expedite the process. As a result, investigating the influence of Li^+ catalysis was included in the study. Therefore, 5 grams of LNH was added to each 1M liter of the DAP solution to investigate its capability to expedite the stiffening effect of the DAP on the chalk slabs.

Table 2-1: Different Treatments Design

Sample ID	Treatment Condition					
	Concentration (M)	Temperature (C°)	Pressure (psi)	Catalyst	Time (hrs)	
S#1	1	25	0	-	72	
S#2			1,000			
S#3			2,000			
S#4		75	0			
S#5			1,000			
S#6			2,000			
S#7		120	0			
S#8			1,000			
S#9			2,000			
S#10		75	1,000		-	6, 18, 36, and 72
S#11						
S#12						
S#13					LiNO ₃ ·3H ₂ O	6
S#14						
S#15						

The DAP treatment's impact on the chalk's composition, structure, and morphology was thoroughly analyzed using a combination of scanning electron microscope (SEM) techniques, X-ray fluorescence (XRF), and XRD. First, a small cube was extracted from the treated samples to be imaged at the nanoscale level with Zeiss Gemini 450 SEM at the Center for Integrative Petroleum Research, King Fahd University of Petroleum and Minerals Dhahran, Saudi Arabia. The hydrothermal synthesis of HAP from DAP and CaCO_3 often leads to the formation of different HAP morphologies, which can be attributed to several factors, including the reaction conditions, reactant concentrations, and the presence of additives. Hence, the SEM is useful for characterizing and analyzing the hydrothermally formed HAP because it provides insights into its nanoscale structure and behavior.

Additionally, determining the depth of a chemical reaction within a solid surface can be a complex process that requires various techniques, depending on the type of reaction and the surface being studied. The XRF is a valuable tool for exploring the distribution and formation of minerals in porous media. Therefore, Bruker M4 Tornado XRF was utilized for elemental distribution. It is a non-destructive tool widely used in geology and environmental science, providing valuable information about diverse materials' elemental composition and mapping.

In this study, a sample with dimensions of 34x76.2x177.8 mm was subjected to 72 hrs. of treatment in the aging cell at 75 °C and 1,000 psi to investigate the reaction of DAP with the sample bulk. First, the sample was cut across its length to get the invasion depth of the DAP reaction. Subsequently, the samples were scanned with the XRF to compare the elemental composition with another intact sample. Furthermore, performing depth

profiling is essential in determining the depth of the reaction. The concentration of HAP was determined by tracking the presence of phosphorus, which was measured across and along the sample's surface at five different lines.

Finally, mineralogical characterization of the chalk samples was done with powder X-ray diffraction (XRD). A finely ground powder was obtained from a small portion of the treated chalk; the powder was then analyzed using the PANalytical Empyrean diffractometer, an advanced XRD instrument within a 2θ range of 0° to 70° . The SEM, XRF, and XRD analyses provided valuable insights into the chalk's composition, structure, and morphology when contrasted with the untreated samples' results. The comprehensive experimental procedure is depicted in **Figure 2-2**.

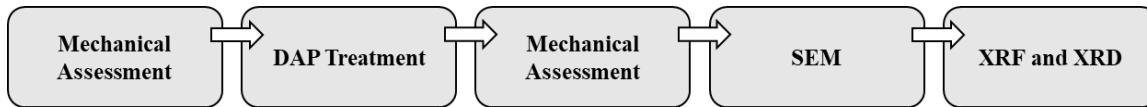


Figure 2-2: Workflow of the Experimental Analyses.

2.2.3 Statistical Significance

The elastic stiffness of chalk varies randomly along the surface within a certain range, making it mandatory to statistically validate the elastic stiffness improvement. The repeated experiments were intentional to reduce the uncertainty in the obtained results and to acquire more data to validate the results statistically. Therefore, statistical significance testing determines whether the elastic stiffness improvement was due to the treatment or just the result of a chance. Thus, the analysis of variance (ANOVA) technique was used to compare the means of treated and untreated elastic stiffness distributions to reveal if the treatments significantly affected chalk elastic stiffness. In addition, Tukey's HSD was

utilized when statistical significance was present. Tukey's HSD is a statistical method used to compare the means of multiple groups and determine which groups are significantly different from each other.

Furthermore, pair-wise comparisons were generated to visually represent this test's results, displaying the mean difference between each group alongside confidence intervals and significance levels. Where the confidence interval excludes zero, statistical significance exists between the two groups at the chosen significance level (generally 0.05). The data visualization and computations were made in Rstudio 2023.03.1.

2.3 Results

2.3.1 Temperature-Pressure Interaction Effect on Stiffness

The various treatments increased the 'samples' elastic stiffness, as illustrated in **Figure 2-3**. Each sample has two distributions: pre-elastic stiffness on the left and post-elastic stiffness on the right. However, the extent of this increase varied depending on the temperature and pressure conditions. Specifically, the effect of temperature on elastic stiffness was evident when comparing samples treated at elevated temperatures (75 and 120 °C) to those treated at lab ambient temperature (24 °C). At 2,000 psi and 24, 75, and 120 °C temperatures, average elastic stiffness increased by 46%, 108%, and 138%, respectively. A similar trend was observed across different temperatures and ambient pressures. However, the stiffness of Sample #5 exceeded expectations, exhibiting a larger-than-anticipated. It showed an increase of 181% following treatment at 75 °C and 1,000 psi. Conversely, the increase in elastic stiffness of Sample #8, treated at 75 °C and 2,000 psi, appeared to be less than

expected. In contrast, the increased elastic stiffness with the increase in treatment pressure did not exhibit a clear trend at different temperatures.

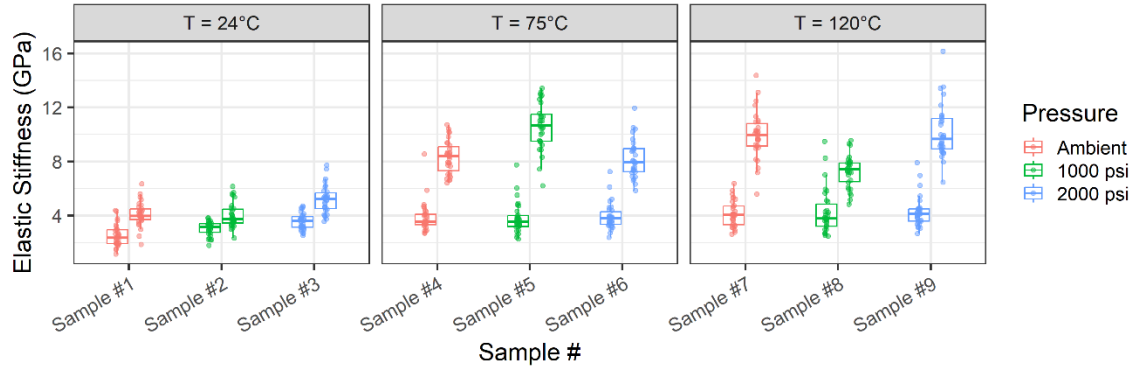


Figure 2-3: Pre- and Post-Elastic Stiffness Distribution Under Varying Pressure and Temperature Treatments.

A one-way ANOVA was conducted to examine the effects of different factors on elastic stiffness, such as sample, pressure, temperature, and pre/post-elastic stiffness, one at a time. In comparison, two-way ANOVA examines two independent variables' impact on a dependent variable. The one-way ANOVA results showed that the sample, temperature, and pre/post-elastic stiffness significantly impacted elastic stiffness. In contrast, the impact of pressure was statistically significant but relatively minor compared to the impact of temperature.

Furthermore, a two-way ANOVA was conducted to analyze the effects of pressure, temperature, and their interaction on elastic stiffness, and the results indicated that all three factors had a significant impact, as presented in **Table 2-2**.

Table 2-2: Two-way ANOVA Analysis of Temperature and Pressure as Factors.

Factor	Degree of Freedom	Sum sq.	Mean sq.	F value	Pr(>F)	p
Temperature	2	427	213.28	32.535	4.69e-14	< .001
Pressure	2	99	49.72	7.585	0.000565	< .001
Temperature: Pressure	4	284	70.99	10.830	< 2e-16	< .001

In addition, Tukey's HSD was utilized to analyze the differences in elastic stiffness means associated with pressure. The Tukey family-wise confidence level is typically expressed as a percentage. It represents the probability that the confidence interval captures the true difference between any two groups in a multiple comparison test. For example, if the Tukey family-wise confidence level is set to 95%. In that case, there is a 95% chance that the confidence interval calculated for each pairwise comparison includes the true difference between the group means. Tukey's HSD analysis shows that the mean elastic stiffness for 0 psi pressure significantly differed from that for pressure levels of 1,000 and 2,000 psi. However, no significant difference between 1,000 and 2,000 psi pressure was observed as the confidence level contains 0 (see **Figure 2-4**).

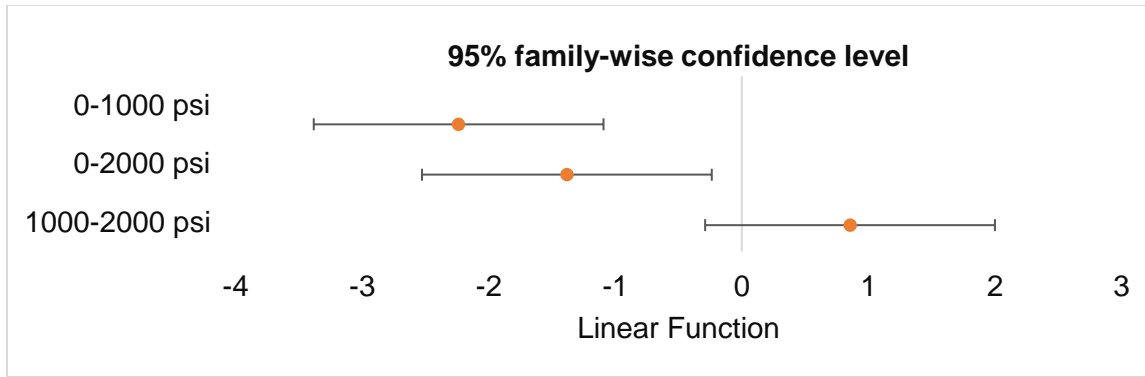


Figure 2-4: Tukey's HSD for Comparison Among Different Pressure Groups.

The statistical study showed that the temperature positively affected chalk elastic stiffness after DAP treatment, whereas the pressure had a slightly negative impact. The usual reservoir pressure and temperature values vary greatly depending on the reservoir and location. In addition, the pressure and temperature combination of 1,000 psi and 75°C significantly increased the elastic stiffness of the surface of chalk. Therefore, these precise parameters were used in the next experiments to imitate downhole circumstances better.

2.3.2 Treatment Duration Effect on Stiffness

The results showed a clear and consistent increase in elastic stiffness across all three experiments, with the elastic stiffness of the samples increasing as they were treated for longer periods (see **Figure 2-5**). At 72 hrs., the samples exhibited the greatest increase in elastic stiffness, and there were no indications of stabilization, indicating that there is potential for further increases in elastic stiffness if the treatment were to be extended for a longer period. Specifically, at the 72-hour mark, the increase in average elastic stiffness for Sample #10, Sample #11, and Sample #12 was 411%, 261%, and 233%, respectively.

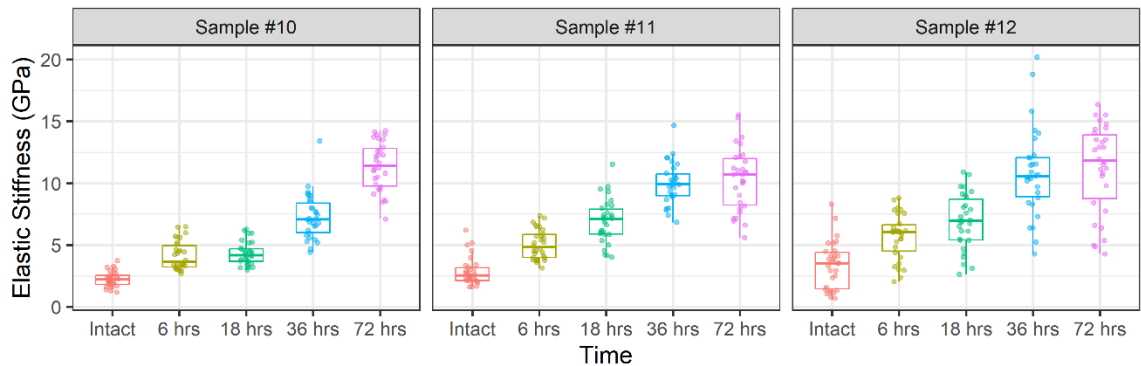


Figure 2-5: Pre- and Post-Elastic Stiffness Distribution Under Increasing Time Treatments.

2.3.3 Catalysis Effect on Stiffness

After undergoing a 6-hour treatment, Samples #13, #14, and #15 displayed an increase in average elastic stiffness. However, no tangible difference was visually observed when comparing the elastic stiffness distributions of the three treated samples with the LNH in the DAP solution to that treated with DAP only (Sample #10), as depicted in **Figure 2-6**. The three samples subjected to treatment with LNH catalysis exhibited an increase in elastic stiffness on average of 84% compared to 61% in the untreated sample.

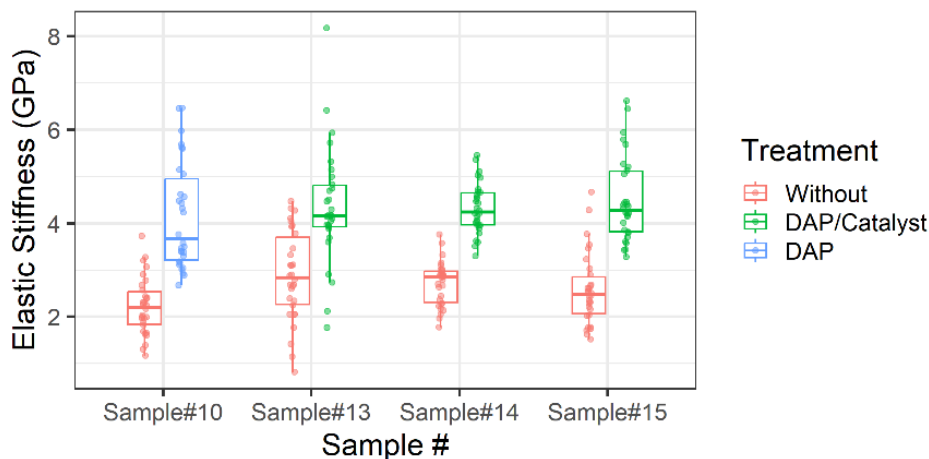


Figure 2-6: Pre- and Post-Elastic Stiffness Distribution for Catalyzed and Uncatalyzed Treatments

Therefore, ANOVA analysis was conducted to validate the results statistically, where the results are arranged in **Table 2-3**. The effect of the treatment is statistically significant and large, but the catalyst effect is significant and small. This finding suggests that the LNH slightly impacted the elastic stiffness properties of the sample. In this case, the result is significant in the sense that it is unlikely to have occurred by chance, but it may be small enough that it is not practically significant.

Table 2-3: Two-way ANOVA Analysis of Temperature and Pressure as Factors.

Factor	Degree of Freedom	Sum sq.	Mean sq.	F value	Pr(>F)	p
Pre/post-elastic stiffness	1	178.9	178.86	238.181	< 2e-16	< .001
Catalyst	1	6.2	6.20	8.258	0.00443	< .001

2.3.4 Determination of Reaction Depth Using XRF

In the XRF analysis, a pseudo-orange color was utilized to denote phosphorous, where the orange hue gradient represents the variation in phosphorous concentration. A brighter color indicates a higher phosphorous concentration, which indicates the presence of HAP and vice versa (see **Figure 2-7a&b**). As a result, the treated sample displayed an increased phosphorous intensity across the surface (**Figure 2-7b**). In addition, a higher intensity of the color was observed along the edges of the sample, indicating a higher phosphorous content.

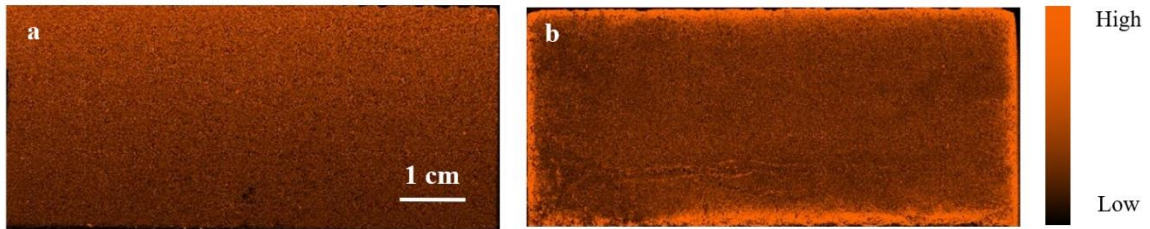


Figure 2-7: Pseudo-colored Images Showing Phosphorous Concentration in a. Untreated, b. Treated Chalk Samples.

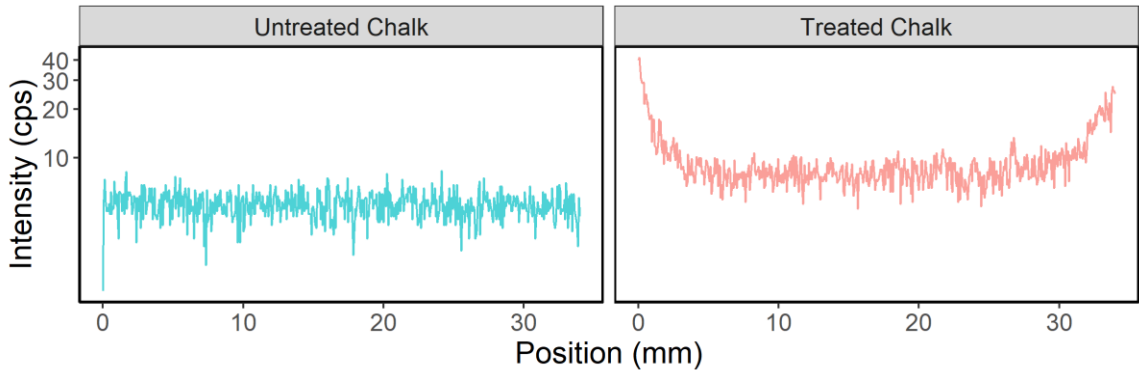


Figure 2-8: Intensity of Phosphorous with Location Across the Untreated and Treated Samples.

Then, the average intensity values were plotted against the position. The treated sample showed higher phosphorous intensity in the interior, with an average value of 8 cps compared to an average value of 5 cps corresponding to the untreated sample. Also, the treated sample showed a noticeable increase in gradient towards the edges, with the effect becoming more pronounced at a distance of 5 mm from the edge, as shown in **Figure 2-8**. The level of phosphorous intensity reaches its peak at the superficial layer when it comes in direct contact with the solution, with values of up to 40 CPS recorded.

2.3.5 Characterization of Mineral Composition Using XRD and EDS

Figure 2-9 presents the XRD spectra of the untreated chalk and the treated chalk powder. Both spectra have been plotted on a single figure to analyze the impact of the DAP treatment on the baseline chalk mineralogy. The spectrum corresponding to the treated chalk displays new peaks at approximately 2θ values of 26, 32, 34, 46, 50, and 53, annotated with black arrows in the plot.

Furthermore, according to the EDS analysis, the virgin sample had a high calcite content, approaching purity with over +99% calcite present. In comparison, the treated samples showed a significant increase in HAP percentage, representing approximately 20% of the extracted sample near the surface.

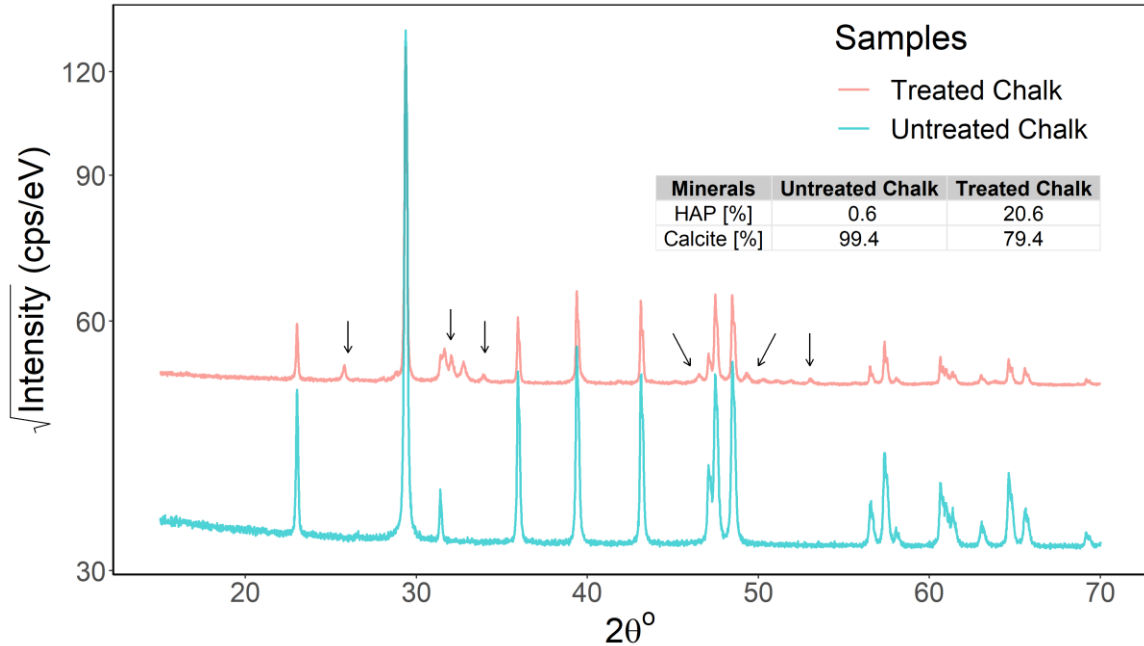


Figure 2-9: XRD Spectra of Powder from Treated and Untreated Chalk Samples.

2.3.6 Morphological Changes Observed with SEM

Initially, a sample of untreated chalk was scanned to represent the unaltered calcite grain structure, as illustrated in **Figure 2-10a**. The scans showed that individual grains are distinct and exhibit differences in size and shape. Next, the treated samples were scanned to visualize the DAP-induced alterations in the calcite. The SEM images revealed the presence of heterogenous morphologies of HAP in shape and size, as shown in **Figure 2-10b-e**. The formed HAP shapes are a few hundred nanometers with various shapes, including needle-like, rod-like, plate-like, and rose-like.

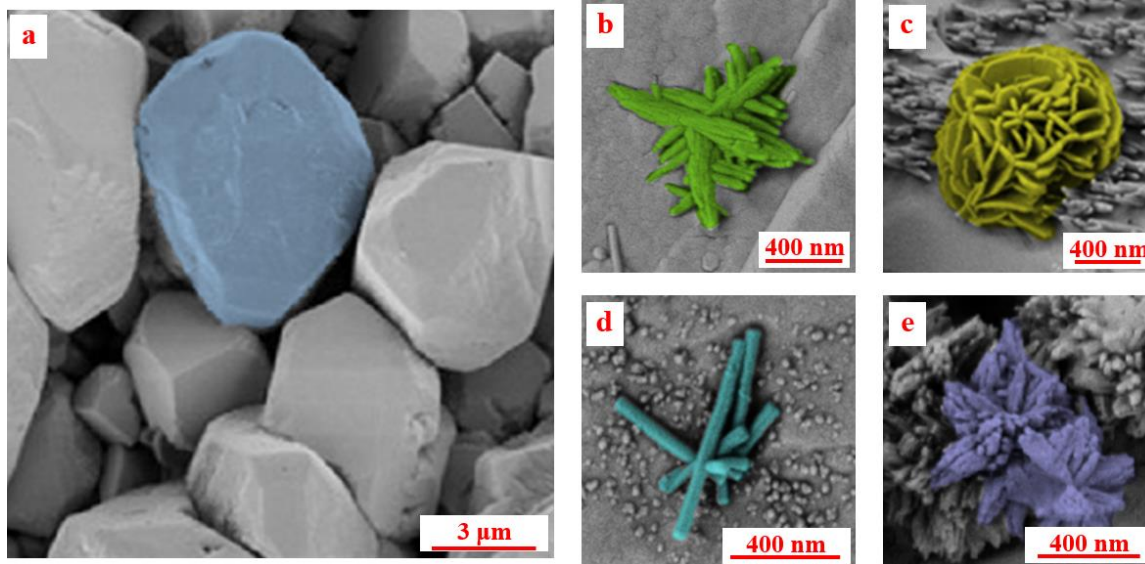


Figure 2-10: Colored SEM Images of a. Intact Separate Calcite Grains, b. Needle-shaped HAP Crystals, c. Rose-shape HAP Crystals, d. Rod-shape HAP Crystals, e. Spikey -shape HAP Crystals.

Figure 2-11a, 11c, and 11e display uncolored SEM images that reveal the host calcite grains and the distinct HAP crystals of various shapes formed under different conditions. In contrast, **Figure 2-11b, 11d, and 11f** show the same SEM images but with pseudo coloring applied to highlight each HAP shape and differentiate them from the host calcite grains. The HAP crystal formations were influenced by variations in the calcite grains' size, shape, and orientation, resulting in different shapes under different pressure and temperature conditions within the same chalk sample. However, certain HAP shapes were more dominant at each pressure and temperature combination. For instance, needle-like, platy hemisphere-like, and sheet-like HAP crystals were observed when chalk reacted with DAP at 2,000 psi and temperatures of 25, 75, and 120 °C, respectively, as depicted in **Figures 11a, 11c, and 11e**. The colored images provide a clear depiction of the formation

of needle-shaped HAP (in green), platy hemisphere-shaped HAP (in yellow), and sheet-shaped HAP (in brown), particularly at the contact points between the calcite grains, which appear faded blue, as shown in **Figures 11b, 11d, and 11f**, respectively. The behavior of the samples treated at 1,000 psi and various temperatures closely resembled those treated at 2,000 psi and different temperatures. The assortment of shapes and the most prominent shapes exhibited remarkable similarity under these conditions. The samples subjected to ambient pressure displayed miscellaneous shapes, with sheets being abundant at 25 °C and needles being prominent at 120 °C. However, the crystals formed under these conditions appeared smaller and more sparsely distributed.

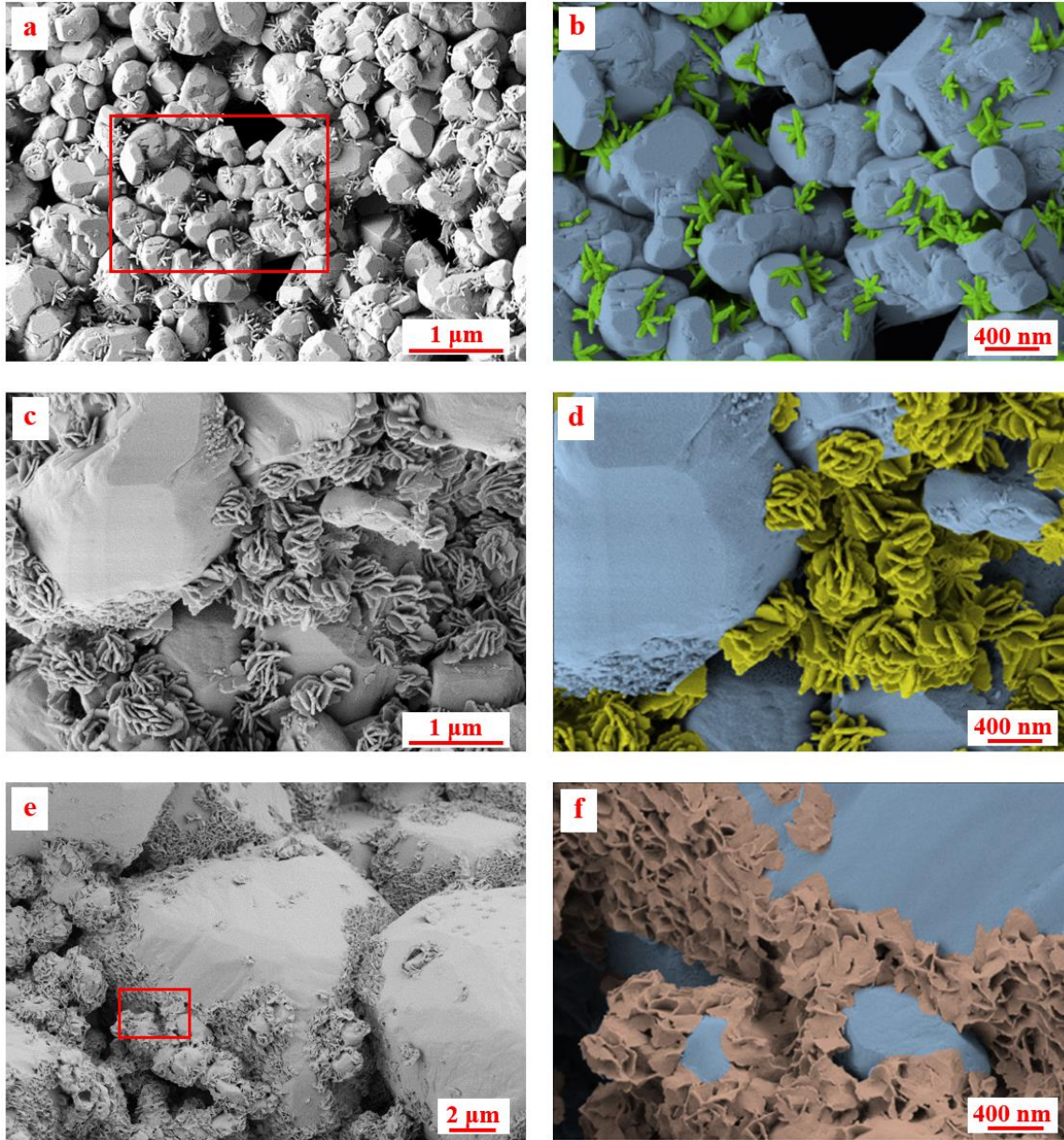
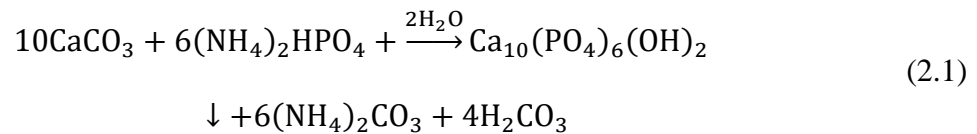


Figure 2-11: SEM Images of a. Treated Chalk Samples at 2,000 psi and 25 °C Showing Calcite and Needle-like HAP, b. Colorized and Closer View of Image 11a, c. Treated Chalk Samples at 2,000 psi and 75 oC, d. Colorized and Closer View of Image 11c, e. Treated Chalk Samples at 2,000 psi and 120 °C, and f. Colorized and Closer View of Image 11e

2.4 Discussion

The effect of pressure on the elastic stiffness of the chalk samples was not as pronounced as that of temperature, suggesting that temperature plays a more significant role in controlling the chalk's reaction kinetics and resulting mechanical properties. Higher temperatures improved the elastic stiffness as it positively affected the DAP-calcite reaction, which was coherent with the literature. As with most chemical reactions, increasing the temperature increases the reaction rate according to the Arrhenius equation (Smith, 2008). On the contrary, there was no clear trend of the elastic stiffness distribution with increasing the pressure from ambient to 2,000 psi.

There were two competing factors justifying the small effect of pressure. First, the DAP-calcite reaction yielded carbonic acid (H_2CO_3), as emphasized in Equation 1.



However, carbonic acid is not a stable compound under normal conditions, and it typically decomposes into carbon dioxide (CO_2) and water (H_2O) through the following reaction:



Therefore, the partial pressure of carbon dioxide (CO_2) can affect the equilibrium position of the decomposition reaction (Darroudi & Searcy, 1981). According to Le Chatelier's principle, increasing the partial pressure of CO_2 shifts the equilibrium of the reaction in the direction that produces more CO_2 . This effect means that at higher CO_2 pressures, the equilibrium will favor the left-hand side of the reaction (the solid CaCO_3)

and inhibit the decomposition of calcite. The effect of CO₂ pressure on the decomposition of calcite is related to the solubility of CO₂ in water. When CO₂ is dissolved in water, it forms carbonic acid (H₂CO₃), which can react with CaCO₃ to form soluble calcium bicarbonate (Ca(HCO₃)₂). This reaction reduces the concentration of carbonate ions (CO₃²⁻) in the solution and slows down calcite decomposition. Therefore, at higher CO₂ pressures, more CO₂ can dissolve in water, leading to a higher concentration of carbonic acid and a slower decomposition rate. Overall, while pressure does not significantly affect the decomposition of calcite, the partial pressure of CO₂ can affect the reaction's equilibrium position and the decomposition rate.

Additionally, this study indicates the critical role of reaction duration in determining the mechanical characteristics of chalk. According to the results, extended reaction times resulted in more pronounced improvements in the elastic stiffness of chalk samples, suggesting that additional time may be required to achieve maximum mechanical performance. Notably, even after 72 hrs. of reaction, the elastic stiffness did not achieve an equilibrium state, implying that more time may yield greater improvement in the elastic stiffness. Interestingly, these observations are consistent with earlier research conducted by (Sassoni et al., 2011), who reported comparable reaction kinetics of Indiana limestone treated with DAP solutions at different concentrations. Specifically, the elastic modulus of dry samples attained maturity after two days in higher concentrations of 1 and 4.4 M, while it took four days in concentrations of 0.1 and 0.5M at room temperature. Therefore, to achieve optimal mechanical outcomes in chalk, careful consideration of the duration of treatment and DAP concentration is essential. Although the utilization of residual effluents from each cycle in the following cycle was implemented, the release of CO₂ gas had a

significant impact on driving the reaction forward, leading to an increased stiffening effect. This finding further reinforces the ongoing discourse surrounding the influence of CO₂ partial pressure. Furthermore, this observation serves as compelling evidence, substantiating the superiority of the cycled treatment, conducted for an identical duration of 72 hrs., in augmenting the stiffening effect on the chalk compared to the continuous treatment.

Furthermore, the conversion of calcium carbonate in the reaction is influenced by factors other than temperature and reaction duration, including the liquid-solid (L/S) ratio, precursor shape, and specific surface area. As per the literature, these parameters play a crucial role in determining the efficiency of the reaction. For instance, (Ashokan et al., 2022)) found that micron size calcium carbonate was consumed within 2 hrs via dissolution precipitation reaction. The process involved adding the calcium carbonate to a solution of DAP, where the Ca/P ratio was kept at 1.67, and the pH was maintained at 10. Compared to calcium carbonate powder, the porous chalk reaction is expected to be slower due to the limited surface area of the former. A larger surface area allows more reactants to come into contact, resulting in a faster reaction.

Therefore, the rate of the DAP-CaCO₃ reaction needs to be optimized to achieve the desired outcome for field applications. The catalytic effect observed in chemical reactions is essentially an alternative to temperature's ability to provide additional energy to reactant molecules; as temperature increases, reactant molecules gain more kinetic energy and collide with greater frequency, leading to increased reaction rates. A catalyst provides an alternative route to products with lower energy demand. This phenomenon is well-documented in the academic literature and explains the relationship between temperature

and reaction kinetics (Eliason & McMahon, 1981). As a result, the reactants form the products more quickly. However, the effect of temperature on the DAP-calcite reaction may also depend on other factors, such as the specific conditions of the reaction and the catalytic agents present.

Since porous media have limited reactivity, introducing a catalyst is another way to increase the reaction rate other than temperature. However, it was revealed that LNH has a statistically minor effect on the treated chalk's elastic stiffness.

The minor effectiveness of LNH on the DAP-calcite reaction can be attributed to various factors. One possible reason is the insufficient concentration of the catalyst, which could result in a suboptimal reaction rate. Specifically, the catalyst concentration of 5 g/L may not be adequate to accelerate the reaction effectively.

The XRF findings suggest that HAP was precipitated throughout the sample due to its permeability, allowing the DAP solution to permeate inside. Additionally, the concentration of the precipitated HAP followed a gradient pattern. The concentration of HAP was initially highest at the sample's surface and progressively decreased towards the interior, eventually reaching a constant value beyond a distance of 5 mm from the surface. The concentration gradient can be attributed to the larger volume of solution in direct contact with the edges and the ease of the reaction at the edges compared to the pores spaces. These results shed light on the behavior of HAP in porous samples and highlighted the importance of considering permeability in such studies. The results agree with the study by Possenti et al. (2020), who utilized Synchrotron radiation μ X-ray diffraction to find the depth of treatment. Their results show that the DAP consolidating treatment causes a

noteworthy crystallization of Ca and P-bearing compounds several millimeters from the treated limestone surface. Another study by Osticioli et al. (2017) investigated the extent of penetration of ammonium oxalate and DAP on tablets of pure CaCO_3 and degraded marble samples. The results of the micro-Raman analysis show that a homogeneous distribution of whewellite inside the substrates down to a depth of ~1 mm was detected, which became larger in highly degraded regions of the marble substrate. In addition, calcium phosphates in HAP were detected at greater depth (down to 2.5 mm), confirming better consolidating properties of DAP with respect to ammonium oxalate. Anfosso et al. (2023) reported successful treatment in improving the 'stones' strength up to a depth of 1 mm despite the low DAP concentration. They found that the treated Lecce Stone absorbed less water than untreated ones, and their abrasion resistance was twice as much as the untreated samples up to a depth of 1 mm. However, the abrasion resistance remained constant below a depth of 1 mm, similar to the untreated specimens.

The peaks observed for HAP at XRD results are consistent with the characteristic peaks of stoichiometric HAP concerning JCPDS file no. 9-432. The XRD findings are consistent with previous studies in the literature (Chen & Shen, 2020). After analyzing the mineral composition, it was determined that the powder obtained from the near surface of the treated sample contains 20.6% of HAP. However, it should be noted that the amount of HAP formed varies depending on the location where the powder was extracted from the sample. Also, the XRD finding is consistent with the concentration gradient observed from the XRF analysis. The XRF results indicate that the near-surface has a higher concentration of phosphorous and, consequently, HAP. As a result, the quantification only reflects the relative mineralogy amounts of the extracted piece and not the entire sample.

The different observed HAP shapes were reported in the literature. For instance, Samarkin et al. (2023) conducted a study where they observed the formation of rod-shaped crystals at a temperature of 80 °C. However, in the current study, when pressure was applied, a mixture of needles and rod-like structures was observed at a slightly lower temperature of 75 °C. This finding indicates that pressure might play a role in determining the type of crystals formed. Furthermore, the abundance of minerals formed in this study was lower than in their experiments conducted under normal atmospheric pressure. The observation supports the notion that applying pressure has a negative impact on crystal formation. Additionally, Lin et al. (2014) provided an overview of the latest techniques used to produce calcium phosphate crystals (including HAP) with controlled sizes ranging from nano- to macroscale, as well as varying shapes such as zero-dimensional particles and spheres, one-dimensional rods, fibers, wires, and whiskers, two-dimensional sheets, disks, plates, belts, ribbons, and flakes, and three-dimensional structures.

The reaction conditions, such as temperature, pressure, and reaction duration, can also significantly influence the formation of HAP crystals with different morphologies. For example, a high reaction temperature can lead to the formation of larger HAP crystals. In comparison, a lower temperature can lead to the formation of smaller HAP crystals with different morphologies (Kim & Ohtsuki, 2016). On top of that, the micro-heterogeneity of the chalk samples is expected to promote the variation in newly formed minerals. Contrary to the case of using a precursor, it was feasible to control the shape of the HAP crystals generated under hydrothermal conditions by selecting starting materials that raise the level of supersaturation in the solution (Goto et al., 2012) or selecting the calcite growth plane (Kim et al., 2012). Moreover, Neira et al. (2009) achieved the desired morphology of

the HAP crystals by precisely controlling the decomposition rate of urea and the initial component concentration during the hydrothermal process.

In addition, the shape of the crystal can affect its mechanical strength (Dubey & Tomar, 2009). For example, plate-shaped crystals are generally stronger in compression than needle-shaped crystals, which are stronger in tension. This difference in mechanical strength can affect the overall mechanical properties of the material in which the crystals are embedded, as illustrated in **Figure 2-3**.

2.5 Conclusion

The study explored the use of diammonium phosphate (DAP) as a consolidation agent to improve the strength of weak carbonates for hydraulic fracturing applications. First, the study investigates the effects of pressure, temperature, reaction duration, and catalyst addition on the DAP-calcite reaction and hydroxyapatite (HAP) formation. The experiments showed that temperature and reaction duration are the most critical factors affecting the DAP-calcite reaction, while the pressure effect is minor. Also, the study used XRF to investigate the consolidating phases' crystal chemistry and penetration depth after treating a porous carbonate stone (Austin Chalk) with DAP. According to the investigations, the formation of HAP was consistent throughout the entire sample, and its concentration was found to increase in the last 5 mm towards the surface. The study yields valuable insight into the newly formed HAP at different depths, shedding light on the diffusion mechanism and reactivity of the substrate. The study's findings suggest that DAP is a reliable agent for consolidating weak carbonates and is promising for improving hydraulic fracture conductivity at reservoir conditions. The results can help optimize

hydraulic fracturing operations in weak carbonate reservoirs, improving production rates and overall well performance.

CHAPTER 3

ENHANCING FRACTURE CONDUCTIVITY IN SOFT

CHALK FORMATIONS WITH DIAMMONIUM

PHOSPHATE TREATMENT: A POTENTIAL

SOLUTION FOR LONG-TERM PERFORMANCE

Abstract

This study aims to address the problem of soft carbonate fracture hydraulic conductivity decline in innately fragile formations or after acid-fracturing stimulation by chemically stiffening the rock surface using a diammonium hydrogen phosphate (DAP) solution. A naturally weak carbonate, Austin chalk was chosen as an ideal specimen. Flat chalk samples reduced elastic modulus (E^*) and roughness were evaluated before and after aging with 1M DAP for 72 hrs. at 75°C and 1000 psi. The fracture gas conductivity of DAP-aged and untreated samples was measured at various flow rates and stresses while recording sample compaction using linear variable differential transformers (LVDTs). The study found that DAP aging increased the E^* of chalk specimens up to 330% of the original value, improving their resistance to deformation and failure under stress by 200 psi. The hydraulic conductivity of DAP-aged samples was at least twice that of untreated samples, with an extended hydraulic fracture conductivity seven times higher than that of the untreated ones.

Scanning electron microscopy (SEM) and dispersive X-ray spectroscopy (EDS) analysis revealed that DAP reacted with the chalk to form hydroxyapatite (HAP), which binds the calcite grains, yielding a stiffer, more deformation-resisting rock surface. Overall, the study demonstrates the potential of chemically enhancing and extending the fracture hydraulic conductivity of weak carbonates using DAP.

Keywords: Hydraulic Fracturing, Hydraulic Conductivity, Chalk, DAP Treatment, Consolidation

3.1 Introduction

Significant hydrocarbon volumes contained in carbonate reservoirs are frequently produced by acid fracturing, which boosts productivity (Kalfayan, 2007). Acid fracturing stimulation is utilized to either bypass near-wellbore damage or increase the well contact area with the formation (William et al., 1979). It entails pumping acid with enough pressure to break down the formation (Schechter, 1991). Then, the acid etches the fracture surfaces unevenly, where the etched fracture length depends on the acid's leak-off and reaction rates (Muecke, 1982).

Acid-fracture conductivity measures the fracture capacity to deliver fluids and depends on several factors related to the rock, acidization conditions, and closure stress (Malagon et al., 2008). For example, factors pertaining to the rock include the dissolution pattern and the rock's mechanical properties after the acid fracturing (Pournik et al., 2010). Rock can be assessed mechanically in various ways. The rock embedment strength representing the surface resistance to deformation under localized loads is plausible in hydraulic fracturing applications. For instance, in the absence of acid-developed channels, (Nierode & Kruk, 1973) showed experimentally by Eq. 1 that weak carbonate hydraulic conductivity ($k_f w_f$)

declines exponentially with the closure stress (σ_c) while it increases with the rock embedment strength (S_{RE}). Furthermore, for any rock type, the conductivity drop rate with closure stress mostly depends on the rock's strength (Gomaa & Nasr-El-Din, 2009; Pournik et al., 2009).

$$k_f w_i = C_1 e^{-C_2 \sigma_c} \quad (3.1)$$

$$C_2 \times 10^3 = 13.9 - 1.3 \ln(S_{RE}) \quad (3.2)$$

where the fracture permeability is denoted by k_f , w_i represents the ideal width of the fracture, C_1 is a constant that signifies the fracture conductivity when stress is zero, where C_2 is another constant that indicates the conductivity decline rate with the closure stress.

Although acid's role in developing rough fracture surfaces is vital, it has a detrimental effect on the rock's mechanical properties (Gong et al., 1999). Nugroho et al. (2022) found that when 15% HCl was added to carbonate samples, the calcite amount was reduced by about 25% from the overall calcite content. Therefore, the higher acid concentration is not always favorable as it could cause excessive etching, leading to a very limited flow capacity (Zhang et al., 2020). Also, Melendez et al. (2007) found that the fracture conductivity is less when acid reduces the rock embedment strength. Moreover, prolonged acid contact with the rock may weaken it, reducing its hydraulic conductivity (Beg et al., 1998; Asadollahpour et al., 2018). Naturally, chalk is soft; therefore, the acid softening is more severe, causing a greater conductivity fall with closure stress (Tariq et al., 2021). Furthermore, increased leakage rates into the rocks also lead to greater strength reduction (Nasr-el-din et al., 2006).

Many approaches were developed to optimize the acid fracture job or mitigate the acid carbonate-destructive effects by manipulating the acid properties or the acidification process. For example, thickening the acid to control the amount of acid leaked into the carbonate yielded higher final conductivity (Almomen et al., 2014; Mehrjoo et al., 2022). Also, emulsified acids with low fluid loss produce lengthy fractures with finite fracture conductivities, which can be advantageous in wells with low closure stress or low permeability (Novotny, 1977). However, the rock was weakened by higher emulsified acid volume fractions, which led to a faster loss of conductivity in the fracture at high closure pressures (Al-Mutairi et al., 2008). Foamed acid is another acid type proposed due to its high viscosity, low fluid loss, and strong fracture-forming ability (Li et al., 2015). In addition, closed fracture acidizing was practiced to promote the development of high-stress enduring channels (Fredrickson, 1986).

The surface texture dominates hydraulic conductivity at low stress, but rock strength becomes more important with higher stress. Therefore, Aljawad et al. (2020) suggested improving the carbonate's mechanical properties to extend the fracture conductivity endurance. Samarkin et al. (2022) comprehensively reviewed the various methods for enhancing the strength of the rocks and their uses in the petroleum industry. For example, precipitating diverse calcium carbonate polymorphs (López-Arce et al., 2010), calcium hydroxide nanoparticles (Ossola et al., 2012), or calcium alkoxides (Erşan et al., 2020) improves the rock's mechanical properties. Furthermore, DAP increased the elastic modulus of limestone by up to 90% (Sassoni et al., 2011), dynamic Young's modulus by 461% (Murru & Fort, 2020), and ultrasonic pulse velocity by up to 540% (Sassoni et al., 2016; Sena da Fonseca et al., 2021) through HAP formation. Finally, Desouky et al. (2021)

simulated the beneficial impact of improving carbonate mechanical characteristics on improving hydraulic fracture conductivity.

Acid etching and consolidation agents can alter the carbonate's mechanical properties. This alteration of carbonate mechanical properties reflects on its deformation when stressed. In this context, the improved carbonate surface stiffness will reduce the carbonate strain, making long-lasting fracture conductivity. Therefore, this study looked at the impact of DAP as a stiffening agent for soft chalk specimens with different stiffness at reservoir conditions. The E^* measurement was analyzed rigorously from a statistical point of view. In all experiments, the flatness of the samples was ensured to track the treatment impact on the hydraulic conductivity. Also, the effect of stiffening on flat fracture hydraulic conductivity was examined in the short run and over extended periods. Finally, the compaction of treated and untreated samples was compared. This study is the first of its kind to prove the concept of improving hydraulic fracture conductivity through rock stiffening using the standard API conductivity cell.

3.2 Experimental Design

In this study, several laboratory tests were executed to determine the effectiveness of chalk stiffening using DAP on generating lasting fracture hydraulic conductivity in flat Austin chalk specimens. Chalk is a typical carbonate rock in its inherent heterogeneity. In this study, we conducted experiments on samples based on both randomization and direct assignment. The chalk samples are first split into two groups: the treatment group and the control group. Then, while the control group was kept intact, the treatment samples were treated with DAP under predefined conditions. After the DAP treatment, the remaining

experiments for both groups were the same. **Figure 3-1** gives a holistic view of the experimental work, which will be discussed in more detail in the following sections.

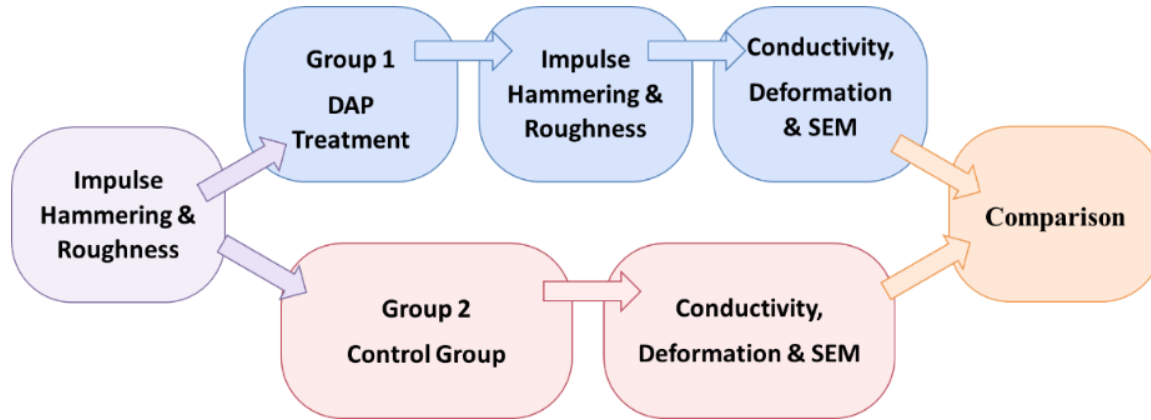


Figure 3-1: Flow chart of the experimental work.

3.2.1 Materials

Because Austin chalk is a weak carbonate and reacts with the DAP, it was chosen for this study. Austin chalk is also naturally weaker than other carbonates, making stiffening by the chemical treatment noticeable. Slabs of 3.40 cm x 7.62 cm x 17.78 cm were employed for the experimental analyses, which were visually inspected to choose those with as few vugs and fractures as possible. Moreover, they were selected flat to minimize the impact of roughness. Proving the concept with rough samples is challenging as it will be difficult to conclude if conductivity improvement was due to stiffening or roughness. DAP was chosen as the consolidation agent in this study with a 1M concentration. It is prepared by dissolving 132.06 g of the DAP salt in 1 L of deionized water.

3.2.2 Instruments and Procedure

As the fracture features highly impact the hydraulic conductivity, the fracture surface of each chalk slab is scanned with the surface roughness analyzer (SRA) to get the roughness

distribution. The texture of the sample surface is captured by a precise profilometer utilizing the confocal microscopy technique. By stacking 2D images, each with a minute depth of focus, achieving a height resolution of a few micrometers is possible. A non-destructive mechanical assessment of the rock slabs is essential for the samples to be further analyzed. Therefore, AutoScan was adopted for rock mechanical properties evaluation. It employs impulse hammering to map non-destructively the variability in mechanical properties like E^* . Eq. 3 defines the reduced elastic modulus, which exhibits a strong correlation with the unconfined compressive strength (UCS) as determined by scratch testing (Gramin et al., 2016). In addition, mechanical properties derived from the AutoScan significantly correlated with those of the conventional triaxial test (Hussain et al., 2019). AutoScan is easy, affordable, and quick in characterizing the rock's elastic property, enabling repeated measurement after some mechanical properties-changing intervention.

$$E^* = \frac{E}{(1 - \nu^2)} \quad (3.3)$$

where E is the sample elastic modulus, and ν is the sample Poisson's ratio.

In each conductivity experiment, the two samples representing the treatment group are treated with the 1M DAP solution for 72 hrs in a cell pressurized to 1,000 psi and put in an oven at 75 °C. The DAP treatment was done in an aging cell composed of steel with a capacity of 3 liters. The samples are vacuumed, saturated, and aged in the cell for a specific time.

Visualization of the changes at the microscale provides important insights into how the DAP works. Therefore, the scanning electron microscope (SEM) was employed to acquire images at different magnifications. Small 1 cm cubes of untreated and treated chalk were prepared for the SEM imaging. The SEM used in this study is the Gemini 450 SEM. The device combines the capacity for advanced analytics as EDS with ultrahigh-resolution images.

The ACM-3000 acid fracture conductivity system was used to evaluate the fracture conductivity. The system's basic components are illustrated in **Figure 3-2**. It has a hast alloy cell, top piston, bottom piston, jack, LVDTs, mass flow controller, back pressure regulator, nitrogen gas source, and pressure gauges connected to the data acquisition system. The Hastelloy cell accommodates the samples and allows gas flow through the fracture at different stresses. The stresses are applied in the loading frame by the jack, where the jack's force is transmitted and distributed by the top piston. Also, the top piston movement due to sample deformation under stress is monitored by the LVTDs mounted on them.

Furthermore, specific nitrogen flow is allowed by the mass flow controller, providing an adequate nitrogen gas flow. Finally, applying back pressure by the back-pressure regulator keeps a constant pressure in the flow path. Therefore, the pressure values can be gauged, and conductivity can be evaluated by Eq. 4 (Wang, 2015).

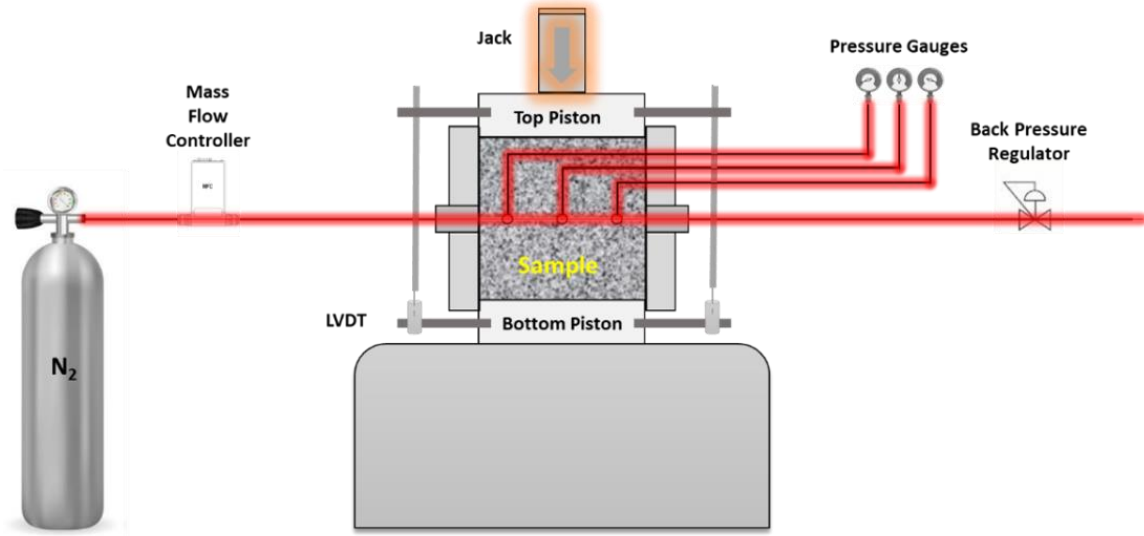


Figure 3-2: A schematic for the fracture conductivity apparatus.

$$\frac{p_{\text{cell}} \Delta p M}{ZRTL} = \frac{1}{k_f w_f} \frac{q \rho \mu}{h_f} \quad (3.4)$$

where M is molecular nitrogen mass, Z is the compressibility factor, which equals 1 in the standard conditions, R is the universal gas constant, T is the room temperature, L is the distance between pressure ports, q is the nitrogen flow rate, ρ is the nitrogen density, μ is the nitrogen viscosity in room temperature, h_f is the length between pressure ports 1 and 3.

The pressure measured at the first port is p_1 , while p_2 is at the third port.

$$p_{\text{cell}} = \frac{p_1 + p_2}{2} \quad (3.5)$$

$$\Delta p = p_1 - p_2 \quad (3.6)$$

The conductivity k_{fwf} is evaluated by changing the flow rate q and finding the reciprocal of the slope when $\frac{p_{cell} \Delta p_M}{ZRTL}$ is plotted versus $\frac{q\rho\mu}{h_f}$. Typically, the conductivity is calculated by measuring p_1 and p_2 at four different flow rates.

Sample preparation for conductivity measurement is crucial for the success of the experiment. To artificially mimic the fracture whose conductivity will be measured, two sister chalk slabs (**Figure 3-3a**) are put on top of each other (**Figure 3-3b**). After that, the two slabs are attached by aluminum tape to prevent silicon from leaking between them. Meanwhile, white and black liquid silicon is mixed in a 1:1 weight ratio. Then, the attached slabs are put inside a steel mold, pouring the silicon mixture around the slabs to form a sealing layer. The attached slabs are left in the mold for 24 hrs. for the silicon to polymerize, as shown in **Figure 3-4c**. After removing the sample from the mold, a steel tool is used to make three punctures along the fracture, where the pressure will be measured (**Figure 3-3d**). Two holes are made at both ends to allow the gas in and out of the fracture. The fracture aperture is shown in **Figure 3-3e**.

After sample preparation, the sample sides and the cell's inner wall are lubricated with grease to ease the insertion of the sample into the cell. A hydraulic jack forces the sample into the cell until the holes align with the gas inlet, gas outlet, and pressure tabs openings. The top and bottom pistons are placed above and below the sample to transmit loads from the jack. The gas inlet is attached to the nitrogen gas source while the outlet is attached to the back pressure, which keeps constant pressure during gas flow. In this work, the mass flow controller maintains specific gas rates of 200 cc/min to 350 cc/min. Next, four linear variable differential transformers (LVDTs) supports are screwed into the upper and lower

pistons. Then, LVDTs are attached to the supports to measure the deformation occurring with the stress applied by the top jack.

The conductivity of the fracture is evaluated at different stresses, increased incrementally by 100 psi up to 1,500 psi. Nitrogen gas is flown at each stress, and pressure sensors record the stabilized pressures.

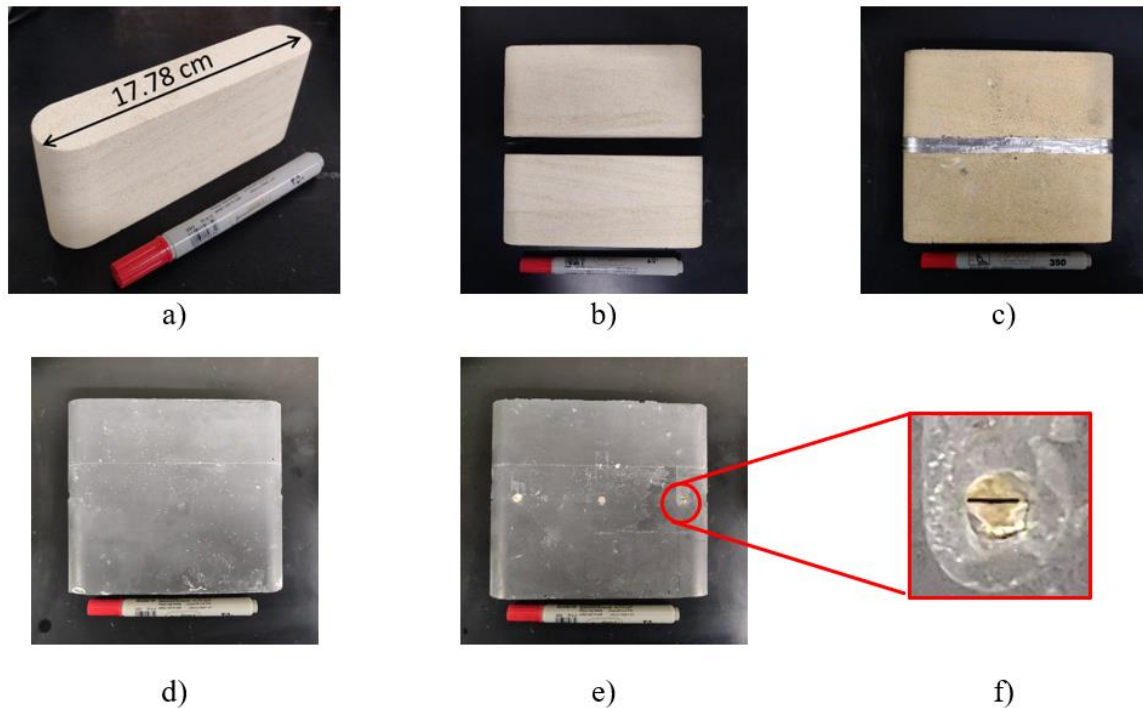


Figure 3-3: Sample preparation for the conductivity experiment.

3.2.3 Statistical Analysis

Chalk pre-/post-treatment E^* measurements and the baseline E^* were examined using analysis of variance (ANOVA) to assess their individual and combined effects on chalk E^* improvement. First, one-way ANOVA was utilized to check the hypotheses: (1) there is no change in chalk E^* after the treatment with DAP. (2) the chalk baseline E^* does not affect

the E* improvement. Furthermore, a two-way ANOVA test was carried out to examine the hypothesis: There is no interaction between factors pre/post-E* and baseline E*. The ANOVA test assumes that observations of each factor are normally distributed, independent, and have equal variances. The assumptions were verified and relaxed if needed. In addition, Tukey's post-hoc test was applied for pairwise comparisons when ANOVA demonstrated significant differences. The R language (version 4.1.0; R Core Team 2022) was used to conduct the statistical analyses within the RStudio environment (version 2022.7.1.554; RStudio Team 2022).

3.3 Results and Discussion

3.3.1 Samples Characterization

Fully controlled experiments on the rocks are almost impossible. However, confounding factors that impact hydraulic conductivity were minimized to the lowest possible level. One major confounding factor is the roughness of the sample surface. Therefore, the hydraulic conductivity experiments were based on well-finished flat Austin chalk samples. Even though the samples appear flat, they are rough at the microscale. Thus, high-resolution surface roughness was acquired using an extremely sensitive profilometer. The profilometer recorded around 1×10^8 data points from the sample surface and considered the mean plane as a reference.

The SRA results revealed that the roughness of the samples used in this study fluctuated around 0.2 mm. Additionally, the root-mean-square height and arithmetic mean height were measured following ISO 25178, yielding values of 0.07 mm and 0.04 mm, respectively. Therefore, the contribution of the roughness to the hydraulic conductivity is

minimal, which is preferred. The similar and low roughness values were intended to assume that the hydraulic conductivity of the fracture is a function of E^* exclusively.

For example, in the first experiment, most surface asperities for all samples fall in ± 0.1 mm from the mean plane, as arranged in **Table 3-1**. Moreover, **Figure 3-4** shows the surface texture and profiles of the surface along both axes for one of the samples used in the second experiment. Also, the roughness was evaluated a second time for the samples subjected to the DAP treatment to assess how the treatment affected the surface roughness. The post-treatment roughness was highly similar to the one before the treatment, suggesting that the treatment did not change the surface roughness significantly. Similar observations from the rest of the treated samples confirmed that the DAP reaction did not significantly affect surface roughness.

Table 3-1: Summary of the roughness measurements in mm for the samples used in Experiment #2.

Sample	3C	4C	3T (before)	3T (after)	4T (before)	4T (after)
5 th percentile (mm)	-0.092	-0.103	-0.123	-0.096	-0.106	-0.084
95 th percentile (mm)	0.079	0.093	0.105	0.08	0.089	0.072
5 th -95 th percentile range (mm)	0.171	0.196	0.235	0.175	0.195	0.156

C: Control, T: Treatment

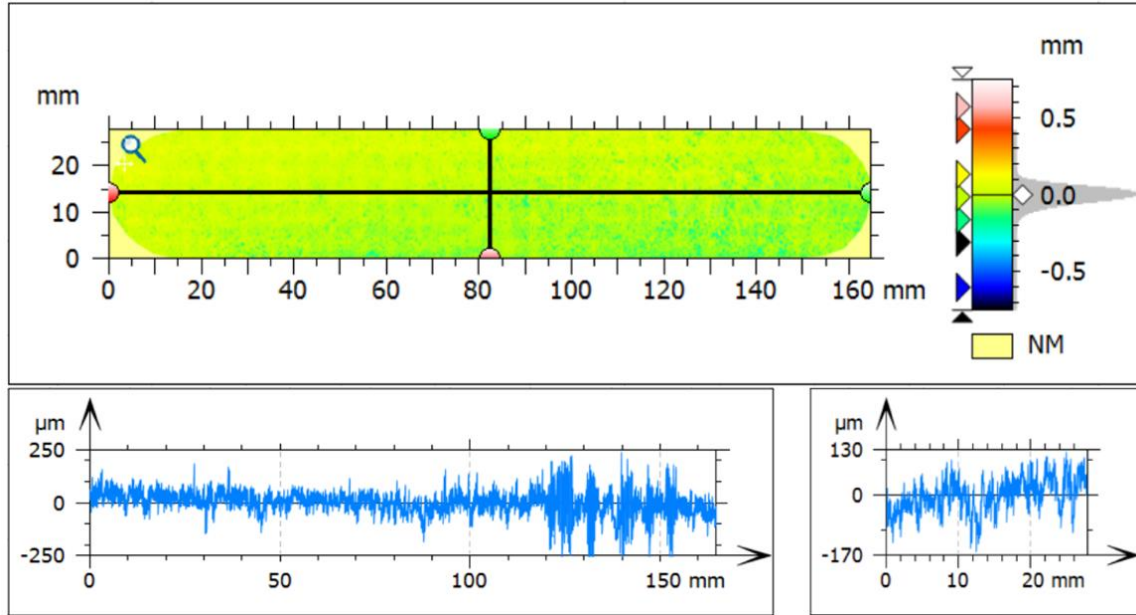


Figure 3-4: Example of surface roughness measurement and profiles along the long and short sides of 3C.

In order to quantify E^* of each sample, the AutoScan was employed to measure E^* on a grid of 30 points, as illustrated in **Figure 3-5**. Collecting numerous values from each sample is mandatory when porous and composite rock as chalk is involved.



Figure 3-5: The chalk sample surface shows E^* measurement grid.

Even though the samples in this study are from the same batch, they exhibit a wide variation in mechanical properties. As measured by AutoScan, E^* demonstrates this variation.

Furthermore, the E^* varies greatly, even within the same sample. Therefore, the variation in E^* was projected to cause variation in the measured hydraulic conductivity, and the effect of the chemical treatment on conductivity, in this case, would be obscured. Therefore, the obtained AutoScan measurements play two vital roles in the mechanical assessment of the chalk samples. First, it gives E^* distribution for each sample. Second, the chalk samples would be grouped according to these values. The collected data from each sample were averaged for a single-point estimate, and the standard deviation was also calculated. Finally, E^* means and standard deviations for all samples were plotted against each other to visualize similar samples. As a result, most chalk samples fit in two compacted clusters, and the rest are sparse over a wide range, as depicted in **Figure 6**. Therefore, four samples were randomly chosen from each compacted cluster to comprise control and treatment groups for each comparative hydraulic conductivity experiment. In one of the experiments, we randomly selected the samples regardless of the clustering or their initial E^* before the hydraulic conductivity experiment.

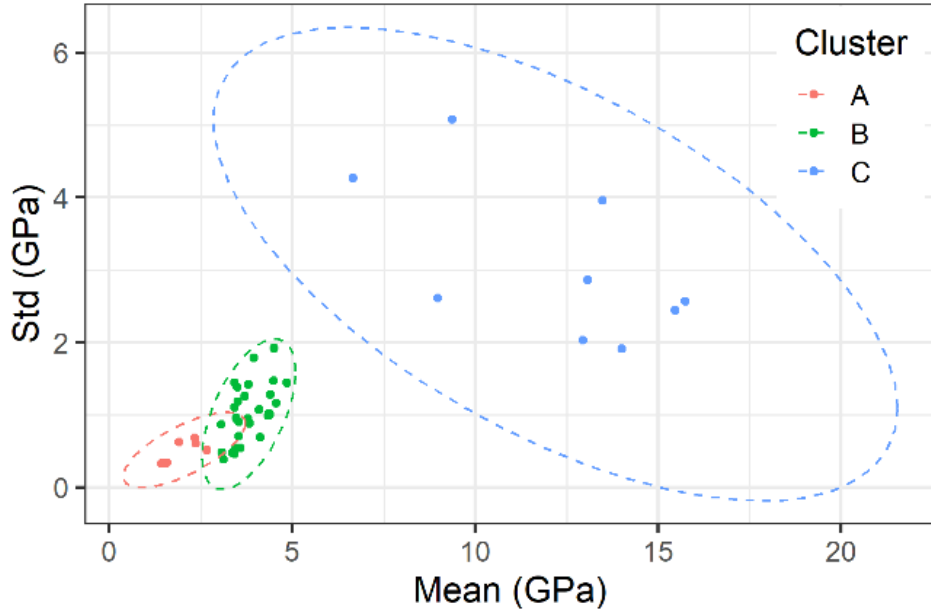
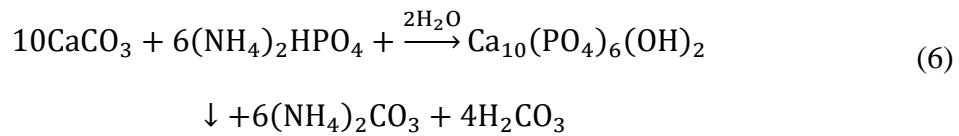


Figure 3-6: Clustering of heterogeneous chalk samples by measuring E^* .

3.3.2 Chemical Treatment and E^* Improvement

This work aims to treat weak chalk samples with DAP to increase their fracture hydraulic conductivity. The chalk can better withstand deformation from localized loads by creating stronger minerals close to the chalk's surface because of the DAP reaction (Samarkin et al., 2023). Equation 1 also shows that a substitution reaction transforms calcite from chalk into HAP (Roy & Linnehan, 1974).



Hence, compared to untreated samples, stiffened chalk samples should have higher hydraulic conductivity values under higher stress.

The first experiment was based on randomly selecting four chalk samples for the control and treatment groups. Later, the DAP solution was applied to two samples. The randomized

experiment is more realistic as it resembles the field condition with no control in the downhole rocks. However, interpreting the results is challenging due to confounding factors, i.e., E^* . For example, the E^* could vary and cover values as low as 1 GPa or as high as 22.5 GPa, as shown in **Figure 3-6**.

For more solid conclusions about DAP treatment on hydraulic conductivity, E^* of the treatment and control groups was comparable in subsequent experiments. All the chalk samples used in Experiment 2 had an average E^* value of approximately 3.42 GPa. **Figure 3-7** shows that the DAP treatment significantly increased the average E^* of the treatment samples in Experiment 2 to 7.41 and 9.53 GPa for 3T and 4T, respectively. This is an increase of 117% for 3T and 177% for 4T. It is important to note that despite having the same initial E^* values and being aged under the same conditions, the treated samples did not show the same E^* improvement. This discrepancy can be attributed to the chalk's heterogeneity. Due to the inherited heterogeneity in the chalk samples, this dispersion is conceivable.

Another experiment was conducted on relatively softer chalk samples than in the previous experiment. The initial average E^* of the samples was around 2 GPa, shown in Figure 3-7 under Experiment 3. The average E^* values of samples 5T and 6T improved significantly with the DAP treatment. Sample 5T average E^* increased from 2.36 GPa to 7.47 GPa, while sample 6T average E^* increased from 1.57 GPa to 6.77 GPa. The DAP treatment raised the average values of samples 5T and 6T by 217% and 331%, respectively. The increase in the case of weaker chalk is higher and more pronounced compared to the previous experiment.

In Experiment 4, the selected samples' E^* was comparable with an average value of 4.4 GPa. However, the post-treatment average E^* was greatly enhanced by 102% for sample 7T and 121% for sample 8T, as shown in **Figure 3-7**.

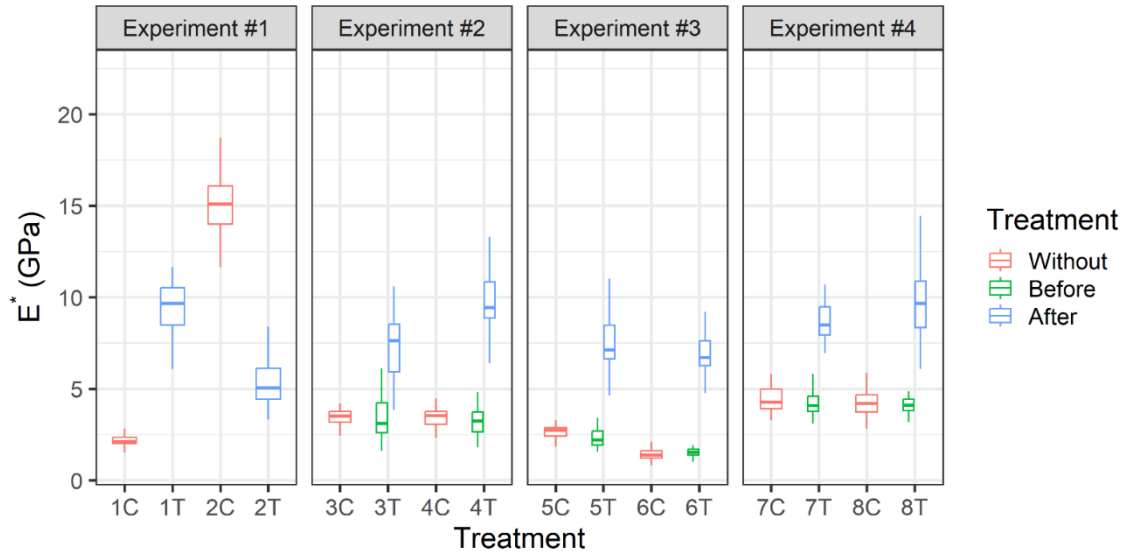


Figure 3-7: Distribution of E^* measurements.

The results of AutoScan's evaluation of all samples' pre-and post-treatment E^* are arranged in **Table 3-2**. For Experiments 1,2 and 3, the short-term hydraulic conductivity was measured, while the long-term hydraulic conductivity was measured in Experiment 4.

Table 3-2: Statistical Summary of E*.

Experiment	Duration	Statistic	Group					
			Control (GPa)		Treatment (GPa)			
1 (Random)	Short		1C	2C	1T		2T	
		$\mu \pm \sigma$	2.3±0.6	15.4±2.44	9.32±1.57		5.29±1.23	
2 (Controlled)	Short		3C	4C	3T Before	3T After	4T Before	4T After
		$\mu \pm \sigma$	3.4±0.5	3.43±0.52	3.42±1.44	7.41±1.81	3.42±1.01	9.53±1.92
3 (Controlled)	Short		5C	6C	5T Before	5T After	6 T Before	6T After
		$\mu \pm \sigma$	2.7±0.5	1.42±0.33	2.36±0.61	7.47±1.51	1.57±0.34	6.77±1.31
4 (Controlled)	Long		7C	8C	7T Before	7T After	8T Before	8T After
		$\mu \pm \sigma$	4.6±1.2	4.33±0.99	4.38±1.01	8.86±1.52	4.37±1.02	9.66±1.78

C: Control, T: Treatment

From the results shown in the table, all treated samples in controlled experiments had an increase in E*. Also, it should be noted that the treatment yields more detectable outcomes when applied to rocks with a lower initial E* coherent with what has been previously described in the literature. For example, Samarkin et al. (2023) reported a notable improvement in chalk E*, especially the weaker ones after DAP treatment.

3.3.3 Statistical Analysis

Experiment 2 has an intermediate baseline E* between the relatively lower baseline E* in Experiment 3 and the relatively higher baseline E* in Experiment 4. The one-way ANOVA

provided evidence that different experiments (each has a different baseline E^*) are likely not equal and statistically significant. Also, the pre/post- E^* factor is statistically significant ($p < .001$). Similarly, the two-way ANOVA showed the statistical significance of both factors, i.e., experiment and pre/post- E^* . However, there is not enough evidence to show these two factors' interaction is significant, as arranged in **Table 3-3**.

Table 3-3: Summary of Two-way ANOVA Analysis.

Parameters	DF	Sum Sq	Mean Sq	F value	Pr(>F)	Significance
Experiment	2	315.2	157.6	75.510	2E-16	0
Pre/ post- E^*	1	2276.5	2276.5	1090.553	2E-16	0
Experiment: Pre/ post- E^*	2	1.2	0.6	0.275	0.759	1
Residuals	354	739.0	2.1			

After showing that there is no statistical significance of the different improvements in E^* from one experiment to another with the DAP treatment, there is no need to perform the Tukey post-hoc test. Therefore, enough evidence does not exist to support that Experiments 1, 2, and 3 have different mean improvements. Furthermore, although the improvement in percentage looks different, the increment in absolute mean E^* values statistically does not look different. Thus, no evidence going from a relatively high baseline E^* to a relatively low one results in more E^* improvement increment.

3.3.4 Hydraulic Conductivity and Deformation

In Experiment 1, across the stress range, the measured hydraulic conductivity of the treated samples is much higher than that of the control group. Additionally, as the stress levels increased, the hydraulic conductivity declined more gently in the treated sample. Moreover, the difference in hydraulic conductivity grew larger with the stress, as appears in **Figure 3-8**. The final hydraulic conductivity of the treated samples is roughly 100 mD.ft, which is one order of magnitude higher than the untreated samples.

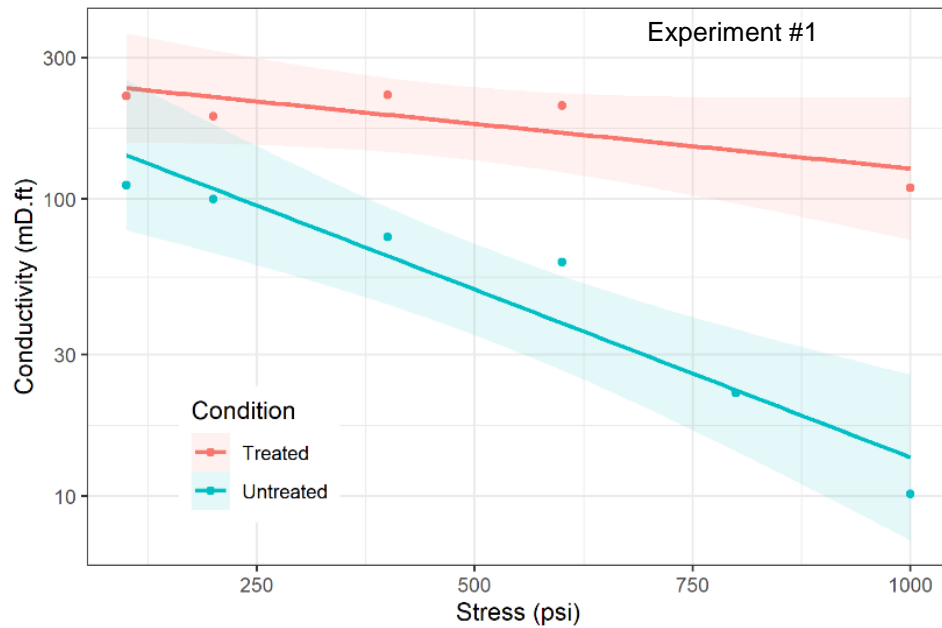


Figure 3-8: Treated and Untreated Hydraulic Conductivity Comparison of Experiment 1.

The difference in conductivity detected in the first experiment might be attributed to the variation observed in the chalk E^* because of the significant fluctuation in the chalk E^* observed in the first experiment. Therefore, the controlled experiments were conducted in the subsequent experiments to determine the causation between the chemical treatment and

the higher hydraulic conductivity. For example, the samples grouped previously based on the E^* would make a fair comparison as their initial stiffness is almost the same.

In Experiments 2 and 3, the hydraulic conductivity of different treated and untreated groups was measured. It can be observed the initial hydraulic conductivity of the untreated samples in Experiment 2 was higher. However, the conductivity of treated samples showed a more gradual fall with increasing stress than the untreated samples due to the DAP treatment's improvement in E^* . As a result, at 1,000 psi, the treated samples' conductivity is more than twice as high as the untreated samples. Beyond the 1,000 psi, the intact sample hydraulic conductivity could not be measured due to rock failure. Nevertheless, the treated sample could withstand stress up to 1,500 psi with even higher final hydraulic conductivity, as illustrated in **Figure 3-9** to the left.

An unusual drop in the conductivity trend of the intact samples beyond 800 psi suggested that the sample failed at that point. The LVDTs readings might give more insights into the sample behavior under increasing stress.

In Experiment 3, the hydraulic conductivity of the treated pair was higher, as **Figure 3-9** to the right shows. Likewise, the break in the conductivity trends manifests a sign of sample cracking under stress.

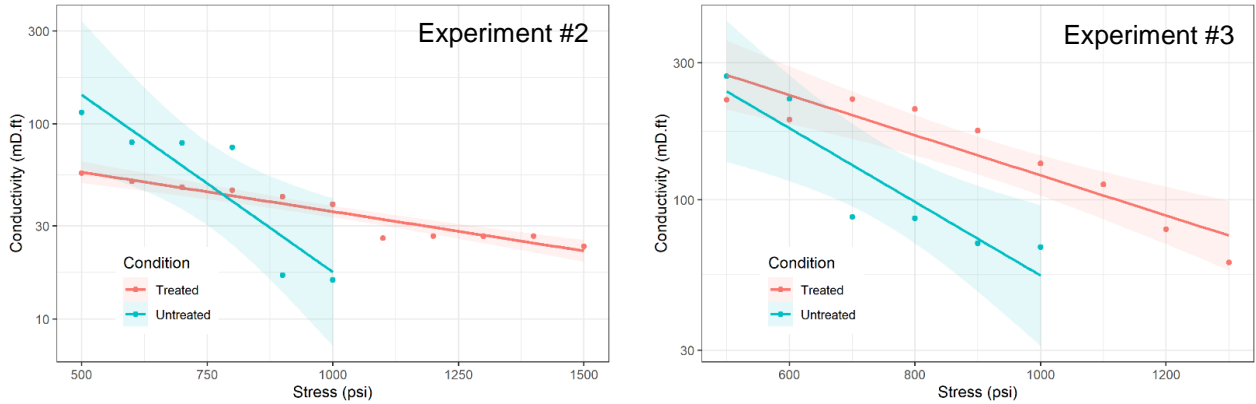


Figure 3-9: Comparison of Hydraulic Conductivity Between Treated and Untreated Samples in Experiments 2 and 3.

The increase in E^* after DAP treatment was observed when reading rock deformations. In **Figure 3-10**, the LVDTs measurement of experiments 2 and 3 for both treated and untreated groups was plotted. Initially, both groups exhibited perfectly linear deformation, while the intact group had slightly higher deformation in Experiment 2. Then, the deformation of the intact group abruptly dropped at 800 psi in Experiment 2 and at 400 psi in Experiment 3, confirming the samples' failure observed in the hydraulic conductivity trends. On the other hand, the treated samples failed beyond 1,000 psi in Experiment 2 compared to 600 psi in Experiment 3. **Table 3-4** presents an overview of the failure onset observed in the treated and untreated samples.

Table 3-4: Failure Stress (psi) as Deduced from LVDT and Conductivity Trendlines.

Experiment	Group	
	Untreated	Treated
#2	800	1000
#3	400	600

Additionally, the compaction of the treated samples was less and more gradual in both experiments. For instance, the total compaction of the treated samples at 1,500 psi was only 1,375 μm , which is 90% less than the 2,600 μm deformation of the untreated samples. Similar behavior was observed in Experiment 3 at 1,000 psi; the untreated sample's deformation was 25% more than the treated one.

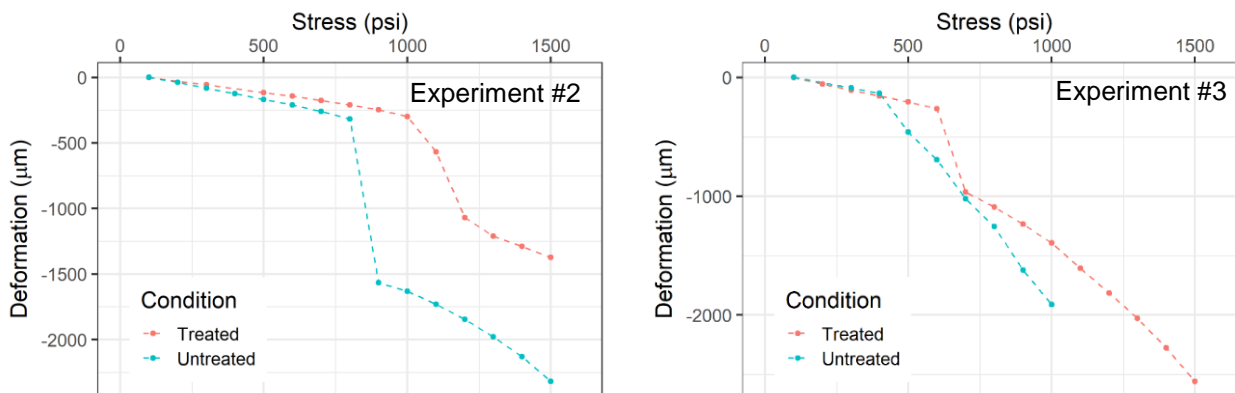


Figure 3-10: Comparison of Compaction Between Treated and Untreated Samples.

In the last experiment, hydraulic conductivity was measured for an extended period. The stress was raised gradually to 1,000 psi and kept constant until the experiment's end, extending it to 160 hrs. As a result of the DAP treatment, the treated samples exhibited

higher stable hydraulic conductivity, averaging around 93 mD.ft compared to only 13 mD.ft in the untreated sample, as seen in **Figure 3-11**.

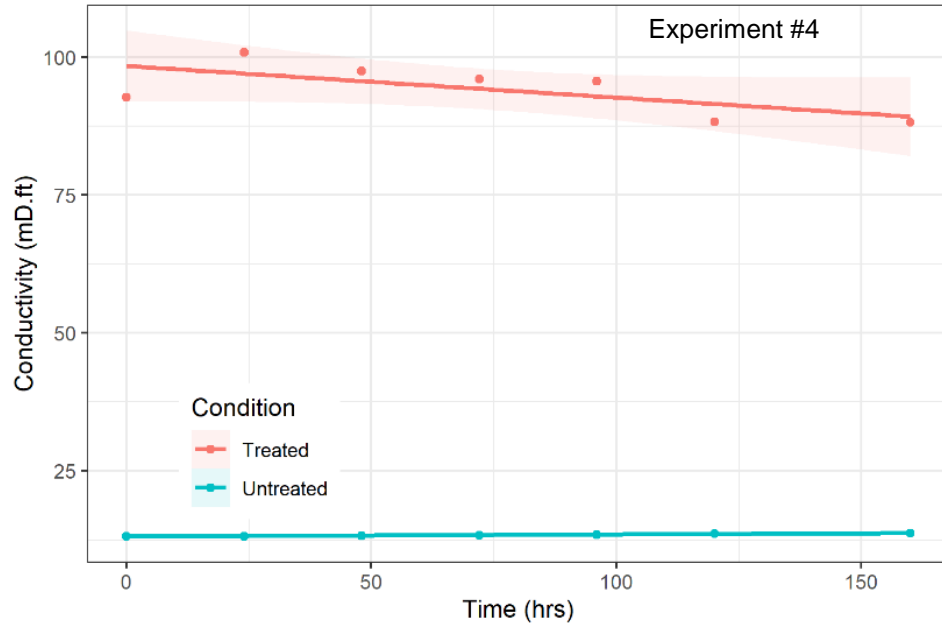


Figure 3-11: The Long-term Conductivity Comparison.

3.3.5 SEM and EDS

The DAP treatment's effect was obvious in the E^* , hydraulic conductivity, and compaction responses. All of the macroscale observations can be related to the changes DAP introduces to the rock at the microscale level. In the case of untreated samples, the calcite grains appear separate, as shown in **Figure 3-12A**. On the other hand, SEM images' investigation of treated samples demonstrates the HAP formation, as shown in **Figure 3-12B:D**. The HAP presence was inferred from the elemental analysis of surfaces (EDS), as demonstrated in **Figure 3-12B**. Furthermore, employing the same technique for elemental quantification at specified locations indicated the values of the constituent elements present in calcite and HAP, which are presented in **Table 3-5**. The literature contains reports of both EDS

analysis and the presence of HAP exhibiting comparable plate-like morphology (Ashokan et al., 2022).

Table 3-5: Elements Composition by Weight (Wt.) Percent as measured by EDS at locations Specified in Figure 12B.

Element	Carbone (C)	Oxygen (O)	Calcium (Ca)	Phosphorous (P)	Silicon (S)
Wt.% @ X	18.69±0.21	52.87±0.24	28.44±0.20	0	0
Wt.% @ O	16.92±0.23	44.83±0.27	36.83±0.24	1.13±0.09	0.29±0.09

HAP efficiently bound the calcite grains by precipitating at the grain-to-grain contact points, as shown in **Figure 12D**. Previous studies showed that treated samples exhibit a significant increase in the dynamic elastic modulus and tensile strength, which is attributed to microcrack reduction and pore filling consequent to the formation of calcium phosphate phases at grain boundaries (Sassoni et al., 2011).

Furthermore, the newly formed HAP has dendrite shapes sprouting from the host calcite grains, interlocking them as visible with higher magnification in **Figure 3-12D**. Kim & Ohtsuki (2016) observed the formation of similar-shaped HAP crystals on the surfaces of the samples, and the size of HAP crystals increased with increasing processing temperature. Thus, HAP's cementing-like effect in the chalk makes it stiffer than intact chalk. Therefore, the deformation becomes less when stresses are applied to the samples. Also, the asperities became stronger and less prone to failure in the treated samples compared to the untreated samples at the same stress. Thus, the stronger asperities supported the load and kept the fracture aperture open to the flow, contrary to the acid

effect on rock compressive strength. Gong et al. (1999) reported that acidification weakens the rock's ability to withstand compression, which makes the surface asperities susceptible to stress deformation. As a result of DAP consolidation, the hydraulic conductivity of the samples subjected to DAP treatment will be higher. In field applications, the utilization of DAP treatment as a secondary injection stage following acid injection has the potential to yield significant benefits. By applying DAP treatment, the stiffness of the fracture surface can be enhanced, which may lead to improved hydraulic fracture conductivity. This enhancement is due to the fact that DAP treatment can promote the deposition of minerals such as HAP onto the fracture surface, which can increase its overall strength and durability. The acid injection will create channels and asperities that improve fracture conductivity, while DAP will sustain long-term fracture conductivity.

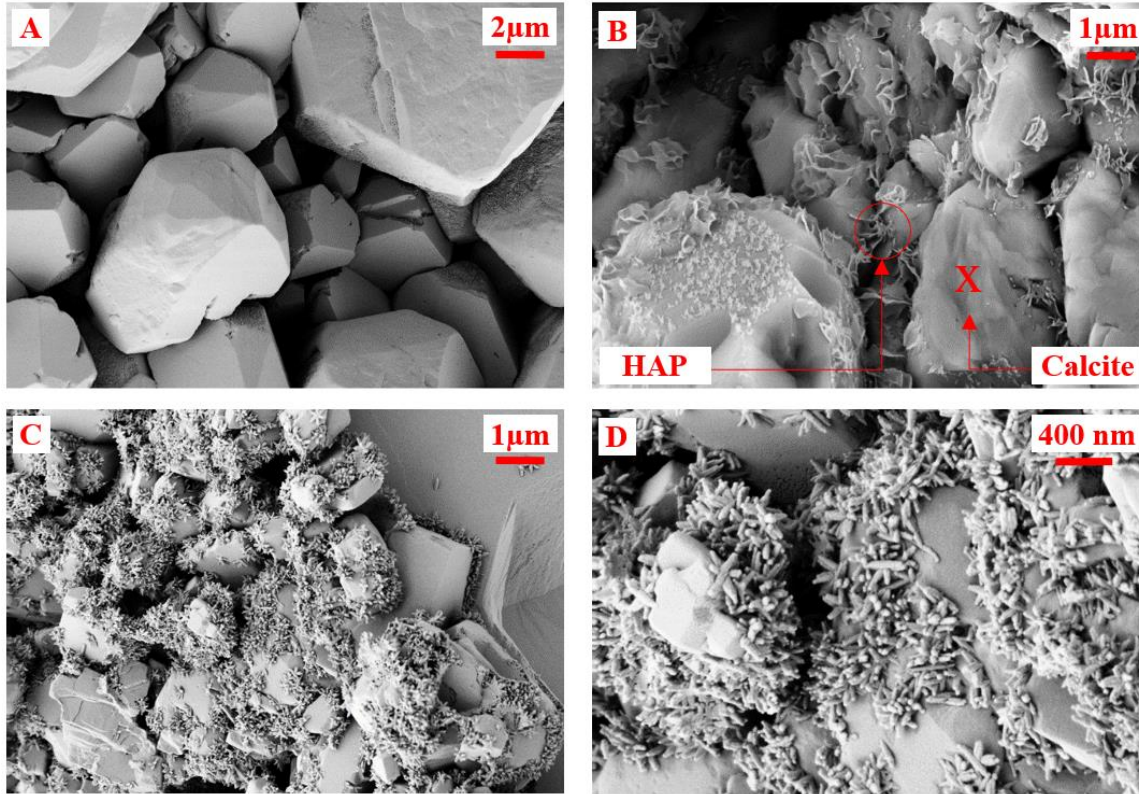


Figure 3-12: SEM image of A) intact chalk sample shows the calcite grains, B) treated chalk with minerals identified with EDS, C) treated chalk sample shows the host calcite grains and the newly formed HAP, and D) closer view of treated chalk sample showing dendrite shape of HAP.

3.4 Conclusion

This study used DAP to consolidate the chalk by inducing HAP precipitation in an exchange reaction with calcite minerals of the chalk samples. As a result, the samples treated with the DAP achieved reduced elastic modulus improvement ranging from 100% to 331% compared to the pre-treatment reduced elastic modulus. The ANOVA results emphasize that baseline-reduced elastic modulus and pre/post-reduced elastic modulus factors are statistically significant and greatly impact reduced elastic modulus mean values.

However, they do not interact, and there is no evidence that relatively softer chalk samples stiffened more than relatively stiffer chalk.

Consequently, improved reduced elastic modulus made the fracture surface more rigid, leading to sustained hydraulic fracture conductivity. For example, in the first experiment, where the samples were randomly selected, the final hydraulic conductivity of the treated samples was 10 times that of the untreated ones.

Nevertheless, it is not recommended to randomly allocate samples to hydraulic conductivity experiments to establish a cause-and-effect relationship, as it could be confusing to understand the findings. Therefore, other controlled experiments were conducted where the samples were selected to have similar initial reduced elastic modulus. Similar to the randomized experiment, the final hydraulic conductivity in the controlled experiments of the samples treated with the DAP is at least twice that of untreated ones. Also, the reduction in hydraulic conductivity of treated samples with stress is less than that of untreated samples in all short-term hydraulic conductivity experiments.

Moreover, the treated samples had higher Failure stress. Similarly, the treated samples extended hydraulic conductivity is considerably higher than those of untreated samples. The obtained results are promising and illustrate the efficacy of the DAP treatment of chalk in sustainably improving the fracture hydraulic conductivity at conditions comparable to the reservoir one.

CHAPTER 4

DIAMMONIUM PHOSPHATE TREATMENT FOR

SUSTAINED HYDRAULIC/ACID FRACTURE

CONDUCTIVITY IN CHALK AND LIMESTONE

FORMATIONS

Abstract

The sustained conductivity of hydraulic/acid fractures is crucial for the continuous and effective production of hydrocarbons. However, hydraulic fractures in soft carbonate formations often experience a reduction in conductivity due to rock deformation and creeping under in-situ stresses. One approach to resolve this issue is to stiffen the fracture surfaces using a consolidating agent. This study examines the application of diammonium hydrogen phosphate (DAP) as an additive to improve the hydraulic/acid fracture conductivity in Indiana limestone and Austin chalk slabs. Initially, flat slabs of Indiana limestone and Austin chalk were subjected to acidization using 15% and 10% hydrochloric acid (HCl) for 10 and 5 minutes, respectively. The resulting surface texture changes were measured using a profilometer. Subsequently, half of the samples underwent treatment in 1M DAP under 1000 psi and 75 °C for 72 hrs. The surface stiffness of the samples was evaluated using nondestructive impulse hammering before and after acid injection and

DAP treatment, while hydraulic/acid fracture conductivity was determined using an API conductivity setup. Following acid injection, the experimental results demonstrate that the stiffness of all the samples was diminished to different degrees. However, intact Indiana limestone samples exhibited increased stiffness after treatment with DAP. Acidized Indiana limestone samples showed partial restoration of their original stiffness with DAP treatment. In contrast, DAP treatment fully restored the stiffness of Austin chalk samples and further enhanced it, resulting in a 2 to 5-fold increase. The increased stiffness observed in the treated samples had a direct impact on short and long-term conductivity. Treated Indiana limestone fractures exhibited double the conductivity of untreated fractures. The improvement in Austin chalk conductivity was even more significant after DAP treatment, resulting in 7 to 8 times higher conductivity in the treated hydraulic/acid fractures. It is worth noting that there was little to no correlation between surface roughness and conductivity, highlighting the significant influence of fracture stiffness on conductivity.

Keywords: Acid Fracturing, Hydraulic Conductivity, Carbonate, DAP Treatment, Consolidation

4.1 Introduction

Carbonate hydrocarbon reservoirs comprise approximately 70% of global oil and gas resources (Guo et al., 2020). These reservoirs are highly valued due to their extensive size and porous characteristics (Li et al., 2018). Given their acid solubility, carbonate hydrocarbon reservoirs can be stimulated through conventional methods, such as matrix acidizing or acid fracturing, based on their permeability range (Palharini Schwalbert et al., 2020). At low reservoir permeability, acid fracturing is the preferred acid stimulation method (Al-Enezi et al., 2017; Mofti et al., 2018; Xiao et al., 2019). Acid fracturing

operation involves the injection of acid at a rate surpassing the breakdown pressure of the carbonate formation, which generates rough acid fractures, resulting in the development of acid fracture conductivity (Aljawad et al., 2019). Economides & Martin (2007) also highlighted that acid fracturing is generally preferable in harder rock formations, as soft formations deform, reducing or nullifying treatment effects. Therefore, acid fracturing is commonly used in lower-permeability carbonate formations that are relatively stiff.

Acid fracture conductivity plays a vital role in acid fracturing operations as it determines the capacity of a hydraulic fracture to deliver reservoir fluids to the wellbore. The optimization of the fracturing process involves considering various factors, with the ultimate success relying on the preservation of conductivity following fracture closure under in situ stress conditions (Al-Ameri & Gamadi, 2020). Hence, laboratory measurements and experiments have further explored the impact of acid parameters (acid type, concentration, temperature, etching time, and injection rate), lithology, and closure stress on fracture morphology and conductivity (Anderson & Fredrickson, 1989; Antelo et al., 2009; Melendez et al., 2007; Nasr-el-din et al., 2008; Navarrete et al., 1998; Nierode et al., 1972; Van Domelen et al., 1994). In addition, geometric characteristics of the acid-etched fracture surface, such as roughness and etching patterns, have been meticulously analyzed to elucidate their relationship with fracture conductivity (Gou et al., 2023; Lu et al., 2017).

Accurately predicting fracture conductivity poses significant challenges due to the complex interplay of various factors, including lithology, rock strength, and closure stress (Motamedi-Ghahfarokhi et al., 2018). Numerous studies have sought to develop models and correlations for estimating fracture conductivity (Akbari et al., 2017). On the

one hand, Rock strength is a key factor that influences fracture conductivity under different closure stresses (Zhou et al., 2021). Furthermore, Nierode and Kruk (1973) have highlighted the exponential impact of rock strength, specifically rock embedment strength, on fracture conductivity. Weaker rocks exhibit a more rapid decline in conductivity. Additionally, the distribution, geometry, and mechanical properties of roughness on the fracture surface can also impact conductivity. Acid injection can modify these properties, resulting in varying levels of emergent acid fracture conductivity (Lai et al., 2019).

It should be noted that conventional acid fracturing techniques can potentially lead to a significant loss of conductivity, either due to excessive acid etching or due to the inherent softness of the carbonate formation (Fredrickson, 1986). In addition, in deep and ultra-deep carbonate reservoirs characterized by high closure stress and deep burial, acid-etched fractures within these formations tend to have low conductivity and are prone to failure. Consequently, well production post-acid fracturing might experience a rapid decline (Ugursal et al., 2019). Thus, the ultimate success of acid fracture stimulation relies heavily on preserving acid fracture conductivity under closure stress (Naik et al., 2020), which is closely linked to the strength of the rock (Tariq et al., 2021).

The acid fracture can be sustained by a chemical treatment to increase the fracture's hydraulic conductivity (DESOUKY et al., 2021d). One approach involves treating weak carbonate samples with DAP, which promotes the formation of stronger minerals near the surface, thereby improving the rock's ability to withstand localized loads (Desouky et al., 2023b, 2023c). This concept draws inspiration from successful efforts to enhance deteriorated carbonate rocks for art preservation (AL-JAWAD et al., 2021), where certain consolidants induce mineral substitution of calcite through dissolution-precipitation

reactions, transforming calcite into stiffer minerals (Samarkin et al., 2022). For instance, Sassoni et al. (2011) demonstrated that DAP forms hydroxyapatite (HAP) in limestone, causing the elastic modulus to increase by 90%. Also, Matteini et al. (2011) reported a 172% increase in dynamic Young's modulus and 27% in ultrasonic velocity after the limestone DAP treatment. Thus, Desouky et al. (2023a) demonstrated that the application of DAP solution to soft flat chalk samples resulted in a substantial enhancement of fracture hydraulic conductivity, which was attributed to the improved mechanical properties of the rock through the formation of HAP.

This article builds upon our prior research, which introduced a novel approach to improve the sustainability of acid fracturing stimulation through chemical means, specifically in soft carbonate reservoirs like chalk. In our previous study, we successfully enhanced the stiffness of the chalk flat surface using DAP, leading to improved conductivity preservation. However, this study expands upon that work by encompassing new carbonate lithology, namely limestone, and addressing the practical challenges associated with the hydraulic conductivity of acid-damaged carbonate rocks. Furthermore, the research examined the roughness caused by acid etching and its potential influence on fracture conductivity. The study outcomes have substantial practical implications, providing valuable insights for designing acid treatments to include a consolidation stage.

4.2 Methodology

4.2.1 Rock Samples

In the experimental phase, Indiana limestone and Austin Chalk rock slabs were utilized, with standard dimensions of 3 inches in height, 1.34 inches in width, and 6.84 inches in length. These dimensions are commonly employed for conducting conductivity experiments. The porosity and permeability ranges for Austin Chalk samples are 8-15 mD and 25-30%, respectively, while for Indiana Limestone samples, the ranges are 8-19 mD for permeability and 14-18% for porosity. The samples were grouped based on their similar initial stiffness to ensure consistency and minimize experimental variations resulting from differences in initial stiffness. This grouping facilitated a systematic comparison between the untreated and DAP-treated samples.

4.2.2 Roughness Measurements

The surface profiles of the rock samples were initially examined for all the samples. A Surface Roughness Analyzer (KRÜSS) equipped with confocal microscopy was utilized to analyze the fracture surface. This technique involves capturing a series of 2D images, each with a limited depth of field, as the optics gradually descend with precise increments. These images are then layered to generate a spatial representation of the surface.

The mean areal roughness profile (S_a) is used to evaluate surface roughness. It quantifies the average distance between the highest peaks and lowest valleys on a surface, indicating the overall roughness level. A higher S_a value indicates a rougher surface with larger deviations in height, whereas a lower S_a value suggests a smoother surface with smaller height deviations. The reference point for S_a is typically the surface's average plane or mean

height. By calculating the vertical distance between the surface's highest and lowest points relative to this reference plane, the S_a value is determined. This standardized measurement enables the evaluation of surface roughness independent of the overall surface height.

S_a is studied for its excellence in describing the orthogonal departure of the fracture edges from a referenced characteristic plane and calculated as:

$$S_a = \frac{1}{NM} \sum_{i=1}^N \sum_{j=1}^M |Z(x_i, y_j)| \quad (4.1)$$

where in the context of the measurement process, N represents the number of measurements taken in the x direction, M represents the number of measurements taken in the y direction, and Z represents the height of the specific point being measured. Moreover, the fracture aperture was deduced by summing the S_a of the two slabs that make up the fracture.

4.2.3 Elastic Stiffness Measurements

The elastic stiffness of the slabs was measured using the AutoScanTM (New England Research) device. This device operates on the principle of impulse hammering to determine stiffness. The assessment of stiffness involves applying a predetermined force to the surface of a rock sample using a standard mass and measuring the sample's time response to the applied force. Hence, the elastic stiffness, represented by Young's modulus, can be quantified by analyzing the rock's response using established models (Gramin et al., 2016). For every sample undergoing DAP treatment, acidization, or a combination of both, a set of 30 elastic stiffness values was collected from the entire surface before and after each intervention.

4.2.4 Acid Etching

In this set of experiments, all Austin chalk and half of Indiana limestone samples underwent acid etching. Before the acid etching process, measurements were taken to assess the stiffness and roughness of the specimens, enabling subsequent comparisons with the etched and DAP-treated states. The acid etching was carried out using the ACM-3000 acid fracture conductivity system (FloxLab). For the etching process, a 10% HCl solution was used for the Austin chalk specimens, while a 15% HCl solution was employed for the Indiana limestone specimens. Two separate rock slabs were placed into the experimental cell, and the acid was pumped through the 3 mm gap between the two specimens at a flow rate of 500 cc/min for 10 minutes in the case of Austin chalk and 5 minutes for the Indiana limestone. Following the etching process, the fracture surface was thoroughly flushed with an equivalent volume of 2% potassium chloride (KCl) brine, as illustrated in **Figure 4-1**.

After removing the samples from the apparatus, an additional rinsing step was performed using deionized water to ensure the removal of any potential residual chemicals (**Figure 4-4A**). Subsequently, the samples were dried for 24 hrs., and their roughness and stiffness were measured again to compare with the initial state. Later, half of the acidized samples underwent treatment with a DAP solution following the described procedures in the next section.

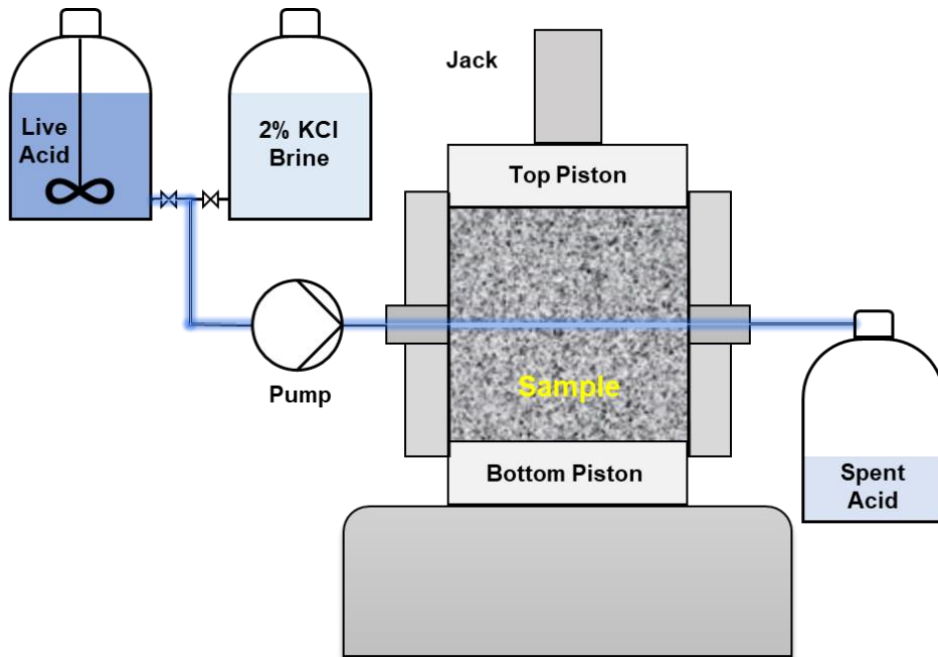


Figure 4-1: Illustration depicting the process of acid etching and subsequent brine flushing.

4.2.5 Specimen's Chemical Treatment

Half of the rock samples underwent treatment using a 1M concentration solution of Diammonium Phosphate (DAP). The treatment involved immersing the rock slabs in pairs in a 3-liter stainless steel cell. To prepare the solution, 396.2 grams of DAP salt were dissolved in 3 liters of deionized water. Before each treatment, the cell was subjected to a 24-hour vacuum with the rock samples inside. This step ensured the penetration of the solution into the pore space of the rock samples, enhancing the stiffening effect. The treatment was carried out at a temperature of 75°C and a pressure of 1,000 psi applied by a sensitive pump for 72 hrs. Following the treatment, the samples were rinsed with deionized water to eliminate any remnant treatment solution and dried for 24 hrs. at the

same temperature as during treatment. The stiffness of these treated samples was then re-evaluated to compare it with the initial and acidized conditions.

In the final preparation step for conductivity measurement, rock slab pairs were joined using aluminum tape (**Figure 4-4B**) and molded with silicon resin to simulate a fracture, as illustrated in **Figure 4-4C**.

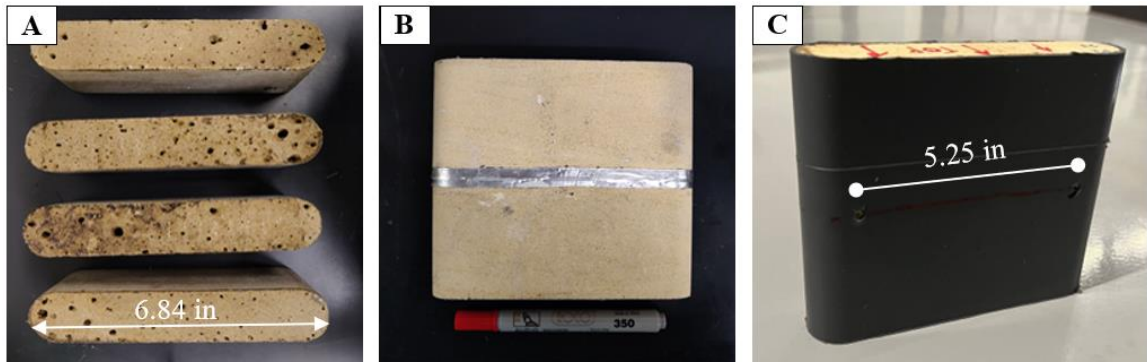


Figure 4-2: A) Samples subjected to acidization B) Attachment of two sister samples to synthesize the fracture C) Molded samples utilized in hydraulic conductivity experiments.

4.2.6 Hydraulic Conductivity Measurements and Deformation

Conductivity experiments were conducted using nitrogen gas in the API ACM-3000 device. For short-term conductivity measurements, the rock samples were subjected to various stress levels in incremental steps. The average deformation of the samples at each stress level was measured using four linear variable differential transformers (LVDTs). Simultaneously, the gas was pumped at four different flow rates, ranging from 200 to 350 cc/min, with a 50 cc/min step size at each stress level, as illustrated in **Figure 4-3**. In the short-term conductivity experiments, the applied stress ranged from 100 to 3,200 psi, with

the maximum stress depending on the initial stiffness of the sample. In the long-term conductivity experiments, a single stress value was applied and maintained for 6 days (144 hrs.), during which the conductivity was measured daily. The conductivity value was determined by calculating the slope of the line generated using the four measurements. The detailed procedure of sample preparation and hydraulic conductivity measurements can be found in **Figure 4-3** from our previous publication (Desouky et al., 2023a).

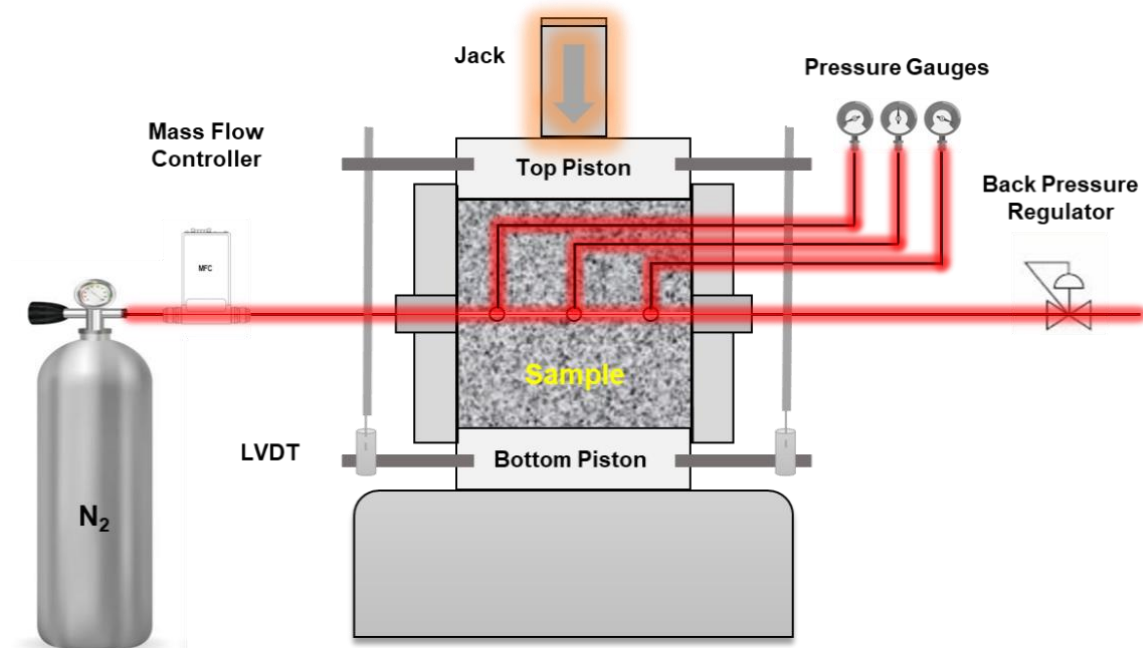


Figure 4-3: Measurement of gas conductivity of the acid fracture and samples' deformations (Desouky et al., 2023a).

Detailed information about the rock samples, including their identification (ID), acidization, DAP treatment, and maximum applied stress during conductivity measurement, is presented in **Table 4-1**.

The table also provides an overview of the experimental arrangement, specifically the grouping of rocks based on their initial stiffness and lithology. Grouping the carbonate samples is essential to address the heterogeneity of the samples and establish a foundation for comparative analysis by selecting similar samples based on stiffness. Additionally, dividing the samples into control and treatment groups within each similarly stiff group serves the purpose of having a benchmark group against which the DAP-treated group can be compared.

Table 4-1: Summary of samples' data and corresponding experimental conditions.

Experiment ID	Sample ID	Lithology	Initial Stiffness (GPa)	Maximum Applied Stress (GPa)	Acidization	DAP Treatment	Tested Conductivity	
Exp. 1	LS1	Limestone	21.11	3,200	X	X	Short/Long	
	LS2		20.91					
Exp. 2	LS3		21.02		2,800	X		✓
	LS4		20.70					
Exp. 3	LS5		24.20	2,800	✓	X	Short	
	LS6		24.37					
Exp. 4	LS7		23.98		✓	✓		
	LS8		24.21					
Exp. 5	Ch1	Chalk	14.00	2,200	✓	X	Short	
	Ch2		15.74					
Exp. 6	Ch3		12.94	2,500	✓	✓		
	Ch4		15.46					
Exp. 7	Ch5		4.11	800	✓	X	Short/Long	
	Ch6		4.48					
Exp. 8	Ch7		4.85	2,000/1,400	✓	✓		
	Ch8		4.50					

LS: limestone, Ch: chalk

4.3 Results

4.3.1 Changes in Elastic Stiffness Following Acid Etching

The elastic stiffness of both Indiana limestone and Austin chalk spanned a wide range. For example, the elastic stiffness of Indiana limestone varied between 20 and 28 GPa, as depicted in **Figure 4-4**. The samples were grouped based on their elastic stiffness as measured by AutoScan before conducting the comparative experiments to ensure a fair comparison. The grouping allowed for the selection of similar samples for each comparative study before and after acid etching or treatment with DAP.

Thus, the elastic stiffness of the available limestone samples was measured, and a mean stiffness plot with a 95% confidence interval was generated. Samples with an initial stiffness of 21 GPa, indicated by a dotted circle in **Figure 4-4**, were selected to compare the conductivity of intact samples with that of DAP-treated ones. Similarly, another group of samples with a similar initial elastic stiffness of 24 GPa, represented by a blue dotted circle in **Figure 4-4**, was chosen to compare acid fracture conductivity between DAP-treated and untreated samples.

The same procedure was followed for the Austin chalk samples, where samples with approximately the same elastic stiffness were selected for each comparative conductivity experiment, as summarized in **Table 4-1**.

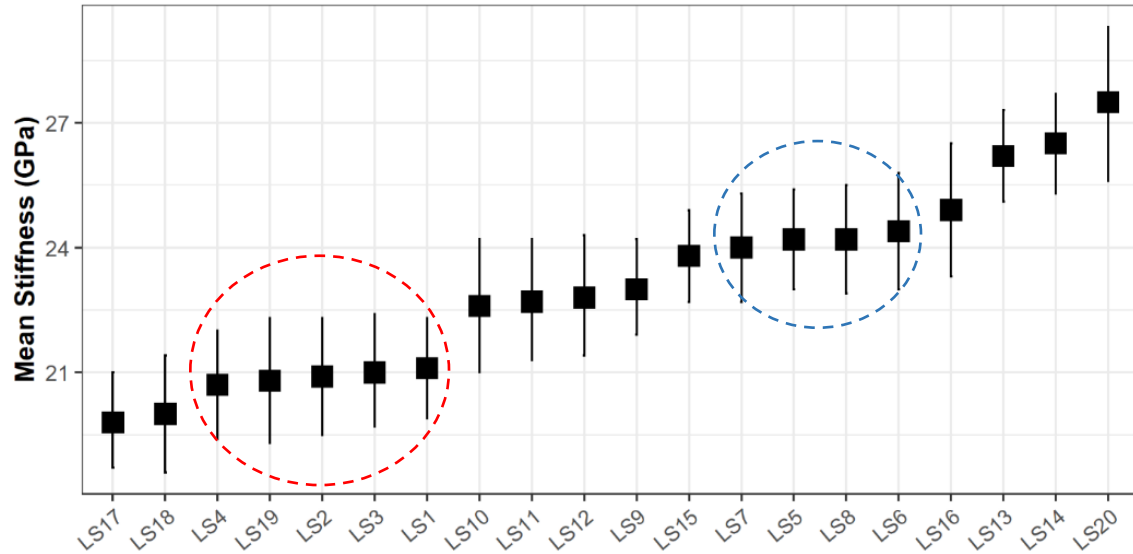


Figure 4-4: Mean stiffness 95% confidence interval of the limestone samples.

In Experiments 1 and 2, the samples had an average initial elastic stiffness value of approximately 21 GPa. While the control group remained unchanged, the treatment group's elastic stiffness increased to 31 GPa after the DAP treatment (i.e., Experiment 3). Notably, LS3 and LS4 exhibited a substantial 49% and 47% increase in elastic stiffness, respectively.

In Experiments 3 and 4, the samples underwent acidization first, significantly reducing their initial elastic stiffness of 24 GPa. During each acid etching process, the bottom sample placed in the API cell experienced the most pronounced reduction in strength. Among the acid-etched Indiana limestone samples, LS6 and LS8 had their elastic stiffness lowered by 23% and 25%, while LS5 and LS7 suffered the greatest reduction with a decrease of 66% and 55%, respectively.

However, after the treatment of samples LS7 and LS8, their elastic stiffness was partially restored. They showed an increase of 9% and 20%, respectively, as depicted in **Figure 4-5**.

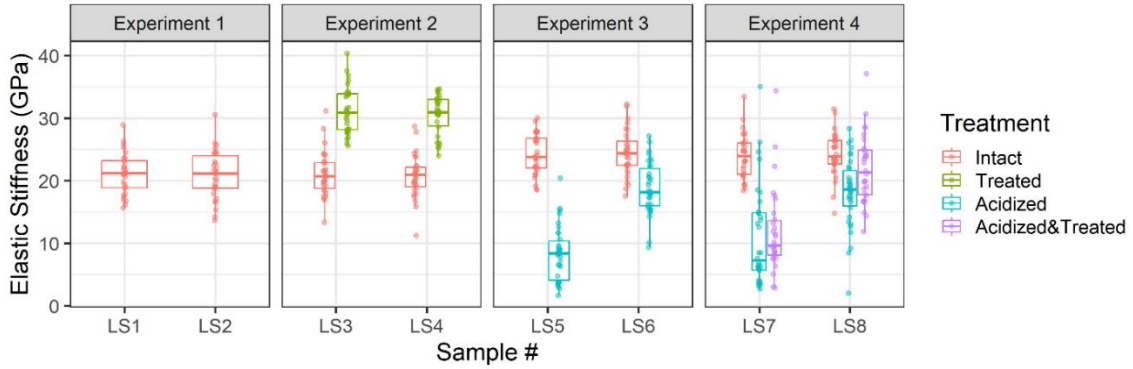


Figure 4-5: Comparison of initial Indiana limestone elastic stiffness and the impact of acid and DAP treatment.

Likewise, the elastic stiffness of the Austin chalk samples decreased as a result of acidization. In general, AutoScan measurements revealed that the acid treatment led to a reduction in stiffness for all the etched samples. Specifically, sample Ch1 experienced a 12% decrease in stiffness, Ch2 decreased by 29%, Ch3 decreased by 4%, and Ch4 decreased by 41%. Notably, the samples used in Experiments 3 and 4, allocated for long-term conductivity, exhibited more significant decreases in stiffness. Sample Ch5 decreased by 52%, Ch6 decreased by 30%, Ch7 decreased by 39%, and Ch8 decreased by 78%.

However, the subsequent treatment with the DAP solution led to the restoration and even enhancement of the initial stiffness levels. The elastic stiffness of samples Ch3, Ch4, Ch7, and Ch8 increased after the DAP treatment. **Figure 4-6** illustrates that the rock samples' initial stiffness was restored and improved beyond their original stiffness levels. For example, sample Ch3 showed a 46% improvement in stiffness compared to the state after

acid treatment. Sample Ch4 exhibited a 71% improvement in stiffness. Additionally, there was a significant enhancement in stiffness for samples Ch7 and Ch8, with remarkable improvements of 334% and 575%, respectively.

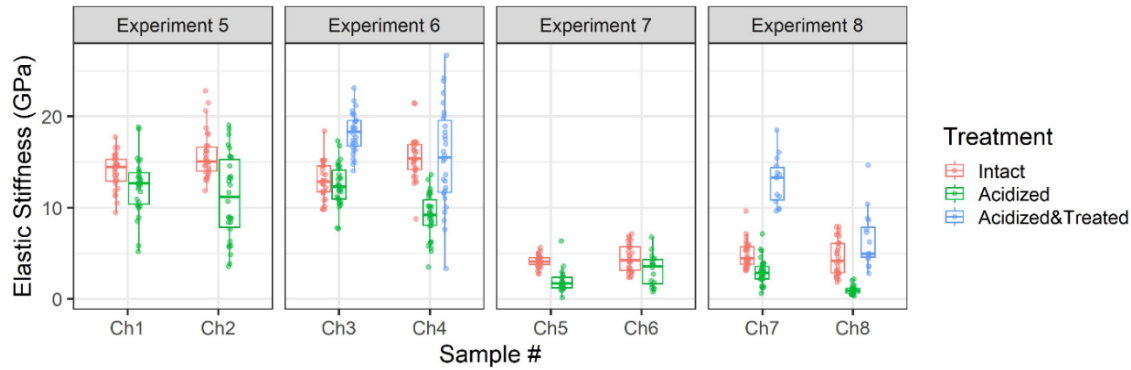


Figure 4-6: Comparison of initial Austin chalk elastic stiffness and the impact of acid and DAP treatment.

4.3.2 Changes in Roughness Following Acid Etching

Examining the surface profiles of rocks before and after acidizing revealed significant changes caused by the acid treatment. Comparing the measurements of S_a provides clear evidence of the impact of the acid treatment on the samples. Initially, the flat samples exhibited an S_a ranging from 0.02 to 0.03 mm. The machined samples exhibit a low S_a , indicating a precise and accurate finish. Moreover, the roughness values are distributed normally around an average plane, as seen in **Figure 4-7A** to the right. Following the acidizing process, there was a significant increase in the S_a of the Indiana limestone samples, with this increase being at least one order of magnitude. The S_a measurements reached values as high as 0.71 mm, as illustrated in **Figure 4-7B**.

Furthermore, the acid treatment led to the formation of irregularities on the surfaces of the Indiana limestone samples, particularly evident in the presence of wormholes, as shown in **Figure 4-7B** and **Figure 4-7C**. Also, the roughness distribution is skewed towards the right, with negative values representing the presence of exceptionally deep valleys that correspond to the wormholes observed. The concentration and sizes of these wormholes were higher near the inlet, while the etching was more pronounced in that area. Additionally, the bottom samples exhibited slightly more etching due to gravity, as observed in **Figure 4-7B**.

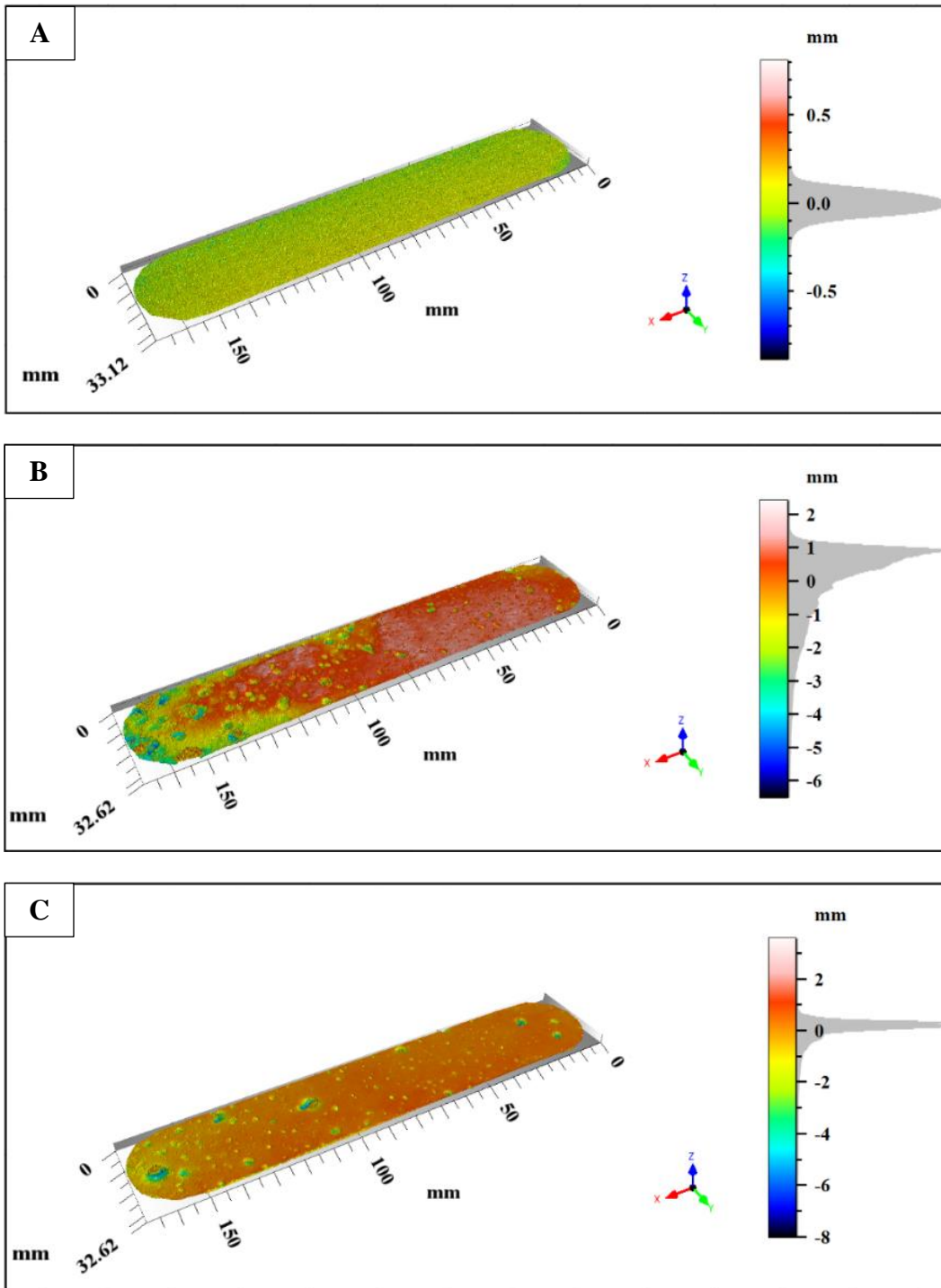


Figure 4-7: Areal mean roughness profile and histogram for A) Sample LS1 without acidization, B) Sample LS5 after acidization, and C) Sample LS6 after acidization.

The etching behavior of the Austin chalk samples shows distinct characteristics. **Figure 4-8** illustrates that the sample AC5 edges have higher elevations than the middle portion. In addition, sample AC6 exhibits a comparable but less pronounced etching in the middle portion, along with the formation of wormholes that resemble those observed in the Indiana limestone samples (**Figure 4-8B**). Notably, the AC6 roughness distribution is left-skewed, accounting for the elevated edges observed during the etching process. The S_a of all the samples and the average fracture width are arranged in **Table 4-2**.

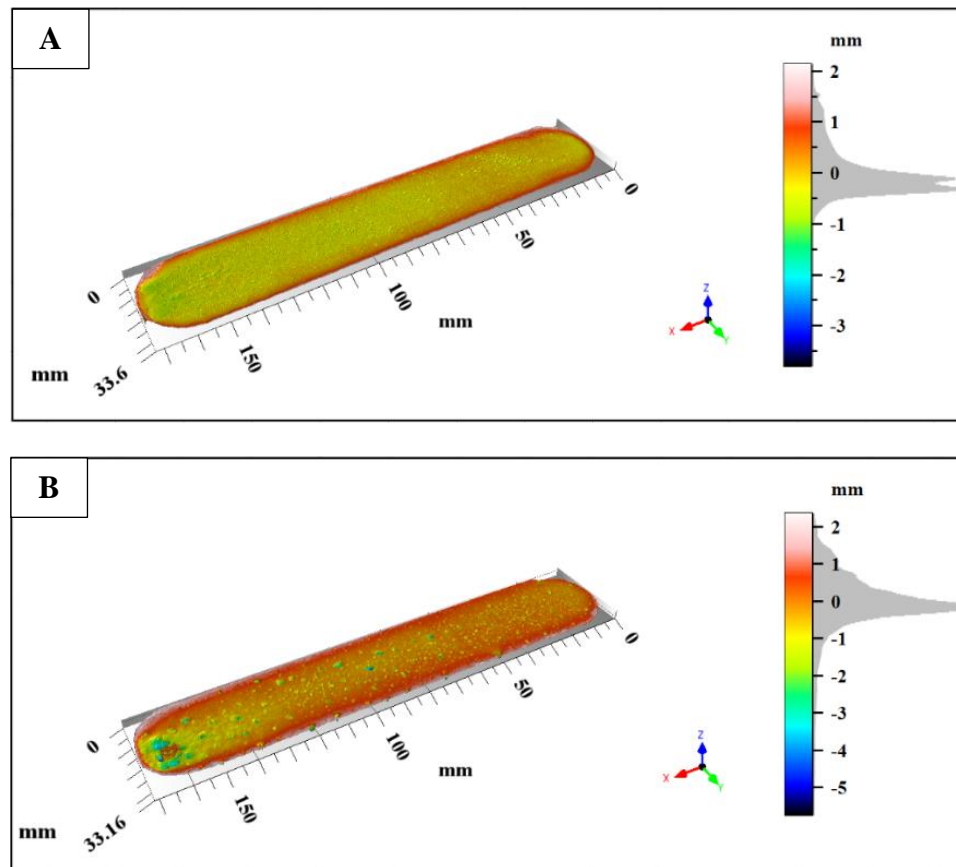


Figure 4-8: Areal mean roughness profile and histogram for A) Sample Ac5 after acidization and B) Sample Ac6 after acidization.

Table 4-2: Summary of the roughness measurements.

Sample ID	S _a (mm)	Mean Fracture Width (mm)	Acidization
LS1	0.03	0.06	X
LS2	0.03		
LS3	0.03	0.05	X
LS4	0.02		
LS5	0.71	1.03	✓
LS6	0.32		
LS7	0.42	0.79	✓
LS8	0.37		
Ch1	0.31	0.71	✓
Ch2	0.4		
Ch3	0.33	0.55	✓
Ch4	0.22		
Ch5	0.62	1.12	✓
Ch6	0.5		
Ch7	1.23	1.82	✓
Ch8	0.59		

LS: limestone, Ch: chalk

4.3.3 Hydraulic/Acid Conductivity

After being treated with DAP, the conductivity measurements of the Indiana limestone samples demonstrated higher values than the untreated samples throughout the entire stress application range, up to 3,200 psi, as illustrated in **Figure 4-9A**. For example, the treated samples exhibited a conductivity of 168 m.D. In contrast, the untreated samples had a conductivity of 97 m.D at 3,200 psi. This trend was similarly observed in the acidized DAP-treated and acidized untreated limestone samples over the 2,800 psi stress application range, as depicted in **Figure 4-9B**. At 2,000 psi, the conductivity of the treated acidized samples was nearly double that of the acidized untreated limestone, with a value of 354 m.D compared to 176 m.D. Additionally, it was observed that the acidized samples displayed higher conductivity values at the same stress levels in Experiments 3 and 4 compared to the corresponding conductivity values in the unacidized samples in Indiana limestone Experiments 1 and 2.

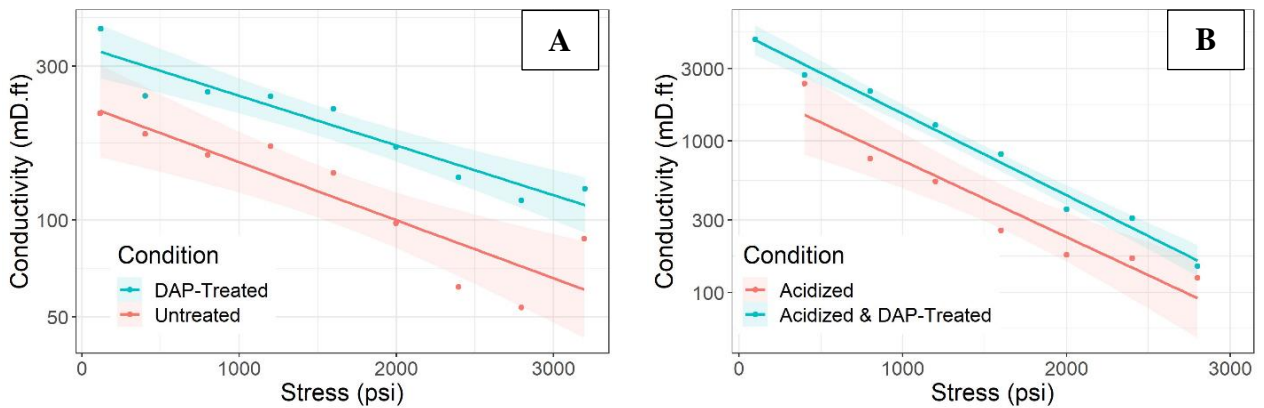


Figure 4-9: Short-term fracture conductivity of Indiana limestone A) Experiments 1 and 2, and B) Experiments 3 and 4.

Indiana limestone Experiments 1 and 2 were extended for 144 hrs. at a 3,200 psi stress to assess the conductivity behavior over time. As depicted in **Figure 4-10**, the long-term conductivity of the untreated limestone samples exhibited fluctuations around 80 m.D, which is 50% lower than the treated samples, which displayed values of 120 m.D. Most conductivity reduction occurred during the short-term conductivity experiment, and the rate of decline decreased over time in a typical exponential pattern. Initially, the decline was relatively rapid as the stress increased, eventually stabilizing at 3200 psi. However, as time progressed, the rate of decline slowed down significantly or almost ceased altogether. This observation implies that the most significant conductivity reduction occurs during the early stages of stress ramping.

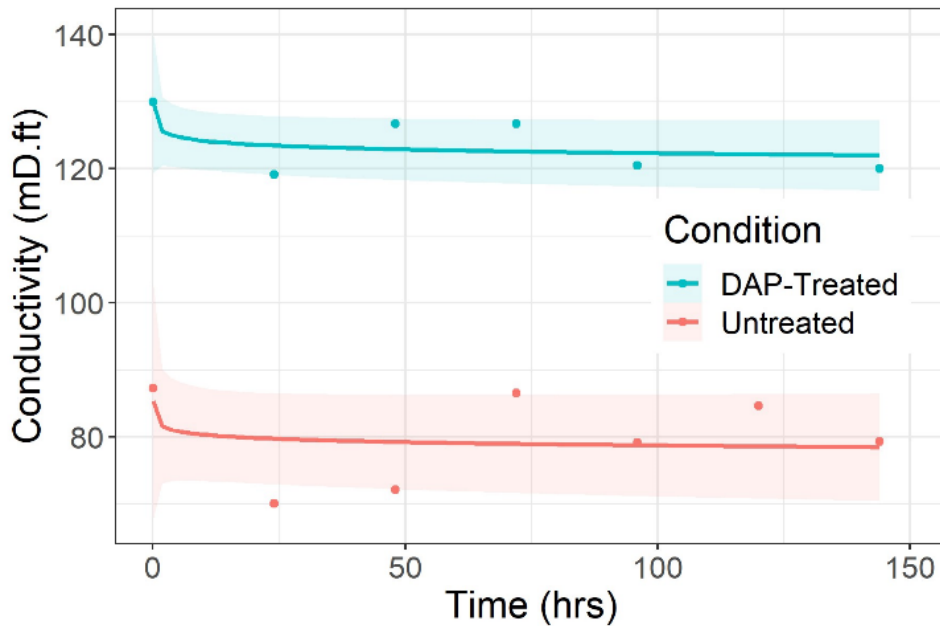


Figure 4-10: Long-term fracture conductivity of Indiana limestone Experiments 1 and 2.

Similarly, the Austin chalk conductivity experiments indicated a noticeable difference between the hydraulic conductivity of the untreated acid fracture and the acid fracture treated with DAP. It can be noticed that the reduction in fracture conductivity was more pronounced in the untreated rock samples compared to the treated ones. Under stress of 2,200 psi, the conductivity of the untreated fracture dropped to approximately 8 md-ft. In contrast, the fracture treated with DAP maintained a conductivity of around 60 md-ft at the same stress level. Additionally, the conductivity of the untreated fractures approached zero at a stress of 2,500 psi, whereas the treated acid fracture sustained its conductivity (**Figure 4-11A**).

It should be noted that chalk samples with an average initial stiffness of 4-4.5 gigapascals (GPa), which was reduced to 1.5-2 GPa, exhibited minimal conductivity at 800 psi stress (**Figure 4-11B**), while the DAP-treated fracture with stiffness of 7-12 GPa maintained high conductivity even under higher stresses. The acidized untreated sample cracked at 800 psi, while the acidized and DAP treated could withstand up to 2,000 psi stress.

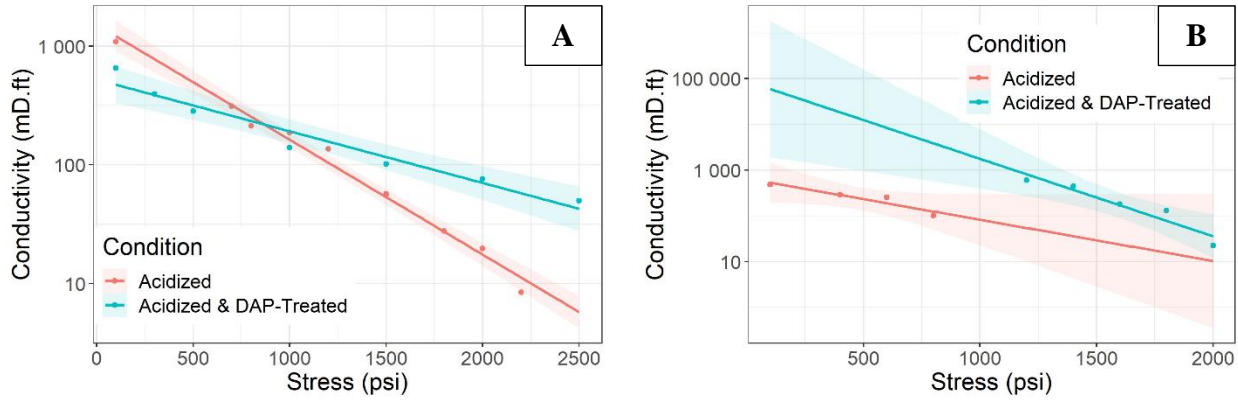


Figure 4-11: Short-term acid fracture conductivity of Austin chalk A) Experiments 1 and 2, and B) Experiments 3 and 4.

The long-term conductivity experiments have demonstrated a positive trend in maintaining enhanced conductivity due to the DAP treatment, as depicted in **Figure 4-12**. The acid-etched and untreated chalk samples were subjected to a stress of 800 psi during the experiments. At this stress level, the initial conductivity measurement was around 100 mD.ft at the start of the experiment. Over a constant stress period of 6 days, the conductivity of the fracture decreased to 30 mD.ft. In contrast, the DAP-treated rock slabs exhibited exceptionally high conductivity when subjected to the same 800 psi stress. Therefore, a higher stress of 1400 psi was applied during the experiment and maintained for 6 days to compare the two experiments' conductivity values. It is noteworthy that chalk samples with an average initial stiffness ranging from 4 to 4.5 GPa typically exhibit limited resistance to high stresses, particularly in the context of acid treatment. Subsequent to acidization, the stiffness of the samples dropped to the range of 1.5-2 GPa, resulting in minimal conductivity at stress levels of 800 psi. In contrast, the DAP-treated fracture, characterized by an improved stiffness ranging from 7 to 12 GPa, maintained significantly

higher conductivity even under elevated stress conditions. Notably, it is important to emphasize that both samples possessed identical stiffness levels prior to the introduction of acid injection and DAP treatment.

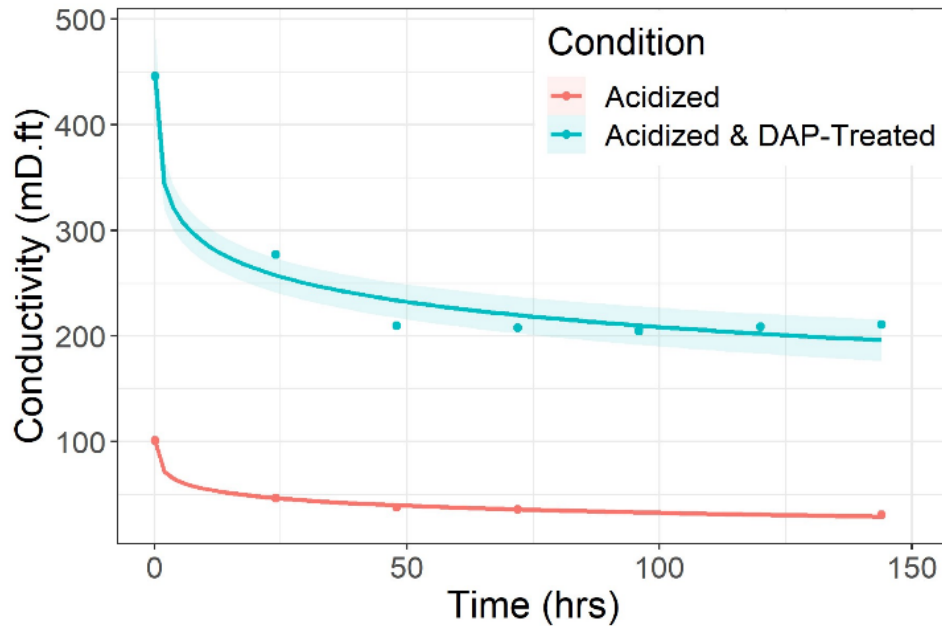


Figure 4-12: Long-term acid fracture conductivity of Austin chalk Experiments 3 and 4.

4.3.4 Deformation

The average deformation of the samples at each stress level, obtained from the four LVDTs, was calculated and plotted in **Figure 4-13**. Experiments 1 and 2 on unacidized Indiana limestone samples showed no significant deformation difference between treated and untreated (**Figure 4-13A**). Both exhibited a small deformation of roughly 150 microns at 1500 psi. At stress levels exceeding 2500 psi, both the treated and untreated samples experienced failure, indicating the importance of not surpassing this stress threshold in subsequent experiments involving similar stiffness levels. However, in Experiments 3 and

4 conducted on acidized samples of Indiana limestone, the recorded deformation was higher than the unacidized samples, with the treated samples showing less deformation (**Figure 4-13B**). At 1500 psi, the untreated samples in Experiment 3 exhibited a deformation of 1200 microns, while the treated samples had a deformation of 950 microns. The deformation trend was mostly linear for all stress values beyond 400 psi until the samples displayed signs of crack initiation, if any.

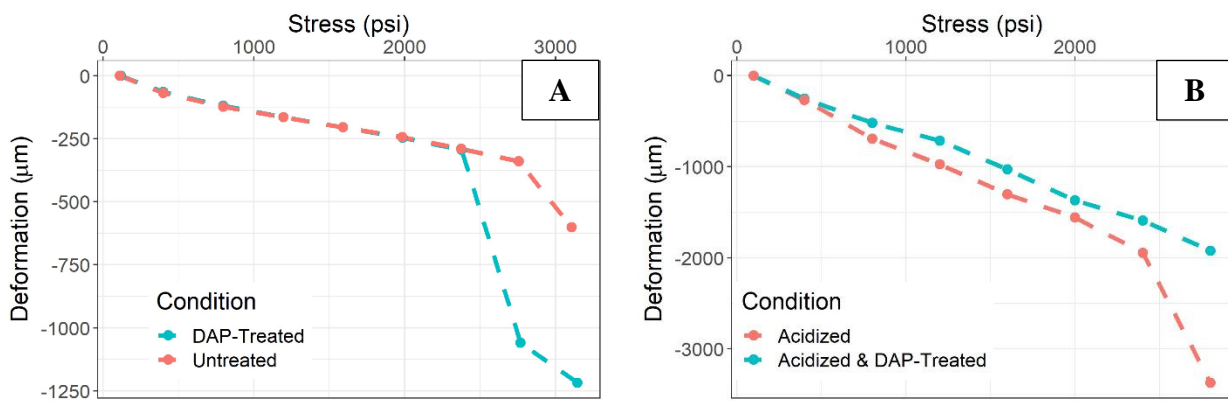


Figure 4-13: Deformation of the samples under stresses for Indiana limestone A) Experiments 1 and 2, and B) Experiments 3 and 4.

Likewise, untreated rock samples exhibited more significant deformation when subjected to applied stress than the DAP-treated samples. **Figure 4-14** illustrates that at 1500 psi, the treated samples showed a deformation of 1355 microns, whereas the untreated acidized chalk samples experienced a deformation of 2800 microns. In general, the deformation between the acidized chalk samples is greater than what was observed in the acidized limestone samples.

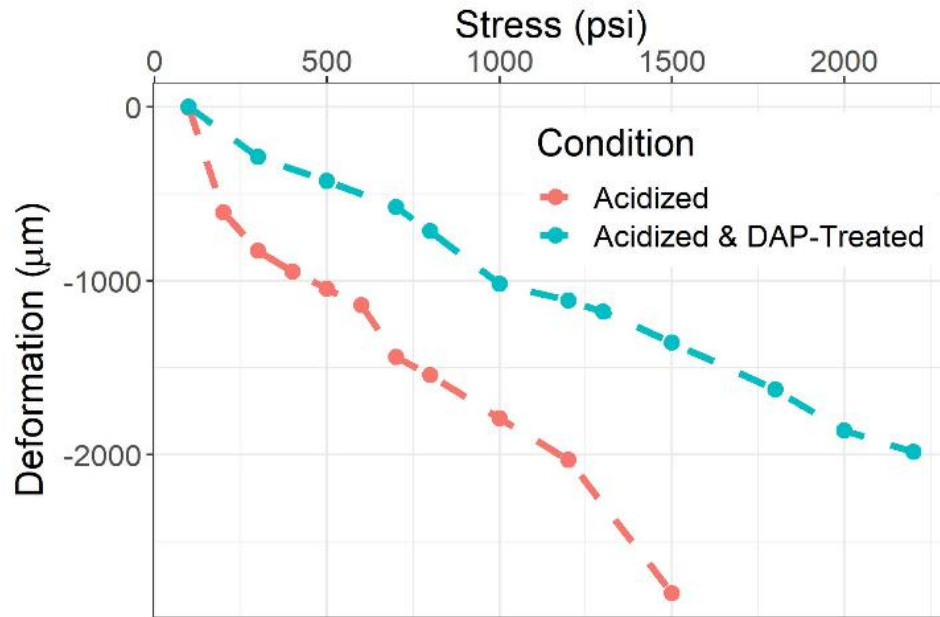


Figure 4-14: Deformation of the samples under stresses for Austin chalk Experiments 1 and 2.

4.4 Discussion

Rock stiffness, which varies among the samples, has a significant impact on fracture conductivity. (Figure 4-4). Clustering the samples could minimize these variations, enabling a fair and unbiased comparison of the results obtained. This approach ensured that similar stiff, flat samples were initially grouped, allowing for a more accurate assessment even when stochastic processes such as acid etching and DAP treatment were involved.

The acid etching process resulted in alterations in the surface morphology of the initially flat carbonate rocks. Therefore, the profilometer scans aimed to capture and describe the surface's essential topographic characteristics and functionality. The profilometer scans emphasized increased roughness, hence a larger calculated average fracture width. However, despite the potentially substantial roughness, its impact on conductivity was not

significant to explain the Indiana limestone conductivity values under low-stress conditions. For instance, when comparing the conductivity of DAP-treated (Experiment 2) and untreated samples (Experiment 1) in Indiana limestone, wider fracture aperture was associated with lower initial conductivity at 100 psi. The observation is plausible as most of the roughness comes from sparse unconnected pits on the limestone fracture surface. Thus, distinguishing between connected and isolated features is as important as analyzing the surface's texture, shape, and orientation (Jiang et al., 2007).

Conversely, in the comparative Experiments 1 and 2 conducted on Austin chalk, higher average width corresponded to higher initial conductivity at the same stress. The acid etching of Austin chalk resulted in sparse pits resembling those found in Indiana limestone, along with a universally shallow channel. Despite being difficult to detect, the presence of this shallow channel in the direction of gas flow contributed to higher conductivity. While some studies suggest a correlation between initial conductivity and the calculated fracture width based on dissolved rock quantity (Nierode & Kruk, 1973), others argue that it depends on the dissolution pattern, which was considered a more accurate approach (Lu et al., 2017; Pournik, 2008). According to Pournik's findings, a correlation exists between the width of a fracture and the presence of asperities. Specifically, when the fracture width is larger, having a higher number of asperities is advantageous for hydraulic conductivity. This relationship enables the fracture to effectively utilize its increased width, leading to a lower contact ratio between the surfaces and higher hydraulic fracture conductivity.

Nevertheless, a more general association can be made between the direction of roughness and the flow direction. Hence, the central shallow channels parallel to the gas flow direction explain the acidized Austin chalk's higher initial conductivity at low stresses.

However, the higher initial acid fracture conductivity did not translate into higher conductivity under stress, as evidenced by the findings of Rodrigues and Medeiros (2011). The results also agreed with (Gou et al., 2021), who stated that having excessive dissolved rock is advantageous for achieving high initial conductivity; however, when subjected to medium and high closure stress, the retention rate of conductivity is the lowest. Therefore, it is plausible to extend the discussion to the behavior of the fracture under the stress application.

The strain results indicate that acidizing increased the normal deformability of fractures compared to non-acidized fractures, as the comparison is shown in **Figure 4-13**. This increase is primarily attributed to the enlargement of the initial aperture and the reduction in the strength properties of the rock. Moreover, when comparing fractures that have undergone treatment following the same acidification conditions, it was observed that fractures with higher normal stiffness corresponding to the treated samples exhibited greater resistance to deformation, as shown in **Figure 4-13B** and **Figure 4-14**. The observation was consistent for the different lithologies involved in the study, i.e., limestone and chalk. In turn, The ability of fractures to resist deformation is a critical factor in determining acid fracture conductivity, especially when increasing the applied stress. Fractures with higher resistance to deformation, attributed to greater rock stiffness, exhibit improved acid fracture conductivity. The enhanced acid fracture conductivity of the treated samples was attributed to their higher stiffness, which helped preserve the integrity of the fracture when subjected to stress. The improved acid fracture conductivity prevented excessive fracture closure and enabled a continuous fluid flow. The results are consistent with our previous publication results and the literature (Asadollahpour et al., 2018).

Furthermore, the increased stiffness of the DAP-treated samples resulted in reduced creep over an extended period, leading to higher long-term fracture conductivity. The treated acidized Indiana limestone, and Austin chalk exhibited improved acid fracture conductivity throughout the extended experiment duration of up to 144 hrs., as the stiffness of these lithologies was enhanced following the DAP treatment.

The dissolution of minerals by acid resulted in a decrease in the elastic stiffness of the rocks, as observed in the AutoScan results, which is consistent with previous research findings. Gong et al. (1999) noted that while acid is essential for creating rough fracture surfaces, it has a detrimental effect on the mechanical properties of the rock. Additionally, Nugroho et al. (2022) found that adding 15% HCl to carbonate samples led to a reduction of approximately 25% in the overall calcite content. Consequently, higher acid concentrations caused excessive etching, limiting the flow capacity (Zhang et al., 2020). Furthermore, Melendez et al. (2007) discovered that the fracture conductivity decreases when acid weakens the embedment strength of the rock.

On the other hand, the DAP treatment was found to enhance the stiffness of the rocks, which aligns with the existing literature. Matteini et al. (2011) explained that DAP treatments consolidate limestone materials by inducing compositional changes. These changes often result in hydroxyapatite (HAP) formation as the primary mineral phase, effectively binding the grains together, as discussed previously in our publication (Desouky et al., 2023a). Overall, the acid treatment reduced the stiffness of the carbonate rocks in the study, leading to lower fracture conductivity over both short and long durations. However, the DAP treatment had the potential to partially or fully restore the stiffness and even enhance it beyond the initial value, resulting in improved fracture conductivity.

4.5 Conclusion

In this study, a series of experiments were conducted to simulate the behavior of acid etching and investigate the effects of DAP treatment on fracture conductivity. The roughness and stiffness were also measured at the initial and acid-etched stages. The acid etching process increased the roughness of the fractures, which enhanced acid conductivity only when aligned with the flow direction. Also, acid etching significantly reduced sample stiffness by up to 80% in some cases. However, DAP treatment under high temperature and pressure conditions restored and improved the initial stiffness beyond its original state. Some samples showed a stiffness improvement of 4 to 6 times compared to their acid-etched condition. The increased stiffness enhanced short-term and long-term acid fracture conductivity. In the case of DAP-treated Indiana limestone, the conductivity was observed to be 50-100% higher compared to intact fractures. Notably, DAP-treated fractures in the Austin chalk formation demonstrated an even more remarkable improvement in conductivity, reaching levels up to 7 to 8 times higher than untreated fractures. These treated samples also demonstrated improved resistance to deformation under applied stresses, indicating enhanced overall strength. Furthermore, acid etching increased the deformability of fractures, resulting in more deformation, exhibiting lower stiffness and lower hydraulic conductivity, especially at high stress levels. The relationship between fracture stiffness and hydraulic conductivity revealed that fractures with higher stiffness had greater conductivity. The DAP treatment mitigated the acid's effects, reducing deformability and increasing conductivity, and the effect is more pronounced when in the softer rock, i.e., Austin chalk. These findings offer valuable insights for implementing this technique in carbonate reservoir stimulation.

CHAPTER 5

CONCLUSION, FUTURE WORK, AND RECOMMENDATION

5.1 Conclusion

The study indicates that the application of DAP treatment is successful in enhancing the stiffness of weak carbonates and improving the conductivity of hydraulic fractures under reservoir conditions. The key findings of the study are as follows:

- Temperature and reaction duration are critical factors influencing the DAP-calcite reaction, while the pressure effect is minor. The study determined that the optimal conditions for the reaction were 1000 psi and 75 °C over 72 hrs. using a 1M DAP.
- The study provides valuable insights into the diffusion and reactivity of the substrate, shedding light on the newly formed HAP at different depths.
- The formation of HAP through the DAP-calcite reaction was consistent throughout the carbonate samples, with higher concentrations observed closer to the surface.
- Acid etching resulted in a substantial decrease in the elastic modulus of Austin chalk by up to 78% and Indiana limestone by up to 66%.
- DAP treatment significantly improved the elastic modulus of Austin chalk samples, ranging from 100% to 575%, with a more pronounced stiffening effect observed in acidized samples with lower elastic modulus.

- In contrast, the DAP treatment of Indiana limestone samples showed a less significant improvement in elastic modulus, ranging from 9% to 49%, with a stronger stiffening effect observed in intact samples.
- The DAP treatment led to an increase in the elastic modulus, resulting in a more rigid fracture surface and long-lasting hydraulic/acid fracture conductivity in both Indiana limestone and Austin chalk samples.
- Controlled experiments show that the hydraulic/acid conductivity of Indiana limestone DAP-treated samples is at least twice that of untreated samples, with reduced sensitivity to stress.
- Furthermore, the enhancement in conductivity of the hydraulic/acid fractures in Austin chalk was particularly notable, with conductivity levels reaching 7 to 8 times higher than untreated fractures.
- DAP treatment mitigated the deformability caused by acid etching, leading to increased fracture stiffness and improved hydraulic conductivity.
- The findings offer valuable insights for the application of DAP treatment in carbonate reservoir stimulation, optimizing hydraulic fracturing operations and enhancing production rates.

5.2 Future Work

Based on the promising outcomes of the study, several areas can be further explored and investigated as follows:

- It is necessary to uncover catalysts that promote the reaction between DAP and calcite to accelerate the stiffening process.

- Alternative chemicals can be examined to explore their potential for achieving more favorable outcomes in terms of carbonate stiffening.
- The potential application of the stiffening achieved through DAP treatment can be explored in various petroleum engineering contexts, such as the stabilization of boreholes drilled in soft formations like chalk.

5.3 Recommendation

It is advisable to take into account some considerations during field trials to achieve comparable positive results in field applications and replicate the findings of the study, for example:

- It is suggested to implement the stiffening innovation described in this study as a supplementary step during acid stimulation operations.
- A comparative analysis should be conducted during field trials to assess the effectiveness of the DAP treatment in real field conditions. This analysis could involve comparing different stages within a single multistage fractured well or evaluating similar wells to evaluate the impact of the treatment in actual field situations.
- The application of the treatment is particularly beneficial in soft formations such as chalk or limestone that have been damaged by acid.
- Conducting a preliminary study of the carbonate formation is recommended to assess the calcite content present in the formation.
- It is important to utilize the exact composition of DAP in the treatment that was used in the laboratory to achieve positive results.

References

- Akbari, M., Javad Ameri, M., Kharazmi, S., Motamedi, Y., & Pournik, M. (2017). New correlations to predict fracture conductivity based on the rock strength. *Journal of Petroleum Science and Engineering*, 152, 416–426. <https://doi.org/10.1016/j.petrol.2017.03.003>
- Al-Ameri, A., & Gamadi, T. (2020). Optimization of acid fracturing for a tight carbonate reservoir. *Petroleum*, 6(1), 70–79. <https://doi.org/10.1016/j.petlm.2019.01.003>
- Al-Enezi, B., Al-Mufarej, M., Ashqar, A., & Navia, A. (2017). First Successful Openhole Lateral Multistage Acid Frac in a Complex Unconventional Carbonate Reservoir North Kuwait. *Day 4 Thu, November 16, 2017*, D041S112R002. <https://doi.org/10.2118/188170-MS>
- Aljawad, M. S., Desouky, M., Sølling, T. I., Amao, A. O., & Al-Ramadan, K. (2020). Improving carbonate rock hardness by consolidating additives to sustain long term fracture conductivity. *Journal of Petroleum Science and Engineering*, 195, 107897. <https://doi.org/10.1016/j.petrol.2020.107897>
- Anderson, M. S., & Fredrickson, S. E. (1987). Dynamic Etching Tests Aid Fracture Acidizing Treatment Design. *All Days*, SPE-16452-MS. <https://doi.org/10.2118/16452-MS>
- Anfosso, M., Matteini, M., Piqué, F., Vicini, S., & Gaggero, L. (2023). Eco-innovation in the conservation of built heritage: Two-steps protocol of Di-ammonium phosphate

application. *Materials Letters*, 333, 133618.
<https://doi.org/10.1016/j.matlet.2022.133618>

Antelo, L. F., Pournik, M., Zhu, D., & Hill, A. D. (2009). Surface Etching Pattern and its Effect on Fracture Conductivity in Acid Fracturing. *All Days*, SPE-119743-MS.
<https://doi.org/10.2118/119743-MS>

Asadollahpour, E., Baghbanan, A., & Hashemolhosseini, H. (2018). Evolution of normal deformability of acidized rock fractures. *Arabian Journal of Geosciences*, 11(21), 652. <https://doi.org/10.1007/s12517-018-3981-9>

Asadollahpour, E., Baghbanan, A., Hashemolhosseini, H., & Mohtarami, E. (2018). The etching and hydraulic conductivity of acidized rough fractures. *Journal of Petroleum Science and Engineering*, 166, 704–717.
<https://doi.org/10.1016/j.petrol.2018.03.074>

Ashokan, A., Kumar, T. S. S., & Jayaraman, G. (2022). Process optimization for the rapid conversion of calcite into hydroxyapatite microspheres for chromatographic applications. *Scientific Reports*, 12(1), 12164. <https://doi.org/10.1038/s41598-022-16579-4>

Ayatollahi, M. R., Najafabadi, M. Z., Koloor, S. S. R., & Petru, M. (2020). Mechanical Characterization of Heterogeneous Polycrystalline Rocks Using Nanoindentation Method in Combination with Generalized Means Method. *Journal of Mechanics*, 36(6), 813–823. <https://doi.org/10.1017/jmech.2020.18>

- Barriuso, B. C., Botticelli, G., Cuzman, O. A., Osticioli, I., Tiano, P., & Matteini, M. (2017). Conservation of calcareous stone monuments: Screening different diammonium phosphate based formulations for countering phototrophic colonization. *Journal of Cultural Heritage*, 27, 97–106. <https://doi.org/10.1016/j.culher.2017.03.002>
- Beg, M. S., Kunak, A. O., Gong, M., Zhu, D., & Hill, A. D. (1998). A Systematic Experimental Study of Acid Fracture Conductivity. *SPE Production & Facilities*, 13(04), 267–271. <https://doi.org/10.2118/52402-PA>
- Broitman, E. (2017). Indentation Hardness Measurements at Macro-, Micro-, and Nanoscale: A Critical Overview. *Tribology Letters*, 65(1), 23. <https://doi.org/10.1007/s11249-016-0805-5>
- Broz, M. E., Cook, R. F., & Whitney, D. L. (2006). Microhardness, toughness, and modulus of Mohs scale minerals. *American Mineralogist*, 91(1), 135–142. <https://doi.org/10.2138/am.2006.1844>
- Chen, R., & Shen, J. (2020). The synthesis of hydroxyapatite crystals with various morphologies via the solvothermal method using double surfactants. *Materials Letters*, 259, 126881. <https://doi.org/10.1016/j.matlet.2019.126881>
- Darroudi, T., & Searcy, A. W. (1981). Effect of carbon dioxide pressure on the rate of decomposition of calcite (CaCO₃). *The Journal of Physical Chemistry*, 85(26), 3971–3974. <https://doi.org/10.1021/j150626a004>

Desouky, M., Aljawad, M. S., Abduljamiu, A., Solling, T., Abdulraheem, A., AlTammar, M. J., & Alruwaili, K. M. (2023). Enhancing Fracture Conductivity in Soft Chalk Formations With Diammonium Phosphate Treatment: A Study at High Temperature, Pressure, and Stresses. *SPE Journal*, 1–11. <https://doi.org/10.2118/215857-PA>

Desouky, M., Aljawad, M. S., Amao, A., AlShehri, D. A., AlTammar, M. J., & Alruwaili, K. M. (2023). Chemical Treatment for Sustainable Acid Fracture Conductivity of Weak Carbonates. *All Days*, ARMA-2023-0447. <https://doi.org/10.56952/ARMA-2023-0447>

Desouky, M., Aljawad, M. S., Solling, T., Abduljamiu, A., Norrman, K., & Alshehri, D. (2021). Improving long-term hydraulic fracture conductivity by alteration of rock minerals. *Journal of Petroleum Science and Engineering*, 196, 108046. <https://doi.org/10.1016/j.petrol.2020.108046>

Desouky, M. H., Aljawad, M. S., AlTammar, M. J., & Alruwaili, K. M. (2023). Maintaining Hydraulic Fracture Conductivity Under High Stresses Through Consolidation with DAP. *Day 2 Mon, February 20, 2023*, D021S075R003. <https://doi.org/10.2118/213670-MS>

DileepKumar, V. G., Sridhar, M. S., Aramwit, P., Krut'ko, V. K., Musskaya, O. N., Glazov, I. E., & Reddy, N. (2022). A review on the synthesis and properties of hydroxyapatite for biomedical applications. *Journal of Biomaterials Science, Polymer Edition*, 33(2), 229–261. <https://doi.org/10.1080/09205063.2021.1980985>

- Dubey, D. K., & Tomar, V. (2009). Role of hydroxyapatite crystal shape in nanoscale mechanical behavior of model tropocollagen–hydroxyapatite hard biomaterials. *Materials Science and Engineering: C*, 29(7), 2133–2140. <https://doi.org/10.1016/j.msec.2009.04.015>
- Eliason, R., & McMahon, T. (1981). Temperature effect on reaction rates. *Journal of Chemical Education*, 58(4), 354. <https://doi.org/10.1021/ed058p354.1>
- Erşan, Y. Ç., Wang, J., Fraeye, D., Boon, N., & De Belie, N. (2020). Surface Consolidation of Maastricht Limestone by Means of *Bacillus Sphaericus* under Varying Treatment Conditions. *Journal of Materials in Civil Engineering*, 32(11), 04020342. [https://doi.org/10.1061/\(ASCE\)MT.1943-5533.0003447](https://doi.org/10.1061/(ASCE)MT.1943-5533.0003447)
- Fredrickson, S. E. (1986). Stimulating Carbonate Formations Using a Closed Fracture Acidizing Technique. *All Days*, SPE-14654-MS. <https://doi.org/10.2118/14654-MS>
- Gomaa, A. M., & Nasr-El-Din, H. A. (2009). Acid Fracturing: The Effect of Formation Strength on Fracture Conductivity. *All Days*, SPE-119623-MS. <https://doi.org/10.2118/119623-MS>
- Gong, M., Lacote, S., & Hill, A. D. (1999). New Model of Acid-Fracture Conductivity Based on Deformation of Surface Asperities. *SPE Journal*, 4(03), 206–214. <https://doi.org/10.2118/57017-PA>
- Goto, T., Kim, I. Y., Kikuta, K., & Ohtsuki, C. (2012). Comparative study of hydroxyapatite formation from α - and β -tricalcium phosphates under hydrothermal

- conditions. *Journal of the Ceramic Society of Japan*, 120(1400), 131–137.
<https://doi.org/10.2109/jcersj2.120.131>
- Gou, B., Guan, C., Li, X., Ren, J., Zeng, J., Wu, L., & Guo, J. (2021). Acid-etching fracture morphology and conductivity for alternate stages of self-generating acid and gelled acid during acid-fracturing. *Journal of Petroleum Science and Engineering*, 200, 108358. <https://doi.org/10.1016/j.petrol.2021.108358>
- Gou, B., Li, X., Guo, J., Liu, W., Zeng, J., He, C., Hu, L., Ren, J., & Dai, Q. (2023). Effect of Acid Type on Acid-Etched Fracture Surface Morphology and Conductivity along the Fracture. *Energy & Fuels*, 37(5), 3709–3722.
<https://doi.org/10.1021/acs.energyfuels.2c04076>
- Guo, J., Gou, B., Qin, N., Zhao, J., Wu, L., Wang, K., & Ren, J. (2020). An innovative concept on deep carbonate reservoir stimulation: Three-dimensional acid fracturing technology. *Natural Gas Industry B*, 7(5), 484–497.
<https://doi.org/10.1016/j.ngib.2020.09.006>
- Hussain, M., Muqtadir, A., Amao, A., Al-Ramadan, K., & Babalola, L. (2019). Destructive vs Non-destructive: Establishing an Empirical Relationship between Impulse Hammer and Triaxial Test - Derived Rock Mechanical Properties. *Proceedings of the 7th Unconventional Resources Technology Conference*. Unconventional Resources Technology Conference, Denver, Colorado, USA.
<https://doi.org/10.15530/urtec-2019-222>
- Jiang, X., Scott, P. J., Whitehouse, D. J., & Blunt, L. (2007). Paradigm shifts in surface metrology. Part II. The current shift. *Proceedings of the Royal Society A:*

Mathematical, Physical and Engineering Sciences, 463(2085), 2071–2099.
<https://doi.org/10.1098/rspa.2007.1873>

Kalfayan, L. J. (2007). Fracture Acidizing: History, Present State, and Future. *All Days*, SPE-106371-MS. <https://doi.org/10.2118/106371-MS>

Kim, I. Y., & Ohtsuki, C. (2016). Hydroxyapatite formation from calcium carbonate single crystal under hydrothermal condition: Effects of processing temperature. *Ceramics International*, 42(1), 1886–1890. <https://doi.org/10.1016/j.ceramint.2015.09.156>

Lai, J., Guo, J., Chen, C., Wu, K., Ma, H., Zhou, C., Wang, S., Ren, J., & Wang, Z. (2019). The Effects of Initial Roughness and Mechanical Property of Fracture Surface on Acid Fracture Conductivity in Tight Dolomite Reservoir. *Day 3 Wed, March 20, 2019*, D032S106R002. <https://doi.org/10.2118/194780-MS>

Li, N., Dai, J., Liu, P., Luo, Z., & Zhao, L. (2015). Experimental study on influencing factors of acid-fracturing effect for carbonate reservoirs. *Petroleum*, 1(2), 146–153. <https://doi.org/10.1016/j.petlm.2015.06.001>

Li, Q., Li, J., Duan, L., & Tan, S. (2021). Prediction of rock abrasivity and hardness from mineral composition. *International Journal of Rock Mechanics and Mining Sciences*, 140, 104658. <https://doi.org/10.1016/j.ijrmms.2021.104658>

Li, Y., Kang, Z., Xue, Z., & Zheng, S. (2018). Theories and practices of carbonate reservoirs development in China. *Petroleum Exploration and Development*, 45(4), 712–722. [https://doi.org/10.1016/S1876-3804\(18\)30074-0](https://doi.org/10.1016/S1876-3804(18)30074-0)

- Lin, K., Wu, C., & Chang, J. (2014). Advances in synthesis of calcium phosphate crystals with controlled size and shape. *Acta Biomaterialia*, *10*(10), 4071–4102. <https://doi.org/10.1016/j.actbio.2014.06.017>
- López-Arce, P., Gomez-Villalba, L. S., Pinho, L., Fernández-Valle, M. E., De Buergo, M. Á., & Fort, R. (2010). Influence of porosity and relative humidity on consolidation of dolostone with calcium hydroxide nanoparticles: Effectiveness assessment with non-destructive techniques. *Materials Characterization*, *61*(2), 168–184. <https://doi.org/10.1016/j.matchar.2009.11.007>
- Lu, C., Bai, X., Luo, Y., & Guo, J. (2017). New study of etching patterns of acid-fracture surfaces and relevant conductivity. *Journal of Petroleum Science and Engineering*, *159*, 135–147. <https://doi.org/10.1016/j.petrol.2017.09.025>
- Ma, G. (2019). Three common preparation methods of hydroxyapatite. *IOP Conference Series: Materials Science and Engineering*, *688*(3), 033057. <https://doi.org/10.1088/1757-899X/688/3/033057>
- Malagon, C., Pournik, M., & Hill, A. D. (2008). The Texture of Acidized Fracture Surfaces: Implications for Acid Fracture Conductivity. *SPE Production & Operations*, *23*(03), 343–352. <https://doi.org/10.2118/102167-PA>
- Matteini, M., Rescic, S., Fratini, F., & Botticelli, G. (2011). Ammonium Phosphates as Consolidating Agents for Carbonatic Stone Materials Used in Architecture and Cultural Heritage: Preliminary Research. *International Journal of Architectural Heritage*, *5*(6), 717–736. <https://doi.org/10.1080/15583058.2010.495445>

- Mehrjoo, H., Norouzi-Apourvari, S., Jalalifar, H., & Shajari, M. (2022). Experimental study and modeling of final fracture conductivity during acid fracturing. *Journal of Petroleum Science and Engineering*, 208, 109192. <https://doi.org/10.1016/j.petrol.2021.109192>
- Melendez, M. G., Pournik, M., Zhu, D., & Hill, A. D. (2007). The Effects of Acid Contact Time and the Resulting Weakening of the Rock Surfaces on Acid-Fracture Conductivity. *All Days*, SPE-107772-MS. <https://doi.org/10.2118/107772-MS>
- Mofti, M. ., Al-Othman, M. ., Alboueshi, A. ., Davis, J. ., Eid, W. ., Allam, A. ., Hamad, A. A., Sadeddin, S. ., Buhamad, A. ., Ashkanani, M. ., Aloun, S. ., Al-Haddad, M. ., & Al-Mehanna, H. . (2018). First Fully Successful Application of a Multistage Acid Fracturing Operation to Stimulate a Carbonate Formation, Resulting in the Implementation in Other Wells in the Mature Bahrah Field, North Kuwait. *Day 3 Wed, January 31, 2018*, D031S018R001. <https://doi.org/10.2118/189353-MS>
- Motamedi-Ghahfarokhi, Y., Ameri Shahrabi, M. J., Akbari, M., & Pournik, M. (2018). New correlations to predict fracture conductivity based on the formation lithology. *Energy Sources, Part A: Recovery, Utilization, and Environmental Effects*, 40(13), 1663–1673. <https://doi.org/10.1080/15567036.2018.1486896>
- Murru, A., & Fort, R. (2020). Diammonium hydrogen phosphate (DAP) as a consolidant in carbonate stones: Impact of application methods on effectiveness. *Journal of Cultural Heritage*, 42, 45–55. <https://doi.org/10.1016/j.culher.2019.09.003>
- Naik, S., Dean, M., McDuff, D., Ranson, A., Jin, X., Zhu, D., & Hill, A. D. (2020). Acid Fracture Conductivity Testing on the Tight Carbonate Ratawi Limestone in the

Partitioned Zone. *Day 2 Tue, January 14, 2020*, D023S127R001.
<https://doi.org/10.2523/IPTC-19724-Abstract>

Nasr-El-Din, H. A., Al-Driweesh, S. M., Metcalf, A. S., & Chesson, J. B. (2008). Fracture Acidizing: What Role Does Formation Softening Play in Production Response? *SPE Production & Operations*, 23(02), 184–191. <https://doi.org/10.2118/103344-PA>

Navarrete, R. C., Miller, M. J., & Gordon, J. E. (1998). Laboratory and Theoretical Studies for Acid Fracture Stimulation Optimization. *All Days*, SPE-39776-MS. <https://doi.org/10.2118/39776-MS>

Neira, I. S., Kolen'ko, Y. V., Lebedev, O. I., Van Tendeloo, G., Gupta, H. S., Guitián, F., & Yoshimura, M. (2009). An Effective Morphology Control of Hydroxyapatite Crystals via Hydrothermal Synthesis. *Crystal Growth & Design*, 9(1), 466–474. <https://doi.org/10.1021/cg800738a>

Nierode, D. E., & Kruk, K. F. (1973). An Evaluation of Acid Fluid Loss Additives Retarded Acids, and Acidized Fracture Conductivity. *All Days*, SPE-4549-MS. <https://doi.org/10.2118/4549-MS>

Nierode, D. E., Williams, B. R., & Bombardieri, C. C. (1972). Prediction of Stimulation From Acid Fracturing Treatments. *Journal of Canadian Petroleum Technology*, 11(04). <https://doi.org/10.2118/72-04-04>

- Novotny, E. J. (1977). Prediction of Stimulation From Acid Fracturing Treatments Using Finite Fracture Conductivity. *Journal of Petroleum Technology*, 29(09), 1186–1194. <https://doi.org/10.2118/6123-PA>
- Nugroho, A., Amanah, N. L., Kamal, H. P., & Angkasa, S. (2022). Acid Treatment on Carbonate Rock: An Effect of HCL Concentration on Rock Properties and Fluid Flowrates. *Journal of Emerging Supply Chain, Clean Energy, and Process Engineering*, 1(1), 7–18. <https://doi.org/10.57102/jescee.v1i1.2>
- Ossola, F., Tomasin, P., De Zorzi, C., El Habra, N., Chiurato, M., & Favaro, M. (2012). New calcium alkoxides for consolidation of carbonate rocks. Influence of precursors' characteristics on morphology, crystalline phase and consolidation effects. *New Journal of Chemistry*, 36(12), 2618. <https://doi.org/10.1039/c2nj40708f>
- Osticioli, I., Botticelli, G., Matteini, P., Siano, S., Pini, R., & Matteini, M. (2017). Micro-Raman analysis on the combined use of ammonium oxalate and ammonium phosphate for the consolidation and protection of carbonate stone artifacts. *Journal of Raman Spectroscopy*, 48(7), 966–971. <https://doi.org/10.1002/jrs.5150>
- Pai, S., M Kini, S., Selvaraj, R., & Pugazhendhi, A. (2020). A review on the synthesis of hydroxyapatite, its composites and adsorptive removal of pollutants from wastewater. *Journal of Water Process Engineering*, 38, 101574. <https://doi.org/10.1016/j.jwpe.2020.101574>

- Palharini Schwalbert, M., Aljawad, M. S., Hill, A. D., & Zhu, D. (2020). Decision Criterion for Acid-Stimulation Method in Carbonate Reservoirs: Matrix Acidizing or Acid Fracturing? *SPE Journal*, 25(05), 2296–2318. <https://doi.org/10.2118/199236-PA>
- Possenti, E., Conti, C., Gatta, G. D., Marinoni, N., Merlini, M., Realini, M., Vaughan, G. B. M., & Colombo, C. (2022). Synchrotron X-ray diffraction computed tomography to non-destructively study inorganic treatments for stone conservation. *IScience*, 25(10), 105112. <https://doi.org/10.1016/j.isci.2022.105112>
- Pournik, M. ., Goma, A. ., & Nasr-El-Din, H. A. (2010). Influence of Acid-Fracture Fluid Properties on Acid-Etched Surfaces and Resulting Fracture Conductivity. *All Days*, SPE-128070-MS. <https://doi.org/10.2118/128070-MS>
- Pournik, M., Zhu, D., & Hill, A. D. (2009). Acid-Fracture Conductivity Correlation Development Based on Acid-Fracture Characterization. *All Days*, SPE-122333-MS. <https://doi.org/10.2118/122333-MS>
- Rodrigues, V. F., & Medeiros, A. C. (2011). Limits of Acid Fracture Conductivity Correlation Improvement Through Acid Fracture Surface Characterization. *All Days*, OTC-22337-MS. <https://doi.org/10.4043/22337-MS>
- Roy, D. M., & Linnehan, S. K. (1974). Hydroxyapatite formed from Coral Skeletal Carbonate by Hydrothermal Exchange. *Nature*, 247(5438), 220–222. <https://doi.org/10.1038/247220a0>
- Samarkin, Y., Aljawad, M. S., Amao, A., Solling, T., Abu-Khamsin, S. A., Patil, S., AlTammar, M. J., & Alruwaili, K. M. (2022). Carbonate Rock Chemical

- Consolidation Methods: Advancement and Applications. *Energy & Fuels*, 36(8), 4186–4197. <https://doi.org/10.1021/acs.energyfuels.2c00232>
- Samarkin, Y., Amao, A., Aljawad, M. S., Solling, T., Al-Ramadan, K., AlTammar, M. J., & Alruwaili, K. M. (2023). Conductivity Enhancement of Fractured Carbonates through High-Temperature Diammonium Hydrogen Phosphate Consolidation: A Preliminary Study. *SPE Journal*, 28(04), 1956–1972. <https://doi.org/10.2118/214657-PA>
- Sassoni, E., Graziani, G., & Franzoni, E. (2016). An innovative phosphate-based consolidant for limestone. Part 1: Effectiveness and compatibility in comparison with ethyl silicate. *Construction and Building Materials*, 102, 918–930. <https://doi.org/10.1016/j.conbuildmat.2015.04.026>
- Sassoni, E., Naidu, S., & Scherer, G. W. (2011a). The use of hydroxyapatite as a new inorganic consolidant for damaged carbonate stones. *Journal of Cultural Heritage*, 12(4), 346–355. <https://doi.org/10.1016/j.culher.2011.02.005>
- Sassoni, E., Naidu, S., & Scherer, G. W. (2011b). The use of hydroxyapatite as a new inorganic consolidant for damaged carbonate stones. *Journal of Cultural Heritage*, 12(4), 346–355. <https://doi.org/10.1016/j.culher.2011.02.005>
- Sena Da Fonseca, B., Ferreira Pinto, A. P., Piçarra, S., Caldeira, B., & Montemor, M. F. (2021). Consolidating efficacy of diammonium hydrogen phosphate on artificially aged and naturally weathered coarse-grained marble. *Journal of Cultural Heritage*, 51, 145–156. <https://doi.org/10.1016/j.culher.2021.08.003>

- Smith, I. W. M. (2008). The temperature-dependence of elementary reaction rates: Beyond Arrhenius. *Chem. Soc. Rev.*, 37(4), 812–826. <https://doi.org/10.1039/B704257B>
- Tariq, Z., Hassan, A., Al-Abdrabalnabi, R., Aljawad, M. S., & Mahmoud, M. (2021). Comparative Study of Fracture Conductivity in Various Carbonate Rocks Treated with GLDA Chelating Agent and HCl Acid. *Energy & Fuels*, 35(23), 19641–19654. <https://doi.org/10.1021/acs.energyfuels.1c03471>
- Ugursal, A. ., Zhu, D. ., & Hill, A. D. (2019). Development of Acid Fracturing Model for Naturally Fractured Reservoirs. *SPE Production & Operations*, 34(04), 735–748. <https://doi.org/10.2118/189834-PA>
- Van Domelen, M. S., Gdanski, R. D., & Finley, D. B. (1994). The Application of Core and Well Testing to Fracture Acidizing Treatment Design: A Case Study. *All Days*, SPE-27621-MS. <https://doi.org/10.2118/27621-MS>
- Viktorov, S. D., Golovin, Yu. I., Kochanov, A. N., Tyurin, A. I., Shuklinov, A. V., Shuvarin, I. A., & Pirozhkova, T. S. (2014). Micro- and nano-indentation approach to strength and deformation characteristics of minerals. *Journal of Mining Science*, 50(4), 652–659. <https://doi.org/10.1134/S1062739114040048>
- Xiao, Y., Wang, H., Guo, J., Lu, L., Cheng, Y., Chen, M., Fan, F., & Xue, H. (2019). Acid Fracturing Was Selected to Stimulate the Potential Production in Low Permeability Reservoirs in Ahdeb Oilfield, Iraq. *Day 3 Wed, March 20, 2019*, D032S064R003. <https://doi.org/10.2118/194900-MS>

- Yaşar, E., & Erdoğan, Y. (2004). Estimation of rock physicommechanical properties using hardness methods. *Engineering Geology*, 71(3–4), 281–288.
[https://doi.org/10.1016/S0013-7952\(03\)00141-8](https://doi.org/10.1016/S0013-7952(03)00141-8)
- Yoshimura, M., Sujaridworakun, P., Koh, F., Fujiwara, T., Pongkao, D., & Ahniyaz, A. (2004). Hydrothermal conversion of calcite crystals to hydroxyapatite. *Materials Science and Engineering: C*, 24(4), 521–525.
<https://doi.org/10.1016/j.msec.2004.01.005>
- Zhang, H., Zhong, Y., Zhang, J., Zhang, Y., Kuang, J., & Yang, B. (2020). Experimental research on deterioration of mechanical properties of carbonate rocks under acidified conditions. *Journal of Petroleum Science and Engineering*, 185, 106612.
<https://doi.org/10.1016/j.petrol.2019.106612>
- Zhang, R., Hou, B., Zhou, B., Liu, Y., Xiao, Y., & Zhang, K. (2020). Effect of acid fracturing on carbonate formation in southwest China based on experimental investigations. *Journal of Natural Gas Science and Engineering*, 73, 103057.
<https://doi.org/10.1016/j.jngse.2019.103057>
- Zhang, X., & Vecchio, K. S. (2007). Hydrothermal synthesis of hydroxyapatite rods. *Journal of Crystal Growth*, 308(1), 133–140.
<https://doi.org/10.1016/j.jcrysgro.2007.07.059>
- Zhou, B., Jin, Y., Xiong, W., Zhang, J., Lai, J., & Fang, Q. (2021). Investigation on surface strength of acid fracture from scratch test. *Journal of Petroleum Science and Engineering*, 206, 109017. <https://doi.org/10.1016/j.petrol.2021.109017> |

Vitae

Name: MAHMOUD HASSAN DESOUKY

Nationality: Egyptian

Date of Birth:5/28/1991

Email: mahmoudhassan1001@yahoo.com

Address: Rose Alyousif street 9th settlement, Obour City, 11828, greater Cairo, Egypt

Academic Background: Petroleum Engineering

Education: Petroleum Engineering Ph.D., KFUPM, 2023

Petroleum Engineering MSc., KFUPM, 2019

Petroleum Engineering BSc., Suez University, 2013

Publications:

Aljawad, M. S., Aljulaih, H., Mahmoud, M., & Desouky, M. (2019). Integration of field, laboratory, and modeling aspects of acid fracturing: A comprehensive review. *Journal of Petroleum Science and Engineering*, 181, 106158. <https://doi.org/10.1016/j.petrol.2019.06.022>

Aljawad, M. S., Desouky, M., Sølling, T. I., Amao, A. O., & Al-Ramadan, K. (2020). Improving carbonate rock hardness by consolidating additives to sustain long term fracture conductivity. *Journal of Petroleum Science and Engineering*, 195, 107897. <https://doi.org/10.1016/j.petrol.2020.107897>

- Desouky, M., Al-Jawad, M., El-Tammar, M., & El-Ruwaili, K. (2023, March 7). *Maintaining Hydraulic Fracture Conductivity Under High Stresses through Consolidation with DAP*. Middle East Oil, Gas and Geosciences Show. <https://doi.org/10.2118/213670-MS>
- Desouky, M., Aljawad, M. S., Abduljamiu, A., Solling, T., Abdulraheem, A., AlTammar, M. J., & Alruwaili, K. M. (2023). Enhancing Fracture Conductivity in Soft Chalk Formations With Diammonium Phosphate Treatment: A Study at High Temperature, Pressure, and Stresses. *SPE Journal*, 1–11. <https://doi.org/10.2118/215857-PA>
- Desouky, M., Aljawad, M. S., Alhoori, H., & Al-Shehri, D. (2020, December 1). *Evaluating the Effects of Acid Fracture Etching Patterns on Conductivity Estimation Using Machine Learning Techniques*. SPE Europec. <https://doi.org/10.2118/200527-MS>
- Desouky, M., Aljawad, M. S., Amao, A., AlShehri, D. A., AlTammar, M. J., & Alruwaili, K. M. (2023, June 25). *Chemical Treatment for Sustainable Acid Fracture Conductivity of Weak Carbonates*. 57th U.S. Rock Mechanics/Geomechanics Symposium. <https://doi.org/10.56952/ARMA-2023-0447>
- Desouky, M., Aljawad, M. S., Solling, T., Abduljamiu, A., Norrman, K., & Alshehri, D. (2021). Improving long-term hydraulic fracture conductivity by alteration of rock minerals. *Journal of Petroleum Science and Engineering*, 196, 108046. <https://doi.org/10.1016/j.petrol.2020.108046>

Desouky, M., Alqubalee, A., & Gowida, A. (2023). Decision Tree Ensembles for Automatic Identification of Lithology. *SPE Symposium: Leveraging Artificial Intelligence to Shape the Future of the Energy Industry*.
<https://onepetro.org/SPEIOGS/proceedings/22AIS/D011S003R001/515684>

Desouky, M. H. (2019). *Enhancement and Prediction of Long-Term Acid Fracture Conductivity* [M.S., King Fahd University of Petroleum and Minerals (Saudi Arabia)].
<https://www.proquest.com/docview/2720970326/abstract/F9EB498F7EF447A2P/Q/1>

Desouky, M. H., Aljawad, M. S., SOLLING, T., AlTammar, M. J., & Alruwaili, K. M. (2023). *Method for stabilizing wellbore, stabilized wellbore and wellbore stabilizing fluid* (United States Patent US20230295482A1).
<https://patents.google.com/patent/US20230295482A1/en>

DESOUKY, M., Jawad, M. A., & SOLLING, T. I. (2022). *Rock hardness for hydraulic fracturing and art preservation* (United States Patent US11492494B2).
<https://patents.google.com/patent/US11492494B2/en>

Desouky, M., Mustafa, A., Aljawad, M., Solling, T., & Dvorkin, J. (2022, June 6). *Sustaining Wormholes Mechanical Stability in Weak Acidized Carbonates Using Consolidants*. SPE EuroPEC - Europe Energy Conference featured at the 83rd EAGE Annual Conference & Exhibition. <https://doi.org/10.2118/209702-MS>

Desouky, M., Tariq, Z., Al jawad, M., Alhoori, H., Mahmoud, M., & Abdulraheem, A. (2021). Development of Machine Learning Based Propped Fracture Conductivity

Correlations in Shale Formations. *SPE Middle East Oil and Gas Show and Conference*, D031S031R005. <https://onepetro.org/SPEMEOS/proceedings-abstract/21MEOS/3-21MEOS/474455>

Desouky, M., Tariq, Z., Aljawad, M. S., Alhoori, H., Mahmoud, M., & Abdulraheem, A. (2021). Machine Learning-Based Propped Fracture Conductivity Correlations of Several Shale Formations. *ACS Omega*, 6(29), 18782–18792. <https://doi.org/10.1021/acsomega.1c01919>

Desouky, M., Tariq, Z., Aljawad, M. S., Alhoori, H., Mahmoud, M., & AlShehri, D. (2020). Data-Driven Acid Fracture Conductivity Correlations Honoring Different Mineralogy and Etching Patterns. *ACS Omega*, 5(27), 16919–16931. <https://doi.org/10.1021/acsomega.0c02123>

Murtada, A.-J., Desouky, M., Solling, T., Alramadan, K., & Abduljamiu, A. (2022). *Method of improving rock hardness in carbonate formations*. Google Patents. <https://patents.google.com/patent/US11365345B2/en>

Mustafa, A., Desouky, M., Aljawad, M. S., Solling, T., & Dvorkin, J. (2023). Sustaining Wormholes Mechanical Stability in Weak Acidized Carbonates Using Consolidants. *Rock Mechanics and Rock Engineering*. <https://doi.org/10.1007/s00603-023-03285-4>